

ISSN 1881-7831 Online ISSN 1881-784X

DD & T

Drug Discoveries & Therapeutics

Volume 8, Number 6
December, 2014



www.ddtjournal.com

DD & T

Drug Discoveries & Therapeutics



ISSN: 1881-7831
Online ISSN: 1881-784X
CODEN: DDTRBX
Issues/Year: 6
Language: English
Publisher: IACMHR Co., Ltd.

Drug Discoveries & Therapeutics is one of a series of peer-reviewed journals of the International Research and Cooperation Association for Bio & Socio-Sciences Advancement (IRCA-BSSA) Group and is published bimonthly by the International Advancement Center for Medicine & Health Research Co., Ltd. (IACMHR Co., Ltd.) and supported by the IRCA-BSSA and Shandong University China-Japan Cooperation Center for Drug Discovery & Screening (SDU-DDSC).

Drug Discoveries & Therapeutics publishes contributions in all fields of pharmaceutical and therapeutic research such as medicinal chemistry, pharmacology, pharmaceutical analysis, pharmaceuticals, pharmaceutical administration, and experimental and clinical studies of effects, mechanisms, or uses of various treatments. Studies in drug-related fields such as biology, biochemistry, physiology, microbiology, and immunology are also within the scope of this journal.

Drug Discoveries & Therapeutics publishes Original Articles, Brief Reports, Reviews, Policy Forum articles, Case Reports, News, and Letters on all aspects of the field of pharmaceutical research. All contributions should seek to promote international collaboration in pharmaceutical science.

Editorial Board

Editor-in-Chief:

Kazuhisa SEKIMIZU
The University of Tokyo, Tokyo, Japan

Co-Editors-in-Chief:

Xishan HAO
Tianjin Medical University, Tianjin, China
Norihiro KOKUDO
The University of Tokyo, Tokyo, Japan
Hongxiang LOU
Shandong University, Ji'nan, China
Yun YEN
City of Hope National Medical Center, Duarte, CA, USA

Chief Director & Executive Editor:

Wei TANG
The University of Tokyo, Tokyo, Japan

Managing Editor:

Hiroshi HAMAMOTO
The University of Tokyo, Tokyo, Japan
Munehiro NAKATA
Tokai University, Hiratsuka, Japan

Senior Editors:

Guanhua DU
Chinese Academy of Medical Science and Peking Union Medical College, Beijing, China

Xiao-Kang LI
National Research Institute for Child Health and Development, Tokyo, Japan
Masahiro MURAKAMI
Osaka Ohtani University, Osaka, Japan
Yutaka ORIHARA
The University of Tokyo, Tokyo, Japan
Tomofumi SANTA
The University of Tokyo, Tokyo, Japan
Wenfang XU
Shandong University, Ji'nan, China

Web Editor:

Yu CHEN
The University of Tokyo, Tokyo, Japan

Proofreaders:

Curtis BENTLEY
Roswell, GA, USA
Thomas R. LEBON
Los Angeles, CA, USA

Editorial and Head Office:

Pearl City Koishikawa 603,
2-4-5 Kasuga, Bunkyo-ku,
Tokyo 112-0003, Japan
Tel.: +81-3-5840-9697
Fax: +81-3-5840-9698
E-mail: office@ddtjournal.com

Drug Discoveries & Therapeutics

Editorial and Head Office

Pearl City Koishikawa 603, 2-4-5 Kasuga, Bunkyo-ku,
Tokyo 112-0003, Japan

Tel: +81-3-5840-9697, Fax: +81-3-5840-9698
E-mail: office@ddtjournal.com
URL: www.ddtjournal.com

Editorial Board Members

Alex ALMASAN (Cleveland, OH)	Rodney J. Y. HO (Seattle, WA)	Sridhar MANI (Bronx, NY)	Yuhong XU (Shanghai)
John K. BUOLAMWINI (Memphis, TN)	Hsing-Pang HSIEH (Zhunan, Miaoli)	Tohru MIZUSHIMA (Tokyo)	Bing YAN (Ji'nan, Shandong)
Jianping CAO (Shanghai)	Yongzhou HU (Hangzhou, Zhejiang)	Abdulla M. MOLOKHIA (Alexandria)	Yasuko YOKOTA (Tokyo)
Shousong CAO (Buffalo, NY)	Yu HUANG (Hong Kong)	Yoshinobu NAKANISHI (Kanazawa, Ishikawa)	Takako YOKOZAWA (Toyama, Toyama)
Jang-Yang CHANG (Tainan)	Hans E. JUNGINGER (Marburg, Hesse)	Weisan PAN (Shenyang, Liaoning)	Rongmin YU (Guangzhou, Guangdong)
Fen-Er CHEN (Shanghai)	Amrit B. KARMARKAR (Karad, Maharashtra)	Rakesh P. PATEL (Mehsana, Gujarat)	Guangxi ZHAI (Ji'nan, Shandong)
Zhe-Sheng CHEN (Queens, NY)	Toshiaki KATADA (Tokyo)	Shivanand P. PUTHLI (Mumbai, Maharashtra)	Liangren ZHANG (Beijing)
Zilin CHEN (Wuhan, Hubei)	Gagan KAUSHAL (Philadelphia, PA)	Shafiqur RAHMAN (Brookings, SD)	Lining ZHANG (Ji'nan, Shandong)
Shaofeng DUAN (Lawrence, KS)	Ibrahim S. KHATTAB (Kuwait)	Adel SAKR (Cairo)	Na ZHANG (Ji'nan, Shandong)
Chandradhar DWIVEDI (Brookings, SD)	Shiroh KISHIOKA (Wakayama, Wakayama)	Gary K. SCHWARTZ (New York, NY)	Ruiwen ZHANG (Amarillo, TX)
Mohamed F. EL-MILIGI (6th of October City)	Robert Kam-Ming KO (Hong Kong)	Yuemao SHEN (Ji'nan, Shandong)	Xiu-Mei ZHANG (Ji'nan, Shandong)
Hao FANG (Ji'nan, Shandong)	Nobuyuki KOBAYASHI (Nagasaki, Nagasaki)	Brahma N. SINGH (New York, NY)	Yongxiang ZHANG (Beijing)
Marcus L. FORREST (Lawrence, KS)	Toshiro KONISHI (Tokyo)	Tianqiang SONG (Tianjin)	(As of December 2014)
Takeshi FUKUSHIMA (Funabashi, Chiba)	Chun-Guang LI (Melbourne)	Sanjay K. SRIVASTAVA (Amarillo, TX)	
Harald HAMACHER (Tübingen, Baden-Württemberg)	Minyong LI (Ji'nan, Shandong)	Hongbin SUN (Nanjing, Jiangsu)	
Kenji HAMASE (Fukuoka, Fukuoka)	Xun LI (Ji'nan, Shandong)	Chandan M. THOMAS (Bradenton, FL)	
Junqing HAN (Ji'nan, Shandong)	Jikai LIU (Kunming, Yunnan)	Murat TURKOGLU (Istanbul)	
Xiaojiang HAO (Kunming, Yunnan)	Xinyong LIU (Ji'nan, Shandong)	Fengshan WANG (Ji'nan, Shandong)	
Kiyoshi HASEGAWA (Tokyo)	Yuxiu LIU (Nanjing, Jiangsu)	Hui WANG (Shanghai)	
Waseem HASSAN (Rio de Janeiro)	Xingyuan MA (Shanghai)	Quanxing WANG (Shanghai)	
Langchong HE (Xi'an, Shaanxi)	Ken-ichi MAFUNE (Tokyo)	Stephen G. WARD (Bath)	

Review

- 232 - 237 **Drug induced pulmonary parenchymal disease.**
Rajendra Prasad, Pawan Gupta, Abhijeet Singh, Nitin Goel

Brief Reports

- 238 - 244 **Several herbal compounds in Okinawa plants directly inhibit the oncogenic/aging kinase PAK1.**
Binh Cao Quan Nguyen, Nozomi Taira, Shinkichi Tawata
- 245 - 248 **Clinical features of 80 cases of tinea faciei treated at a rural clinic in Japan.**
Hikomitsu Noguchi, Masatoshi Jinnin, Keishi Miyata, Masataro Hiruma, Hironobu Ihn

Original Articles

- 249 - 254 ***In vitro* and *in vivo* anti-MRSA activities of nosokomycins.**
Ryuji Uchida, Hideaki Hanaki, Hidenori Matsui, Hiroshi Hamamoto, Kazuhisa Sekimizu, Masato Iwatsuki, Yong-Pil Kim, Hiroshi Tomoda
- 255 - 261 **Human RNA polymerase II-associated protein 2 (RPAP2) interacts directly with the RNA polymerase II subunit Rpb6 and participates in pre-mRNA 3'-end formation.**
Shotaro Wani, Yutaka Hirose, Yoshiaki Ohkuma
- 262 - 267 **Development of mucoadhesive buccal films from rice for pharmaceutical delivery systems**
Siriporn Okonogi, Sakornrat Khongkhunthian, Sanchai Jaturasitha
- 268 - 275 **Ion-exchange complex of famotidine: sustained release and taste masking approach of stable liquid dosage form.**
Reham Mokhtar Aman, Mahasen Mohamed Meshali, Galal Mahmoud Abdelghani

CONTENTS

(Continued)

Case Report

- 276 - 279 **Central nervous system infection with non-tuberculous mycobacteria: A report of that infection in two patients with AIDS.**
Rentian Cai, Tangkai Qi, Hongzhou Lu

Subject Index

- 280 - 284 **Subject Index (PDF)**

Guide for Authors

Copyright

Drug induced pulmonary parenchymal disease

Rajendra Prasad*, Pawan Gupta, Abhijeet Singh, Nitin Goel

Department of Respiratory Medicine, Vallabhbhai Patel Chest Institute, University of Delhi, Delhi, India.

Summary

Drug-induced pulmonary parenchymal disease (DIPPD) can be caused by a variety of agents, including antibiotics, chemotherapeutic drugs, antiarrhythmic agents and non-steroidal anti-inflammatory drugs (NSAIDs). DIPPD includes acute bronchospasm, organizing pneumonia, alveolar hypoventilation and hypersensitivity reactions. History, physical examination and investigations are required mainly to exclude other causes of lung diseases. Investigations may include chest radiography, pulmonary function testing and bronchoscopy with bronchoalveolar lavage (BAL). Recognition of DIPPD is difficult because the clinical, radiologic, and histologic findings are nonspecific. Management includes drug withdrawal and in some cases corticosteroid therapy. In this article we reviewed the various drugs known to cause pulmonary parenchymal diseases, various patterns of parenchymal diseases observed and their management.

Keywords: Pulmonary disease, bronchospasm, organizing pneumonia

1. Introduction

Pulmonary toxicity has been linked to increasing number of drugs since the late 19th century. With the advancement in development of new drugs, more drugs are now associated with lung diseases. In 1880, Osler described heroin-induced pulmonary edema during an autopsy (1). Drugs can affect any part of lung but parenchyma is most frequently involved. Currently, more than 350 agents are associated with drug induced pulmonary parenchymal diseases (DIPPD) (2,3). While uncommon, pulmonary adverse reactions often lead to significant physiologic impairment and/or necessitate intervention (4). Although drug-induced pulmonary diseases (DIPPD) vary in their pathophysiology, presentation and prognosis but diagnosis and treatment approach is similar in all groups. DIPPD is primarily a diagnosis of exclusion. Proper diagnosis requires a high index of suspicion and familiarity with the clinical syndromes associated with DIPPD. The present article aims to review the various drug induced pulmonary parenchymal diseases and their management.

2. Pathogenesis

Drug induced pulmonary parenchymal disease generally involves pulmonary parenchyma but can also involve the airways in addition. Mechanisms include direct oxidative injury, cytotoxic effects on alveolar capillary endothelial cells, immune-mediated lung injury and amphophilic medications causing deposition of phospholipid within the cells. These result in a variety of clinical and histologic patterns including bronchospasm, pneumonitis, pulmonary fibrosis, hypersensitivity reaction and non-cardiogenic pulmonary edema that has been mentioned in Table 1.

2.1. Bronchospasm

Drug induced bronchospasm can be triggered by any drug delivery route (aerosol, oral, IV or topical). Acute bronchospasm may be seen within few minutes of drug administration. Symptoms may manifest as wheezing and shortness of breath. Chest radiographs may show hyperinflation. Drugs cause bronchoconstriction by direct effect on airway smooth muscle by β blockers (5) and anticholinergic (6), inhibitory action on cyclooxygenase by aspirin (7), irritation of airways *via* a vagal reflex by ipratropium bromide and cromoglycate (8), release of substances causing bronchoconstriction by morphine (9), IgE mediated type I hypersensitivity reaction by penicillin (10) and enzymatic degradation

*Address correspondence to:

Dr. Rajendra Prasad, Vallabhbhai Patel Chest Institute, University of Delhi, Delhi, India.
E-mail: rprasadkgmc@gmail.com

Table 1. Drugs causing various patterns of pulmonary parenchymal disorders

Condition	Offending drugs	References
Bronchiolitis obliterans organizing pneumonia	Minocycline, amphotericin-B, bleomycin, methotrexate, nitrofurantoin, mitomycin, doxorubicin, acebutolol, amiodarone, ticlopidine, gold, phenytoin, sulfasalazine, L-tryptophan, interferon	17,18
Hypersensitivity lung disease	Ampicillin, bupropion, cytarabine, NSAIDs, sirolimus, penicillin, cephalosporins, phenytoin, carbamazepine, atorvastatin, sulfonamides, ticlopidine, ciprofloxacin, interferon-alfa, trimethoprim-sulfamethoxazole	22,23
Pulmonary eosinophilia	Amiodarone, captopril, bleomycin, gold salts, tryptophan, methotrexate, phenytoin, acetyl-salicylic acid, GM-CSF, minocycline, carbamazepine, penicillamine, sulfasalazine, propylthiouracil, chloroquine, cocaine, diclofenac, heroin, isoniazid, isotretinoin, zafirlukast	44-46
Pulmonary edema	Cytarabine, amlodipine, heroin, gemcitabine, cyclosporine, verapamil, interleukin, epinephrine, aspirin, methotrexate, acetazolamide, propoxyphene, ethchlorvynol, tocolytic agents, propranolol, nitric oxide, chlorthiazide, thiethylperazine, methotrexate, tretinoin, nitomycin, ketoprofen, heroin, methadone, protamine, clozapine	48-50
ARDS	Cytarabine, vinblastine, vincristine, nitrofurantoin, antineoplastic and immunosuppressant agents, recombinant GM-CSF, infliximab, talc, amiodarone, immunoglobulin	51-53

of other drugs in the liver by rifampicin (11). Common causes of drug-induced acute bronchospasm include non-steroidal anti-inflammatory drugs (NSAIDs), aspirin and beta-blockers. Other drugs like angiotensin converting enzyme (ACE) inhibitors, cephalosporins, hydrocortisone, nitrofurantoin, penicillin, and tamoxifen can also cause this manifestation (4). Contrast media used in radiology that contains iodine and the iron dextran compound Imferon may provoke severe anaphylactic responses. Hydrocortisone may cause paradoxically worsening of asthma by unknown mechanism (12). In patients with asthma and chronic obstructive pulmonary disease (COPD) who have a component of reversible airflow limitation, acute bronchospasm with beta-blockers is more likely. However, in one study, patients with COPD and coronary artery disease benefited from β -blockers; thus, β -blockers use in patients with COPD is not avoided (13,14). Up to 20% of asthmatic patients cannot tolerate aspirin and other NSAIDs (15).

2.2. Bronchiolitis obliterans organizing pneumonia (BOOP)

Bronchiolitis obliterans is a chronic form of airflow limitation characterized by inflammation and small airways occlusion (16). BOOP is a histopathologic reaction to a nonspecific inflammatory insult and can occur after exposure to a number of drugs (17,18). Symptoms may include nonproductive cough and shortness of breath with bilateral crackles. Imaging shows patchy airspace infiltrates peribronchial or subpleural in location with air trapping. Spirometry may reveal decreased Forced Expiratory Volume (FEV1) and forced expiratory flow at 25% to 75% of forced

vital capacity (FEV 25-75%). Diffusing capacity is reduced. Lung biopsy may demonstrate intraluminal buds of granulation tissue with preserved lung architecture. BOOP is treated with drug withdrawal and corticosteroids and has favourable outcome.

2.3. Hypersensitivity lung disease

Drug-induced hypersensitivity syndrome (DIHS), also called drug rash with eosinophilia and systemic symptoms (DRESS), is a severe reaction occurring 1-8 weeks after drug introduction. It is an immune mediated reaction involving cytokine and T-lymphocyte activation. Any drug can cause hypersensitivity syndrome. It may present with Loffler syndrome characterized by cough, dyspnea, fever, rash, blood eosinophilia and fleeting pulmonary infiltrates. Hypersensitivity lung disease may also manifest as chronic eosinophilic pneumonia. Patients may present with sub-acute low-grade fever, weight loss and nonproductive cough. Chest radiographs shows patchy peripheral airspace consolidation. Bronchoscopy with bronchoalveolar lavage (BAL) can confirm the diagnosis by revealing eosinophilia (more than 25% eosinophils). Drug-induced hypersensitivity pneumonitis is a pulmonary syndrome characterized by a complex immunological reaction (19). Patients may present with acute, sub-acute or chronic symptoms of fever, chills, malaise and dyspnea. Spirometry demonstrates a reduced Forced Vital Capacity (FVC) and Diffusion Lung Capacity for carbon monoxide (DLCO). High Resolution Computed Tomography (HRCT) scan Chest may reveal bilateral upper lobe-predominant ground-glass opacities, centrilobular nodules and air trapping on expiratory scans. In chronic cases, HRCT may show fibrotic changes, including

honeycombing and traction bronchiectasis (20). Lung biopsy may demonstrate loosely formed granulomas near the terminal bronchioles and lymphocytic and plasma cell infiltration of the alveolar walls. Pathology may demonstrate a Non-specific interstitial pneumonia (NSIP) or Usual interstitial pneumonia (UIP) pattern (20). Management includes drug withdrawal, but in some cases corticosteroid therapy may be helpful. The common examples of drugs associated with a hypersensitivity pneumonitis include nitrofurantoin and methotrexate (21).

2.4. Alveolitis

Most common mechanism of drug-induced alveolitis is allergic reactions. Cyclophosphamide and nitrofurantoin release toxic oxygen species or Acrolein (24). Bleomycin may cause proliferation of fibroblasts and penicillamine may impair collagen formation (25,26). Patients with alveolitis may present with shortness of breath and cough. Chest radiograph shows diffuse patchy infiltration. Drug reaction should be kept in differential diagnosis in all patients presenting with diffuse lung infiltrates. HRCT Chest may reveal early symmetric reticular interstitial markings progressing to fibrotic changes. Pulmonary function tests demonstrate restrictive changes with decreased DLCO and reduced FVC and Total Lung Capacity (TLC). Bleomycin is the most common chemotherapeutic agent, while amiodarone is the most common non-chemotherapeutic agent resulting in alveolitis (27). Phenytoin and carbamazepine are the anticonvulsant drugs that can cause alveolitis. Among cardiac drugs, amiodarone is most frequently associated with alveolitis (28). Amiodarone has a prolonged action and resolution of pulmonary abnormalities occur on withdrawal of drug. Sulfasalazine is the one of the common anti-inflammatory drugs associated with alveolitis (29) and the reaction is due to hypersensitivity to the sulphapyridine moiety (30).

2.5. Drug-induced lupus erythematosus

Drug-induced lupus erythematosus reactions are most commonly due to hydralazine, procainamide, isoniazid, quinidine, phenytoin and penicillamine (4,31-33). Symptoms begin insidiously after taking the drug for many months. Patients may complain of dyspnea, fever, rash, arthralgias, and joint swelling along with systemic symptoms. Pleuritis presenting with pleural effusion is the most common pulmonary manifestation reported in 50-80% of patients. In drug-induced lupus erythematosus, antinuclear antibodies or anti-histone antibodies are positive, while anti-double stranded DNA is negative. Chest radiograph may reveal bilateral infiltrates, pneumonitis, atelectasis and/or pleural effusions. Pleural fluid glucose is usually normal.

The treatment involves discontinuation of the drugs. If the drug is used, use in minimal dose along with corticosteroids.

2.6. Alveolar hemorrhage

Diffuse alveolar hemorrhage is characterized by the accumulation of red blood cells in the alveolar spaces (34). Patients with alveolar hemorrhage present with hemoptysis, dyspnea, anemia and bilateral infiltrates. Drug induced alveolar hemorrhage may represent a hypersensitivity reaction, an injury to the alveolar capillary basement membrane or a coagulation defect. Drugs that may cause coagulation defects are oral anticoagulants, fibrinolytics and platelet glycoprotein inhibitors (35), drugs resulting in hypersensitivity reaction are propylthiouracil, penicillin, sulfasalazine and hydralazine and drugs having direct toxicity are amiodarone, gefitinib, sirolimus and crack cocaine (36-38). Diagnosis requires bronchoscopy in which serial BAL samples reveal increasingly hemorrhagic fluid along with appearance of new infiltrates on chest radiograph. Lung biopsy is rarely required. Withdrawal of the drug or reversal of a coagulation defect is helpful in alveolar hemorrhage.

2.7. Interstitial fibrosis

Inflammation of the lung interstitium is the most common manifestation of DIPPD. Childhood and old age are associated with an increased risk of drug toxicity. Interstitial fibrosis occur when drug reach higher tissue concentrations in the lung by biotransformation process which increases the toxicity by producing reactive metabolites or by consequences of bioactivation which are lung-specific (39). By causing disruption of the oxidant/antioxidant balance, oxygen may precipitate DIPPD (40). Similarly, radiation therapy by synergistic effect with bleomycin can cause lung toxicity. Patients may present with nonproductive cough and dyspnea. HRCT Chest may demonstrate basilar sub-pleural reticular infiltrates; diffuse fibrosis with traction bronchiectasis and honeycombing. Spirometry reveals a restrictive physiology and a reduced DLCO. Lung biopsy demonstrates lymphoid aggregates and plasma cells infiltrating the alveolar septa and the peribronchial spaces. Interstitial fibrosis can also be found (41). In drug-induced NSIP, interstitial inflammation is more homogeneous and cellular than that seen in UIP. This is a progressive disease with poor response to therapy. In acute amiodarone toxicity, mortality may approach 40-50%, despite drug withdrawal and corticosteroid therapy. Drugs causing pulmonary fibrosis are adalimumab, amiodarone, bleomycin, chlorambucil, cyclophosphamide, gold, interferon, infliximab, methotrexate, nitrofurantoin, paclitaxel, penicillamine, phenytoin, sirolimus and statins.

2.8. Eosinophilic lung disease

Pulmonary manifestations of drug induced eosinophilic lung diseases are simple pulmonary eosinophilia, acute eosinophilic pneumonia, chronic eosinophilic pneumonia, Churg-Strauss syndrome and eosinophilic pleural effusion. Drug induced eosinophilic lung disease is a diagnosis of exclusion. Thus, history and physical examination are required for the diagnosis. Laboratory investigation is helpful to exclude other diseases. Blood eosinophil count is frequently elevated. Chest radiograph is often helpful to diagnose other lung diseases that may mimic drug induced lung disease. BAL may demonstrate elevated percentage of eosinophils and lymphocytes (42). Eosinophilic lung disease can be suspected by the finding of an increased number of eosinophils in the blood or BAL fluid of a patient who has pulmonary symptoms or infiltrates on chest radiograph. Lung biopsy is non-specific and rarely required. Symptoms may resolve with discontinuation of the drugs and rarely treatment with corticosteroids is required. Both idiopathic and drug induced acute eosinophilic pneumonia mimic radiologically (43). Minocycline has been reported to cause acute eosinophilic pneumonia (44). Drug induced acute eosinophilic pneumonia recur on re-challenge with offending drug. Churg-Strauss syndrome can be the result of leukotriene inhibitors like zafirlukast and montelukast (45). Whether leukotriene inhibitors cause Churg-Strauss syndrome or their use as a steroid sparing agents in asthmatics allows the development of symptoms of occult Churg-Strauss syndrome is unknown (46). The clinical and radiological presentation of idiopathic and drug induced Churg-Strauss syndrome are similar. Treatment requires long-term corticosteroids and cytotoxic medications.

2.9. Pulmonary edema and acute respiratory distress syndrome

Pulmonary edema and Acute Respiratory Distress Syndrome (ARDS) are common manifestations of drug induced lung disease. Clinical features mimic other causes of pulmonary edema. Clinical features may include dyspnea, tachypnea and hypoxemia. Pathogenesis is unknown for most drugs. Idiosyncratic reaction is most common mechanism followed by capillary leak, anaphylaxis and hypervolemia for drug induced pulmonary edema. Increased permeability leads to protein and fluid to enter the lung interstitium and alveolar spaces. Chest radiograph may show alveolar and interstitial infiltrates. Unlike cardiogenic pulmonary edema, cardiomegaly and vascular redistribution are absent. Diagnosis is based on exclusion of other causes. Most reactions are self-limited. Treatment includes oxygen and diuretic therapy. Corticosteroids role is controversial. Positive pressure ventilation may be

required in severe cases (47). Symptoms may recur on re-challenge.

3. Diagnosis

Establishing a direct relationship between the administration of a drug and the development of lung disease is the first step toward determining drug induced pulmonary parenchymal disease. Drug initiation always precedes clinical symptoms. The time to develop a drug-induced lung parenchymal injury may be quick in the case of bronchospasm, or several years in the case of drug induced pulmonary fibrosis. The diagnostic approach requires review of the patient's presentation and medical history with current and past medication use, including dosages and schedule. There are no definitive symptoms, physical examination, laboratory and radiographic features associated with DIPPD. Acute bronchospasm is characterized by obstructive changes, including a reduced FEV1 and FEV1/ FVC ratio with a significant bronchodilator response. Bronchiolitis obliterans may be suggested by evidence of fixed obstructive lung disease, initially manifested by a reduced FEF1, followed by decreasing FEV25-75 with a low FEV1/ FVC ratio without a bronchodilator response. Pulmonary fibrosis is suggested by a restrictive pattern with a decreased FVC and TLC. Gas exchange is impaired due to ventilation-perfusion mismatching and decreased DLCO due to impaired diffusion across the abnormal interstitium. Arterial blood gas analysis may reveal hypoxemia at rest but should have also arterial oxygen saturation determined during exertion by performing six-minute walk test, because many patients with only mild disease undergo desaturation with exertion despite normal saturation at rest. Complete blood cell count with differential, sputum studies, and serological findings such as rheumatoid factor or anti nuclear antibody and echocardiography are necessary to exclude other causes. Fiberoptic bronchoscopy with BAL may be indicated in case of non-conclusive noninvasive diagnostic measures. BAL findings in drug-induced hypersensitivity pneumonitis include lymphocytosis > 50% and a decreased CD4 to CD8 ratio. Eosinophilic pneumonia is characterized by an elevated BAL eosinophil count > 25% (54). BAL findings in alveolar hemorrhage reveal hemosiderin-laden macrophages and an increasingly bloody return from repeated BAL saline aliquots. BAL fluid often has foamy macrophages in patients taking amiodarone. Cytotoxic pneumonitis due to chemotherapeutic agents generally has a neutrophil predominance. Bronchoscopy with negative culture results helps in ruling out infectious causes. But these findings indicate medication exposure and do not necessarily establish drug toxicity. Sensitivity of open lung or surgical biopsy is not high but can be useful in diagnosing hypersensitivity pneumonitis, bronchiolitis obliterans and organizing pneumonia. They can exclude

the possibility of alternative disease or infection.

4. Management

Management of pulmonary drug reactions consists in stopping the offending drug and substituting with less harmful one. Occasionally, corticosteroid therapy may be used. In BOOP, hypersensitivity pneumonitis and eosinophilic pneumonia, corticosteroids can hasten resolution of symptoms, but in pulmonary fibrosis, pulmonary vascular disease and bronchiolitis obliterans, corticosteroids have no role. If allergy is suspected, a challenge test can be carried out after an interval during which the drug is not taken. Hyposensitization, or induction of tolerance, can be done if the drug is essential, all alternatives are unsatisfactory and the reaction is likely to be allergic or idiosyncratic. Clinicians must educate the patients about the potential adverse effects of the drug before starting treatment. Those who develop drug toxicity should be advised to avoid the drug in the future.

5. Conclusion

Currently there are several drugs that can be recognized as offending agent for DIPPD. At present, there is no consensus for a definite diagnostic workup approach in patients with a suspicion of DIPPD. Although lung biopsies are not pathognomonic for drug toxicity and correlation with clinical, laboratory, and radiologic data is essential, they can be considered as a powerful tool in the evaluation of suspected by helping to exclude underlying disease or infection and documenting the pattern of parenchymal injury. Therefore, it is important for physicians to be familiar with iatrogenic diseases for which their patients are at risk. The information is helpful in making the diagnosis of drug toxicity as well as guiding the optimal management of the patient in near future.

References

1. Sternbach G. William Osler: Narcotic-induced pulmonary edema. *J Emerg Med.* 1983; 1:165-167.
2. Rosenow EC 3rd. Drug-induced pulmonary disease. *Dis Mon.* 1994; 40:253-310.
3. Ozkan M, Dweik RA, Ahmad M. Drug-induced lung disease. *Cleve Clin J Med.* 2001; 68:782-785.
4. Raissy HH, Harkins M, Marshik PL. Drug-induced pulmonary disease. *Pharmacotherapy: A Pathophysiologic Approach.* 7th ed., McGraw-Hill, New York, USA, 2008; pp. 521-534.
5. Decalmer PBS, Chatterjee SS, Cruikshank JM, Benson MK, Sterling GM. Beta-blockers and asthma. *Br Heart J.* 1978; 40:184-189.
6. Fratto C. Provocation of bronchospasm by eye drops. *Ann Intern Med.* 1978; 88:362.
7. Sanak M, Simon HU, Szczeklik A. Leukotriene C4 synthase promoter polymorphism and risk of aspirin-induced asthma. *Lancet.* 1997; 350:1599.
8. Connolly CK. Adverse reaction to ipratropium bromide. *Br Med J.* 1982; 285:934.
9. Gilman AG, Goodman LS, Rall TW, Murad F. *The Pharmacological Basis of Therapeutics.* 7th ed., Macmillan, New York, USA, 1985; p. 507.
10. Coutts II, Dally MB, Newman Taylor AJ. Asthma in workers manufacturing cyclosporins. *Br Med J.* 1981; 283:950.
11. Powell-Jackson PR, Gray BJ, Heaton RW, Costello JF, Williams R, English J. Adverse effect of rifampicin administration on steroid-dependent asthma. *Am Rev Respir Dis.* 1983; 128:307.
12. Dajani BM, Sliman NA, Shubair KS, Hamzeh YS. Bronchospasm caused by intravenous hydrocortisone sodium succinate (Solu-Cortef) in aspirin sensitive subjects. *J Allergy Clin Immunol.* 1984; 68:201.
13. Salpeter S, Ormiston T, Salpeter E. Cardioselective beta-blocker use in patients with reversible airway disease. *Cochrane Database Syst Rev.* 2001; 2:CD002992.
14. Au DH, Bryson CL, Fan VS, Udriș EM, Curtis JR, McDonnell MB, Fihn SD. Beta-blockers as single-agent therapy for hypertension and the risk of mortality among patients with chronic obstructive pulmonary disease. *Am J Med.* 2004; 117:925-931.
15. Babu K, Salvi S. Aspirin and asthma. *Chest.* 2000; 118:1470-1476.
16. Visscher DW, Myers JL. Bronchiolitis: The pathologist's perspective. *Proc Am Thorac Soc.* 2006; 3:41-47.
17. Cordier JF. Organizing pneumonia. *Thorax.* 2000; 55:318-328.
18. Erasmus JJ, McAdams HP, Rossi SE. Drug induced lung injury. *Sem Roentgen.* 2002; 37:72-81.
19. Bourke SJ, Dalphin JC, Boyd G, McSharry C, Baldwin CI, Calvert JE. Hypersensitivity pneumonitis: Current concepts. *Eur Respir J Suppl.* 2001; 32:81S-92S.
20. Silva CI, Churg A, Muller NL. Hypersensitivity pneumonitis: Spectrum of high-resolution CT and pathologic findings. *AJR.* 2007; 188:334-344.
21. Louie S, Lillington GA. Low dose methotrexate pneumonitis in rheumatoid arthritis. *Thorax.* 1986; 41:703-704.
22. Lantuejoul S, Brambilla E, Brambilla C, Devouassoux G. Statin-induced fibrotic nonspecific interstitial pneumonia. *Eur Respir J.* 2002; 19:577-580.
23. Schwaiblmair M, Behr W, Haeckel T, Märkl B, Foerg W, Berghaus T. Drug-induced infiltrative lung disease: *Eur Respir J.* 2001; 18:93s-100s
24. Martin WJ. Nitrofurantoin: Evidence for the oxidant injury of lung parenchymal cells. *Am Rev Respir Dis.* 1983; 127:482.
25. Kelley J, Newman RA, Evans JN. Bleomycin-induced pulmonary fibrosis in the rat. Prevention with an inhibitor of collagen. *J Lab Clin Med.* 1980; 96:954.
26. Nimni ME, Bavetta LA. Collagen defect induced by penicillamine. *Science.* 1965; 150:905.
27. Camus P, Bonniaud P, Fanton A, Camus C, Baudaun N, Foucher P. Drug-induced and iatrogenic infiltrative lung disease. *Clin Chest Med.* 2004; 25:479-519.
28. Roca J, Heras M, Rodriguez-Roisin R, Magrina J, Xaubet A, Sanz G. Pulmonary complications after long-term amiodarone treatment. *Thorax.* 1992; 47:372.
29. Averbuch M, Halpern Z, Hallak A, Topilsky M, Levo Y. Sulfasalazine pneumonitis. *Am J Gastroenterol.* 1985; 80:343.

30. Thomas P, Seaton A, Edwards J. Respiratory disease due to sulphasalazine. *Clin Allergy*. 1974; 4:41.
31. Bhadra K, Suratt B. Drug-induced lung disease: A state-of-the-art review. *J Resp Dis*. 2009; 30:1-17.
32. Foucher P, Biour M, Blayac JP, Godard P, Sgro C, Kuhn M, Vergnon JM, Vervloet D, Pfitzenmeyer P, Ollagnier M, Mayaud C, Camus P. Drugs that may injure the respiratory system. *Eur Respir J*. 1997; 10:265-279.
33. Birnbaum B, Sidhu GS, Smith RL, Pillinger MH, Tagoe CE. Fulminating hydralazine-induced lupus pneumonitis. *Arthritis Rheum*. 2006; 55:501-506.
34. Fontenot AP, Schwarz MI. Diffuse alveolar hemorrhage. *Interstitial Lung Disease*. 2003; 3:632-656.
35. Kalra S, Bell MR, Rihal CS. Alveolar hemorrhage as a complication of treatment with abciximab. *Chest*. 2001; 120:126-131.
36. Vlahakis NE, Rickman OB, Morgenthaler T. Sirolimus-associated diffuse alveolar hemorrhage. *Mayo Clin Proc*. 2004; 79:541-545.
37. Janjua TM, Bohan AE, Wesselius LJ. Increased lower respiratory tract iron concentrations in alkaloidal ("crack") cocaine users. *Chest*. 2001; 119:422-427.
38. Leki R, Saitoh E, Shibuya M. Acute lung injury as a possible adverse drug reaction related to gefitinib. *Eur Respir J*. 2003; 22:179-181.
39. Schwaiblmair M, Berghaus T, Haeckel T, Wagner T, von Scheidt W. Amiodarone induced pulmonary toxicity: An underrecognized and severe adverse effect? *Clin Res Cardiol*. 2010; 99:693-700.
40. Bast A, Weseler A, Haenen G, den Hartog G. Oxidative stress and antioxidants in interstitial lung disease. *Curr Opin Pulm Med*. 2010; 16:516-520.
41. Huggett M, Armstrong R. Adalimumab-associated pulmonary fibrosis. *Rheumatology*. 2006; 45:1312-1313.
42. Akoun GM, Cadranet JL, Milleron BJ, D'Ortho MP, Mayaud CM. Bronchoalveolar lavage cell data in 19 patients with drug associated pneumonitis (except amiodarone). *Chest*. 1991; 99:98-104.
43. Yokoyama A, Mizushima Y, Suzuki H, Arai N, Kitagawa M, Yano S. Acute eosinophilic pneumonia induced by minocycline: Prominent kerley B lines as a feature of positive re-challenge test. *Jpn J Med*. 1990; 29:195-198.
44. Dussopt C, Mornex JF, Cordier JF, Brune J. Acute eosinophilic lung after a course of minocycline. *Rev Mal Respir*. 1994; 11:67-70.
45. Knoell DL, Lucas J, Allen JN. Churg-Strauss syndrome associated with zafirlukast. *Chest*. 1998; 114:332-334.
46. Weller PF, Plaut M, Taggart V, Trontell A. The relationship of asthma therapy and Churg-Strauss syndrome: NIH workshop summary report. *J Allergy Clin Immunol*. 2001; 108:175-183.
47. Reed CR, Glauser FL. Drug-induced non-cardiogenic pulmonary edema. *Chest*. 1991; 100:1120-1124.
48. Gallerani M, Manzoli N, Fellin R, Simonato M, Orzincolo C. Anaphylactic shock and acute pulmonary edema after a single oral dose of acetazolamide. *Am J Emerg Med*. 2002; 20:371-372.
49. Conces DJ, Kreipke DL, Tarver RD. Pulmonary edema induced by intravenous ethchlorvynol. *Am J Emerg Med*. 1986; 4:549-551.
50. Tweeddale MG. Salicylates and pulmonary edema. *Ann Intern Med*. 1974; 81:710-711.
51. Riegert-Johnson DL, Godfrey JA, Myers JL, Hubmayr RD, Sandborn WJ. Delayed hypersensitivity reaction and acute respiratory distress syndrome following infliximab infusion. *Inflamm Bowel Dis*. 2002; 8:186-191.
52. Verhoef G, Boogaerts M. Treatment with granulocyte-macrophage colony stimulating factor and the adult respiratory distress syndrome. *Am J Hematol*. 1991; 36:285-287.
53. Van Mieghem W, Coolen L, Malysse I, Lacquet LM, Deneffe GJ. Amiodarone and the development of ARDS after lung surgery. *Chest*. 1994; 105:1642-1645.
54. Janz DR, O'Neal HR Jr, Ely EW. Acute eosinophilic pneumonia: A case report and review of the literature. *Crit Care Med*. 2009; 37:1470-1474.

(Received July 7, 2014; Revised December 21, 2014; Accepted December 21, 2014)

Several herbal compounds in Okinawa plants directly inhibit the oncogenic/aging kinase PAK1

Binh Cao Quan Nguyen¹, Nozomi Taira¹, Shinkichi Tawata^{2,*}

¹ Department of Bioscience and Biotechnology, The United Graduate School of Agricultural Sciences, Kagoshima University, Kagoshima, Japan;

² Department of Bioscience and Biotechnology, Faculty of Agriculture, University of the Ryukyus, Senbaru 1, Nishihara-cho, Okinawa, Japan.

Summary

The p21-activated kinase 1 (PAK1) is emerging as a promising therapeutic target, and the search for blockers of this oncogenic/aging kinase would be potentially useful for the treatment of various diseases/disorders in the future. Here, we report for the first time the anti-PAK1 activity of compounds derived from three distinct Okinawa plants. 5,6-Dehydrokawain (DK) and dihydro-5,6-dehydrokawain (DDK) from alpinia inhibited directly PAK1 more strongly than mimosine and mimosinol from leucaena. Cucurbitacin I isolated from bitter melon also exhibited a moderate anti-PAK1 activity. Hispidin, a metabolite of DK, strongly inhibited PAK1 with the $IC_{50} = 5.7 \mu M$. The IC_{50} of three hispidin derivatives (H1-3) for PAK1 inhibition ranges from 1.2 to 2.0 μM , while mimosine tetrapeptides [mimosine-Phe-Phe-Tyr (MFFY) and mimosine-Phe-Trp-Tyr (MFWY)] inhibit PAK1 at nanomolar level (IC_{50} of 0.13 and 0.60 μM , respectively). Thus, we hope these derivatives of hispidin and mimosine could be used as potential leading compounds for developing far more potent anti-PAK1 drugs which would be useful for clinical application in the future.

Keywords: p21-activated kinase 1, 5,6-dehydrokawain, dihydro-5,6-dehydrokawain, mimosine, cucurbitacin I

1. Introduction

The family of p21-activated protein kinases (PAKs) belongs to Ras-related C3 botulinum toxin substrate/cell division control protein 42 (RAC/CDC42)-dependent serine/threonine kinases and in mammals consists of six distinct members (PAK1-6) (1). Among them, PAK2 and PAK4 are absolutely essential for the development of embryos (1,2). However, apparently PAK1 is not essential for embryogenesis, and PAK1-deficient mice look perfectly healthy, and are even resistant to inflammatory diseases, and PAK1-deficient mutant of *C. elegans* lives longer than the wild-type (2).

PAK1 is responsible not only for a variety of

inflammatory diseases such as asthma and arthritis, but also for infection of HIV and influenza virus. In addition, PAK1 is essential for the growth of majority of solid tumors as well as their metastasis and angiogenesis (blood vessel formation required for the growth of solid tumors) (1,2). In other words, hyper-activation or over-expression of PAK1 would shorten the healthy lifespan, in part by causing cancers and a variety of other diseases/disorders such as diabetes (type 2), hyper-tension and Alzheimer's disease (2). Since PAK1 is not essential for the growth of normal cells (2), (unlike the conventional anti-cancer drugs) blocking PAK1 *per se* does not cause any side effect. Thus, selective small molecule PAK1-blockers (natural or synthetic) would have a potentially huge market value for the treatment of a variety of PAK1-dependent diseases/disorders and the longevity as well in the future. Furthermore, considering the well-known fact that people in Okinawa have enjoyed the longest healthy lifespan among Asian population, we recently got interested in testing the possibility that foods or

*Address correspondence to:

Dr. Shinkichi Tawata, Department of Bioscience and Biotechnology, Faculty of Agriculture, University of the Ryukyus, Senbaru 1, Nishihara-cho, Okinawa 903-0213, Japan.

E-mail: b986097@agr.u-ryukyuu.ac.jp

herbal products derived from some of plants uniquely grown in Okinawa might contribute to the longevity among Okinawa people by blocking PAK1.

Leucaena leucocephala and *Alpinia zerumbet*, distributed widely in Okinawa in particular and in subtropical and tropical zones in general, have lent them as multi-purpose plants such as the development of novel cosmetics and medicines (3). *Alpinia* is used in folk medicine for its anti-inflammatory, bacteriostatic, and fungistatic properties (4). The essential oil from its leaves possesses relaxant and anti-spasmodic actions in rat ileum (5). Early data have indicated that mimosine, 5,6-dehydrokawain (DK) and dihydro-5,6-dehydrokawain (DDK), which are major ingredients in leucaena and alpinia, are shown to have various biological activities including anti-fungal, anti-inflammatory, anti-tumor and anti-viral (6,7). In our laboratory, we have prepared several compounds from leucaena and alpinia against HIV-1 integrase and neuraminidase enzymes (7), for inhibition of advanced glycation end products and for prevention of the skin diseases (8,9). Bitter gourd (*Momordica charantia*), known as "goya" in Japan, has been implicated in different pharmacological activities such as anti-

diabetic, anti-bacterial, anti-viral, anti-cancer, and anti-obesity (10). In spite of given diverse biological activities, their anti-PAK1 activity still remained unknown. In this study, we first focused primarily on the potential anti-PAK1 activity of compounds isolated from alpinia, leucaena, and bitter gourd. We then prepared several derivatives from these natural compounds for further potentiation of their anti-PAK1 activity (Figure 1). To the best of our knowledge, this is the very first report showing the direct inhibition of PAK1 by compounds derived from these three Okinawa plants.

2. Materials and Methods

2.1. Chemicals and reagents

Tris(triethylsilyl)silane, resveratrol were obtained from Sigma-Aldrich (Shinagawa-ku, Tokyo, Japan) whereas trifluoromethanesulfonic acid was obtained from Nacalai Tesque (Nakagyo-ku, Kyoto, Japan). Curcumin was purchased from Kanto Chemical Co. (Chuo-ku, Tokyo, Japan). Fmoc-L-amino acids were purchased from Hipep Laboratories (Kamigyo-ku, Kyoto, Japan).

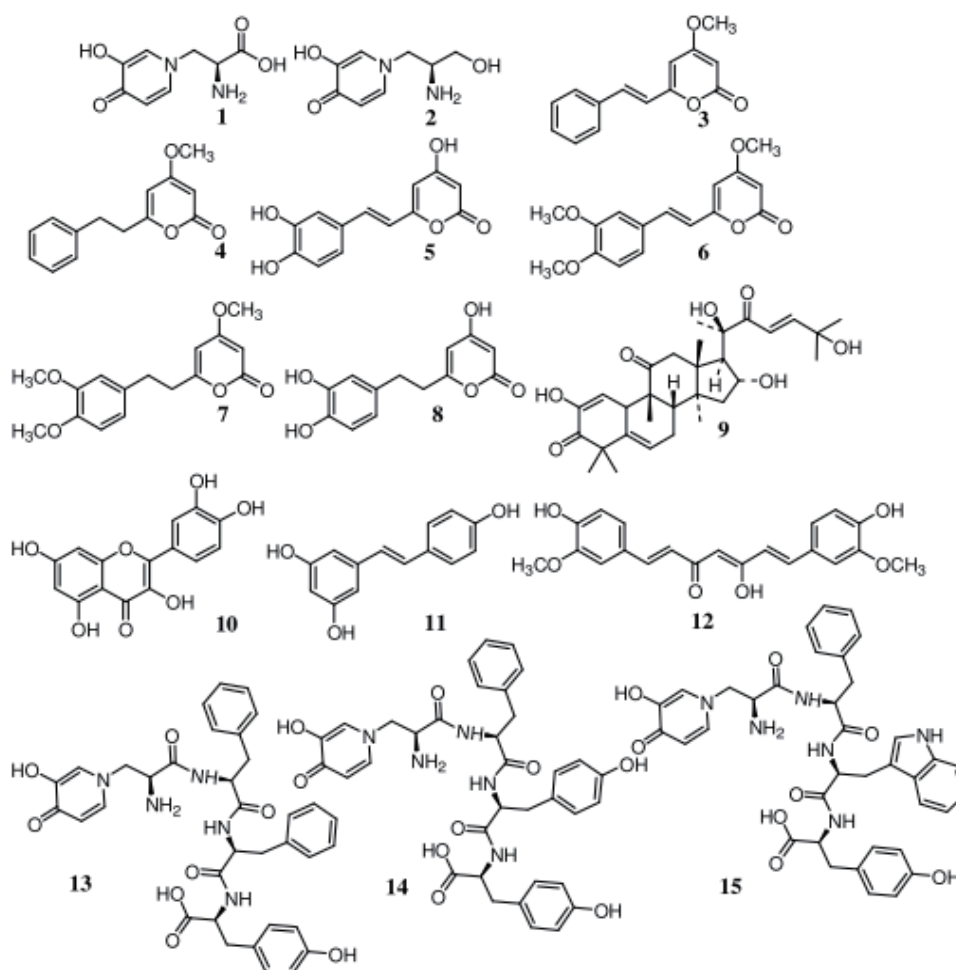


Figure 1. Chemical structures of compounds. Mimosine (1), mimosinol (2), DK (3), DDK (4), hispidin (5), H1 (6), H2 (7), H3 (8), cucurbitacin I (9), quercetin (10), resveratrol (11), curcumin (12), MFFY (13), MFYY (14), MFWY (15).

2-[1H-benzotriazole-1-yl]-1,1,3,3-tetramethyluronium hexafluorophosphate (HBTU) were from Novabiochem (Schuchardt, Hohenbrunn, Germany). Quercetin, wang resin (1% DVB), N,N'-diisopropylcarbodiimide (DIC), N,N'-diisopropylethylamine (DIEA), and 1-hydroxy-1H-benzotriazole (HOBt) were purchased from Wako Pure Chemical Industries (Chuo-ku, Osaka, Japan). Unless otherwise mentioned, all reagents were of analytical grade and were obtained from Wako Pure Chemical Industries and Kanto Chemical Co. The ^1H spectra were recorded on a JEOL JNM-ECA400 (Tokyo, Japan). Chemical shifts are expressed in parts per million (δ) relative to tetramethylsilane (TMS).

2.2. Mimosine isolation from *Leucaena leucocephala* leaves

Samples of *Leucaena leucocephala* leaves were collected at the Faculty of Agriculture, University of the Ryukyus, Okinawa, Japan (lat 26°N, long 127°E). Fresh leaves (1.5 kg) were boiled in 5 L water for 10 min. The cooled liquid extract was sieved by suction filtration in a shaking bath (As One, Nishi-ku, Osaka, Japan) and the filtrate was mixed with ion-exchange resin (2 kg), stirred for 30 min, and left overnight. The resin was rinsed with distilled water 5-6 times and 5 L 80% ethanol was added dropwise to remove chlorophyll. Mimosine was dissolved from the resin with dropwise addition of 6 L of 2 N NH_4OH . The liquid extract was concentrated to a final volume of 300 mL at 40°C under reduced pressure. The solution was adjusted to pH 4.5-5.0 with 6 N HCl and mimosine was precipitated at 4°C overnight. The precipitate was recrystallized from

5 N NaOH (pH 9.0) and 6 N HCl (pH 4.5-5.0) and then allowed to stand at 4°C to give pure mimosine. Mimosine was stored at -20°C until further use (11).

2.3. Preparation of mimosinol from mimosine

Trifluoromethanesulfonic acid (187 μL , 2 mmol) was added to a 25-mL round-bottom flask containing 3.4 mL dichloromethane (CH_2Cl_2). After stirring at room temperature, tris(triethylsilyl)silane solution (618 μL , 2 mmol) was added dropwise and the mixture was stirred at room temperature for 3 h until the solution become clear. Mimosine (0.4 g, 2 mmol) was placed in a round-bottom flask, to which imidazole (0.15 g, 2.2 mmol) and dimethylformamide (DMF): CH_2Cl_2 (3.4 mL, 1:1) were then added. The reaction flask was cooled to 0°C and tris(triethylsilyl)silyl triflate was added dropwise. After the addition was completed, the reaction was stirred at room temperature for 2 h. Mimosine ester was obtained from the filtrate by evaporation. A solution of sodium borohydride (0.28 g, 7.2 mmol) in 3 mL 50% ethanol was added to solution of mimosine ester in 3 mL of 50% ethanol. The resulting mixture was refluxed at room temperature for 5.5 h and the solvent ethanol was evaporated in vacuo. The aqueous solution thus obtained was extracted with ethyl acetate (3×20 mL); the combined extracts were washed with saturated sodium chloride, dried over anhydrous sodium sulfate, and evaporated to give mimosinol as a colorless crystal (352 mg, 95% yield) (Figure 2). ^1H NMR (D_2O , 400 MHz) δ 7.93 (s, 1H, CH), 7.28 (s, 1H, CH), 3.02-2.86 (d, 2H, CH), 2.08-1.91 (s, 2H, CH_2), 1.58-1.54 (m, 2H, CH_2), 1.22-1.11 (m, 1H, CH).

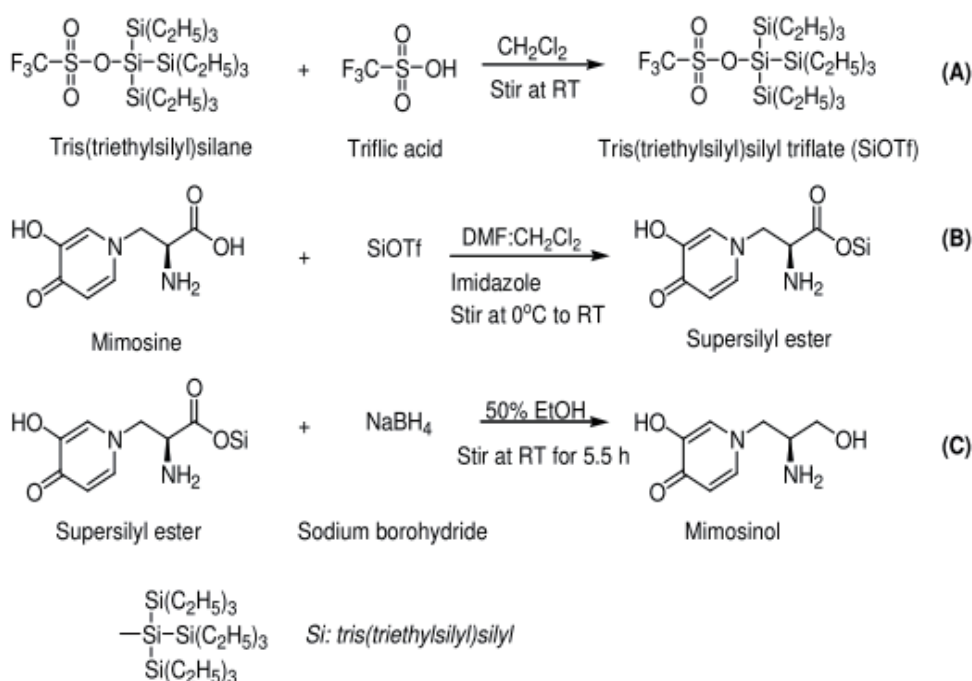


Figure 2. Route for reduction of mimosine to mimosinol. (A) *In situ* generation of tris(triethylsilyl)silyl triflate, (B) Installation of tris(triethylsilyl)silyl group into mimosine, (C) Reduction of mimosine ester to mimosinol using sodium borohydride.

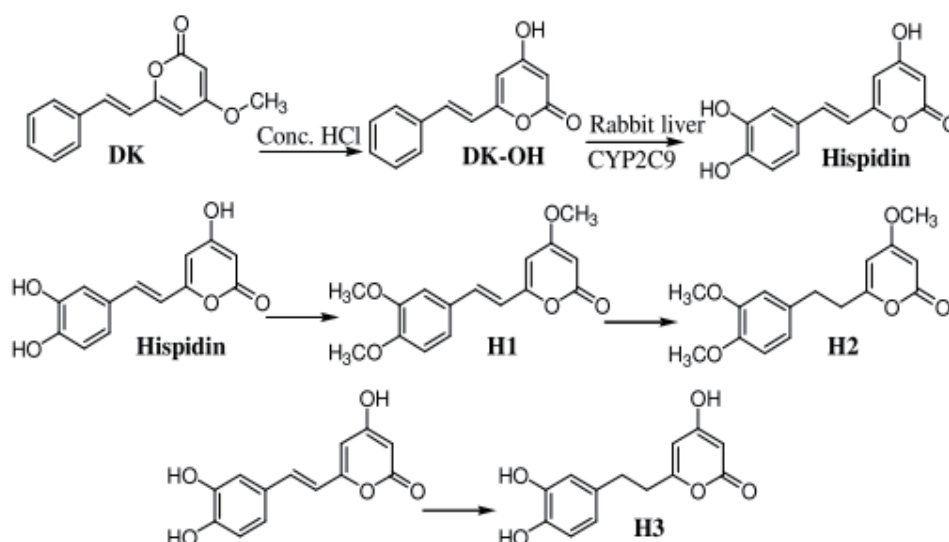


Figure 3. Preparation of hispidin and their derivatives. Bioconversion of 5,6-dehydrokawain (DK) to hispidin by CYP2C9 in the microsomes of rabbit liver. Hispidin derivatives (H1-3) were prepared from hispidin.

2.4. Synthesis of mimosine tetrapeptides

Compounds were prepared according to procedure described previously (12). In brief, Fmoc-L-amino acid (1.6 mmol) was dissolved in 5 mL of dimethylacetamide, followed by adding HOBt (1.6 mmol) and DIC (1.6 mmol). The mixture was added to swollen Wang resin (1 g) in DMF and stirred for 17 h. After deprotection of 9-fluorenylmethoxycarbonyl (Fmoc) with 25% piperidine, the next amino acids were coupled to the resin mixture solution (Fmoc-amino acid/HOBt/HBTU/DIEA = 4:3:3.6:8) and stirred for 1 h to form tripeptides. The Kaiser's test was used to assess the completeness of the coupling reaction. After final coupling with mimosine, the final cleavage was performed by shaking the resin vigorously in 95% trifluoroacetic acid (TFA) for 1 h. The resin was filtered and washed with TFA. The obtained filtrate was precipitated with ice-cold diethyl ether. The resulting precipitate was filtered, washed with diethyl ether, and dried under a vacuum to obtain the desired mimosine tetrapeptides. The purified compounds were evaluated using LC-MS (ESI): m/z $[M-H]^+$ 693.2, 670.1, 654.2 for MFWY, MFYY, and MFFY, respectively.

2.5. Isolation of DDK and DK compounds from *Alpinia zerumbet*

The rhizomes of *alpinia* were collected from the University of the Ryukyus campus, Okinawa, Japan. The rhizomes (2 kg) were boiled in 10 L water for 20 min. The solution was cooled at room temperature and sieved by suction filtration (As One, Nishi-ku, Osaka, Japan). The filtrate was reduced to 1 L under vacuum at 40°C, and extracted with hexane (3 × 500 mL). The organic layer was evaporated to complete dryness under

vacuum. The dried crude extract was boiled in water and filtered hot. The residue obtained was purified by high-performance liquid chromatography (HPLC) (Shimadzu, Nakagyo-ku, Kyoto, Japan) to give DK. The filtrate was crystallized at 4°C, and the crystals were purified further using HPLC to obtain DDK. For purification of DDK and DK, the major peaks were collected using mobile phase including solvent A (0.1% acetic acid in water) and solvent B (0.1% acetic acid in methanol). The gradient elution was performed as follows: 1-10 min, isocratic 50% B; 10-20 min, linear gradient 50-100% B; 20-30 min, isocratic 100% B; 30-35 min, linear gradient 100-50% B. The flow rate and absorbance wavelength were set at 0.8 mL/min and 280 nm, respectively (7).

2.6. Preparation of hispidin and cucurbitacin I compounds

These two compounds were prepared by other group in our laboratory. DK was converted to hispidin by cytochrome P450 2C9 enzyme (CYP2C9) in the microsomes of rabbit liver (Figure 3) (13). Cucurbitacin I was isolated from Okinawa bitter gourd (*Momordica charantia*) fruits.

2.7. Preparation of hispidin derivatives (H1-3)

Hispidin (3 mg) was dissolved in 0.6 mL methanol:CH₂Cl₂ (1:5). The solution was cooled to 0°C, and 0.5 mL of diazomethane in CH₂Cl₂ was added. The mixture was stored overnight at 4°C. Solvents were evaporated, and the residue was purified by silica gel preparative thin layer chromatography (PTLC) to obtain H1 as pale yellow powder (2 mg, 67% yield) (14). Compound H1 (3.5 mg) dissolved in 0.82 mL of MeOH:CHCl₃ (1:1) was stirred for 2 h in the presence

of 10% of Pd/C (0.65 mg). The mixture was filtered and solvent was evaporated in vacuo. Purification was achieved by column chromatography to afford compound H2 as a white solid (3 mg, 85%) (15). The similar procedure was used to prepare H3 from hispidin.

Data for 6-(3,4-dimethoxystyryl)-4-methoxy-2H-pyran-2-one (H1). ¹H NMR (CDCl₃, 400 MHz) δ 7.43 (d, 1H, CH), 7.07 (dd, 1H, CH), 7.00 (d, 1H, CH), 6.85 (d, 1H, CH), 6.43 (d, 1H, CH), 5.89 (d, 1H, CH), 5.46 (d, 1H, CH), 3.91 (s, 3H, OCH₃), 3.89 (s, 3H, OCH₃), 3.81 (s, 3H, OCH₃).

Data for 6-(3,4-dimethoxyphenethyl)-4-methoxy-2H-pyran-2-one (H2). ¹H NMR (CDCl₃, 400 MHz) δ 6.77 (d, 1H, CH), 6.69 (dd, 1H, CH), 6.66 (d, 1H, CH), 5.69 (d, 1H, CH), 5.40 (d, 1H, CH), 3.84 (s, 3H, OCH₃), 3.83 (s, 3H, OCH₃), 3.76 (s, 3H, OCH₃), 2.91 (m, 2H, CH₂), 2.71 (m, 2H, CH₂).

Data for 6-(3,4-dihydroxyphenethyl)-4-hydroxy-2H-pyran-2-one (H3). ¹H NMR (DMSO, 400 MHz) δ 7.29 (d, 1H, CH), 7.20 (dd, 1H, CH), 6.76 (d, 1H, CH), 6.11 (d, 1H, CH), 5.26 (d, 1H, CH), 3.34 (m, 2H, CH₂), 2.99 (m, 2H, CH₂).

2.8. In vitro assay for the kinase PAK1

Its kinase activity was measured by ADP-Glo™ kinase assay kit (Promega, Madison, WI, USA) according to manufacturer's instructions. Human PAK1 (10 μ L) at 25 ng/reaction concentration was incubated with 5 μ L of test compounds at various concentrations for 10 min. The kinase reaction was started by the addition of 2.5 X adenosine triphosphate (ATP)/substrate mix (10 μ L) which was incubated for 40 min. The reaction was terminated by 25 μ L ADP-Glo™ reagent, followed by 40 min incubation. To this reaction mixture was added 50 μ L of the kinase detection reagent which converts adenosine diphosphate (ADP) to ATP that eventually generates a luciferin/luciferase-based fluorescence. After 30 min incubation, luminescence was recorded by MTP-880Lab microplate reader (Corona, Hitachinaku, Ibaraki Japan) with an integration time of 0.5 s per well. Blank wells lacked the test compounds and PAK1 but did include all remaining components. All procedure steps were conducted at room temperature. The percentage inhibition was calculated relative to the control kinase activity without any inhibitor.

3. Results and Discussion

In previous study, we discovered that DK and DDK from alpinia rhizomes as well as mimosine from leucaena leaves are strong inhibitors of HIV-1 integrase and neuraminidase activity (7,12). Interestingly, PAK1 is essential for the replication of several viruses including HIV and influenza virus (2). In this study we found that DK, DDK and mimosine compounds inhibited directly

Table 1. Anti-PAK1 activity of herbal compounds and their derivatives

compound	IC ₅₀ (μ M) for PAK1 inhibition
mimosine	37
mimosinol	30
MFFY	0.13
MFYY	2.3
MFWY	0.60
DK	17.1
DDK	10.3
hispidin	5.7
H1	1.6
H2	1.2
H3	2.0
cucurbitacin I	19
quercetin	340
resveratrol	15
curcumin	7.0

The IC₅₀ values were determined graphically as the concentration of each compound that showed 50% inhibitory activity. M: mimosine, F: phenylalanine, W: tryptophan, Y: tyrosine.

the kinase activity of PAK1. As summarized in Table 1, the anti-PAK1 activity of DK and DDK is significantly better than mimosine and mimosinol. The IC₅₀ values of DK and DDK are 17 and 10 μ M, respectively, while mimosine and mimosinol had the IC₅₀ values of 37 and 30 μ M, respectively. Furthermore, a metabolite of DK called hispidin had a strong anti-PAK1 activity (IC₅₀ = 5.7 μ M), almost equivalent to curcumin (IC₅₀ = 7.0 μ M), but clearly stronger than resveratrol (IC₅₀ = 15 μ M). Considering that one of the benzene rings in resveratrol is simply replaced by an α -pyrone ring in hispidin, it is likely that α -pyrone significantly contributes to an increase in the anti-PAK1 activity. However, Upadhyay *et al.* (7) suggested that the methoxy group at C-5 of DDK and DK could be the major contributor to their anti-HIV activity. Thus, perhaps this methoxy group of DK and DDK could also be attributed to their anti-PAK1 activity, in addition to the α -pyrone ring. In comparison of the anti-PAK1 activity between DK and hispidin, *in vivo* DK could act as a PAK1 inhibitor in two ways, first as DK itself and second after it is converted to hispidin by the enzyme CYP2C9. The anti-PAK1 activity of DK is significantly weaker than its metabolite "hispidin". Thus, it is most likely that the attachment of two OH groups to the benzene ring of DK or DDK contributes to an increase in the anti-PAK1 activity. We further prepared a few hispidin derivatives in an attempt to potentiate their anti-PAK1 activity. As shown in Table 1, the two methoxy derivatives (H1-2) inhibited PAK1 more strongly than hispidin, with the IC₅₀ values ranging from 1.2 to 1.6 μ M.

The anti-PAK1 activity of a few mimosine tetrapeptides was also evaluated. Interestingly, at least two of these peptides inhibited PAK1 at nanomolar level. MFFY and MFWY (IC₅₀ = 0.13 and 0.60 μ M, respectively) were more potent than MFYY (IC₅₀ = 2.3 μ M).

Cucurbitacins, a family of tetracyclic triterpenes, are used in folk and traditional medicine which have selective biological properties against carcinogenesis. Recently, it has been suggested as anti-inflammatory and anti-cancer agents (16). Cucurbitacin I is a triterpenoid compound bearing diverse physiological actions such as inducing apoptosis, blocking cell cycle, inhibiting tyrosine kinase JAK2 (17). Since JAK2 is responsible for the activation of PAK1, this triterpenoid could block PAK1 at least indirectly in cells (18). By isolating cucurbitacin I from bitter melon, we showed for the first time that in fact this compound directly inhibited PAK1 with the IC_{50} of 19 μ M.

By the simple method used in our laboratory, these pyrones (DK, DDK) as well as mimosine and mimosinol can be prepared easily from alpinia and leucaena. Moreover, the synthesis of their derivatives is not costly; thus, in theory, their further chemical modification for creating more potent PAK1-inhibitors could be economically feasible.

In conclusion, we showed for the first time that compounds prepared from alpinia, leucaena and bitter melon directly inhibit PAK1. Although these herbal compounds *per se* are not potent PAK1 inhibitors in comparison with curcumin, we managed to potentiate significantly their anti-PAK1 activity by specific chemical modification. For an instance, the mimosine tetrapeptide MFFY inhibits PAK1 with the IC_{50} around 100 nM. So far the most potent PAK1-specific inhibitors are FRAX486 and FRAX597 with the IC_{50} around 10 nM, although both their cell-permeability and water-solubility/bioavailability are rather poor (19). Thus, we hope that the "MFFY" in particular could serve as the first leading compounds for the development of far more potent and water-soluble anti-PAK1 derivatives which would be useful for clinical application in the future. Furthermore, we are currently measuring their anti-protein kinase B (AKT) activity, to make it sure that they would not cause any side effect *in vivo*, as unlike PAK1, the oncogenic kinase AKT is known to be required for the growth of normal cells, in particular heart development as well. AKT-deficient mice are embryonically lethal, mainly due to the heart failure (2).

Acknowledgements

We express sincere thanks to Dr. Masakazu Fukuta, University of the Ryukyus, Okinawa, Japan, for manuscript revision and his useful comments and suggestions.

References

1. Dummler B, Ohshiro K, Kumar R, Field J. Pak protein kinases and their role in cancer. *Cancer Metastasis Rev.* 2009; 28:51-63.
2. Maruta H. Herbal therapeutics that block the oncogenic

- kinase PAK1: A practical approach towards PAK1-dependent diseases and longevity. *Phytother Res.* 2014; 28:656-672.
3. Tawata S, Fukuta M, Xuan TD, Deba F. Total utilization of tropical plants *Leucaena leucocephala* and *Alpinia zerumbet*. *J Pestic Sci.* 2008; 33:40-43.
4. Zoghbi MGB, Andrade EHA, Maia JGS. Volatile constituents from leaves and flowers of *Alpinia speciosa* K. Schum. and *A. purpurata* (Viell.) Schum. *Flavour Fragr J.* 1999; 14:411-414.
5. Bezerra MAC, Leal-Cardoso JH, Coelho-de-Souza AN, Criddle DN, Fonteles MC. Myorelaxant and antispasmodic effects of the essential oil of *Alpinia speciosa* on rat ileum. *Phytother Res.* 2000; 14:549-551.
6. Corbi PP, Massabni AC, Costa-Neto CM. Synthesis and characterization of a new platinum (II) complex with L-mimosine. *J Coord Chem.* 2005; 58:1477-1483.
7. Upadhyay A, Chompoo J, Kishimoto W, Makise T, Tawata S. HIV-1 integrase and neuraminidase inhibitors from *Alpinia zerumbet*. *J Agric Food Chem.* 2011; 59:2857-2862.
8. Chompoo J, Upadhyay A, Kishimoto W, Makise T, Tawata S. Advanced glycation end products inhibitors from *Alpinia zerumbet* rhizomes. *Food Chem.* 2011; 129:709-715.
9. Chompoo J, Upadhyay A, Fukuta M, Tawata S. Effect of *Alpinia zerumbet* components on antioxidant and skin diseases-related enzymes. *BMC Complementary Altern Med.* 2012; 12:1-9.
10. Hsu C, Hsieh CL, Kuo YH, Huang CJ. Isolation and identification of cucurbitane-type triterpenoids with partial agonist/antagonist potential for estrogen receptors from *Momordica charantia*. *J Agric Food Chem.* 2011; 59:4553-4561.
11. Tawata S. Effective reduction and extraction of mimosine from *L. leucocephala* and the potential for its use as a lead compound of herbicides. In: *Pesticide and Alternatives* (Casida JE, ed.). Elsevier Science Publishers, Amsterdam, Netherlands, 1990; pp. 541-544.
12. Upadhyay A, Chompoo J, Taira N, Fukuta M, Gima S, Tawata S. Solid-phase synthesis of mimosine tetrapeptides and their inhibitory activities on neuraminidase and tyrosinase. *J Agric Food Chem.* 2011; 59:12858-12863.
13. Upadhyay A, Uezato Y, Tawata S, Ohkawa H. CYP2C9 catalyzed bioconversion of secondary metabolites of three Okinawan plants. In: *Proceedings of 16th International Conference on Cytochrome P450* (Shoun H, Ohkawa H, eds.). Nago, Okinawa, Japan, 2009; pp. 31-34.
14. Singh SB, Jayasuriya H, Dewey R, Polishook JD, Dombrowski AW, Zink DL, Guan Z, Collado J, Platas G, Pelaez F, Felock PJ, Hazuda DJ. Isolation, structure, and HIV-1-integrase inhibitory activity of structurally diverse fungal metabolites. *J Ind Microbiol Biotechnol.* 2003; 30:721-731.
15. McCracken ST, Kaiser M, Boshoff HI, Boyd PDW, Copp BR. Synthesis and antimalarial and antituberculosis activities of a series of natural and unnatural 4-methoxy-6-styryl-pyran-2-ones, dihydro analogues and photodimers. *Bioorg Med Chem.* 2012; 20:1482-1493.
16. Hsu YC, Chen MJ, Huang TY. Inducement of mitosis delay by cucurbitacin E, a novel tetracyclic triterpene from climbing stem of *Cucumis melo* L., through GADD45 γ in human brain malignant glioma (GBM)

- 8401 cells. *Cell Death Dis.* 2014; 5:1-9.
17. Shi X, Franko B, Frantz C, Amin HM, Lai R. JSI-124 (cucurbitacin I) inhibits Janus kinase-3/signal transducer and activator of transcription-3 signalling, downregulates nucleophosmin-anaplastic lymphoma kinase (ALK), and induces apoptosis in ALK-positive anaplastic large cell lymphoma cells. *Br J Haematol.* 2006; 135:26-32.
18. Rider L, Shatrova A, Feener EP, Webb L, Diakonova M. JAK2 tyrosine kinase phosphorylates PAK1 and regulates PAK1 activity and functions. *J Biol Chem.* 2007; 282:30985-30996.
19. Dolan BM, Duron SG, Campbell DA, Vollrath B, Rao BSS, Ko HY, Lin GG, Govindarajan A, Choi SY, Tonegawa S. Rescue of fragile X syndrome phenotypes in *Fmr1* KO mice by the small-molecule PAK inhibitor FRAX486. *Proc Natl Acad Sci USA.* 2013; 110:5671-5676.
- (Received December 14, 2014; Revised December 18, 2014; Accepted December 21, 2014)*

Clinical features of 80 cases of tinea faciei treated at a rural clinic in Japan

Hiromitsu Noguchi^{1,3,*} Masatoshi Jinnin², Keishi Miyata³, Masataro Hiruma⁴, Hironobu Ihn²

¹Noguchi Dermatology Clinic, Kumamoto, Japan;

²Department of Dermatology and Plastic Surgery, Kumamoto University, Kumamoto, Japan;

³Department of Immunology, Allergy & Vascular Biology, Kumamoto University, Kumamoto, Japan;

⁴Ochanomizu Institute for Medical Mycology and Allergology, Tokyo, Japan.

Summary

From March 2008 through February 2014, 80 patients aged 1-95 years (43 men and 37 women) were diagnosed with tinea faciei by a rural Japanese clinic. The affected sites were the cheek in 42 patients (52.5%), the auricles and area surrounding the auricles in 16 (20.0%), and the mandible in 12 (15.0%); 33 patients (41.2%) had concurrent ringworm in areas other than the face. Twenty-one patients (26.3%) had applied topical steroids to treat a rash. The pathogen responsible for tinea faciei was *Trichophyton rubrum* in 35 patients (43.7%), *T. tonsurans* in 19 (23.8%), *T. mentagrophytes* in 3 (3.8%), *T. verrucosum* in 2 (2.5%), *T. violaceum* in 2 (2.5%), *Microsporum canis* in 17 (21.3%), and *M. gypseum* in 2 (2.5%). Clinical symptoms were divided into three groups based on the severity of inflammation and the extent of lesions and scored in points. Anthropophilic dermatophytes resulted in a score of 1.82 points for the severity of inflammation and a score of 1.84 points for the extent of lesions while zoophilic dermatophytes resulted in a score of 2.14 points for the severity of inflammation and a score of 1.50 points for the extent of lesions. This indicates that anthropophilic fungi resulted in less inflammation and broader lesions, whereas zoophilic fungi resulted in more intense inflammation and smaller lesions. Patients who had applied topical steroids had a mean score of 1.90 points for the severity of inflammation and a mean score of 2.10 points for the extent of lesions. Patients who had not applied topical steroids had a mean score of 1.95 points for the severity of inflammation and a mean score of 1.59 points for the extent of lesions. The severity of inflammation did not differ significantly. However, lesions were significantly broader in patients who had applied topical steroids than in those who had not applied topical steroids ($p < 0.04$). The severity of tinea faciei is a useful index for the clinical diagnosis of tinea faciei.

Keywords: Clinical features, dermatophytes, dermatophytosis, ringworm, tinea faciei

1. Introduction

Tinea faciei is a rare dermatophyte infection occurring in the glabrous skin of the face, excluding the moustache and beard areas in men (1). Although ringworm of the face is classified as tinea corporis in Japan, it is often called tinea faciei (1,2). Tinea faciei is often difficult to diagnose because of the severe

inflammatory lesions caused by zoophilic fungi and an atypical clinical appearance as a result of topical steroid use (1). Eighty cases of tinea faciei were encountered over the last 6 years at a rural Japanese clinic. Here, the clinical features of these cases have been evaluated by scoring the severity of inflammation and the extent of lesions.

2. Materials and Methods

Eighty patients with tinea faciei were seen by this clinic from March 2008 through February 2014. Tinea faciei was diagnosed by direct microscopic examination using Parker ink KOH staining. Pathogens were identified

*Address correspondence to:

Dr. Hiromitsu Noguchi, Noguchi Dermatology Clinic, 1834-1 Namazu, Kashima-machi, Kamimashiki-gun, Kumamoto 861-3101, Japan.

E-mail: derma@nogcli.jp

by fungal cultures. During the period studied, 10,575 patients with dermatophytosis were seen, accounting for 8.7% of 121,038 outpatients (new patients). Eighty-five patients with tinea faciei accounted for 0.80% of all patients with tinea; the pathogens responsible for that tinea were identified in 80 patients (94.1%).

Specimens were cultured in Sabouraud's cycloheximide chloramphenicol agar at 25°C, and pathogens were identified based on mycological findings. A hairbrush culture (96 spikes) was performed in cases where concurrent tinea capitis was suspected (3).

Clinical symptoms were divided into three groups based on the severity of inflammation and the extent of lesions and these symptoms were scored in points. The severity of inflammation was determined as follows: scaly plaque-like lesions with mild inflammation, 1 point; typical "ringworm" lesions with an annular appearance, 2 points; and vesicular or exudative lesions with intense inflammation, 3 points. The extent of lesions was determined as follows: lesions < 3 cm in diameter, 1 point; lesions 3-6 cm in diameter, 2 points; and lesions > 6 cm in diameter, 3 points. The Kruskal-Wallis and

Mann-Whitney tests were used for statistical processing and a $p < 0.05$ was considered to represent a significant difference.

Patients with multiple lesions or tinea capitis were also given oral terbinafine hydrochloride or itraconazole. Patients with tinea unguium or tinea capitis caused by *Trichophyton tonsurans* received pulsed treatment in 4-week cycles. One cycle consisted of oral medication given for 1 week followed by a 3-week respite. Topical medication was applied until the end of treatment. Therefore, the duration of topical application was the same as the treatment period.

3. Results and Discussion

Patients were 43 men and 37 women aged 1-95 years (mean: 42.8 ± 27.7 years). Of the patients, 31 (38.8%) were < 19 years of age, 21 (26.3%) were 20-59 years of age, and 28 (35.0%) were ≥ 60 years of age. The affected sites were the cheeks in 42 patients (52.5%), the auricles and area surrounding the auricles in 16 (20.0%), and the mandible in 12 (15.0%). Thirty-three



Figure 1. Case 1. The patient had applied a topical steroid to treat a rash. The pathogen responsible for tinea faciei was *Trichophyton rubrum*. Erythematous plaque provided evidence to rule out discoid lupus erythematosus. The severity of inflammation was 1 point, and the extent of the lesion was 2 points.



Figure 2. Case 2. The patient was a 14-year-old judo practitioner. The pathogen responsible for tinea faciei was *Trichophyton tonsurans*. The patient had scaling erythema with infiltration on his left cheek. The severity of inflammation was 3 points, and the extent of the lesion was 1 point.

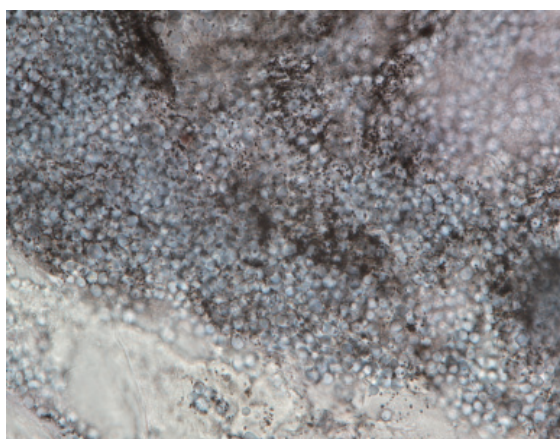


Figure 3. Direct microscopic examination revealed endothrix infection with chains of conidia in and around the hair.

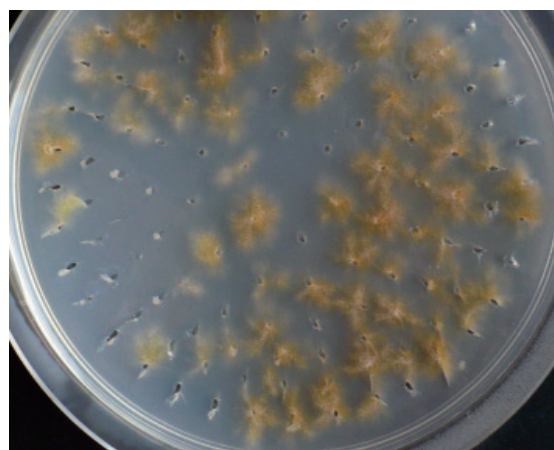


Figure 4. A sample, obtained with a circular hairbrush, was cultured and produced brownish-yellow colonies with powdery surfaces.

Table 1. Clinical Features of Tinea Faciei by Pathogen

Theme	Case	Male/female	Age	Concurrent other type of tinea	Hairbrush test positive	Steroid-modified	Inflammation (score)	Extent (score)	Internal dosing (wks)	Topical application (wks)	Recurrent case
Anthropophilic	56	40/16	42.4	19	10	13	1.82	1.84	2.9	4.9	5
<i>T. rubrum</i>	35	22/13	59.3	16	1	13	1.74	2.29*	2.4	5.3	4
<i>T. tonsurans</i>	19	18/1	15.3	7	8	0	1.95	1.11*	3.9	3.9	1
<i>T. violaceum</i>	2	0/2	3.5	0	1	0	2.00	1.00	2.0	6.5	0
Zoophilic	22	2/20	41.8	8	4	7	2.14	1.50	2.1	5.0	2
<i>T. mentagrophytes</i>	3	1/2	25.0	0	0	1	2.33	1.67	0.7	5.0	0
<i>T. verrucosum</i>	2	0/2	29.5	0	0	1	2.00	1.00	0.5	5.5	0
<i>M. canis</i>	17	1/16	46.1	8	4	5	2.12	1.53*	2.5	4.9	2
Geophilic											
<i>M. gypseum</i>	2	0/2	66.5	0	0	1	3.00	1.00	5.0	6.0	0
Steroid-modified case	21	9/12	54.0	8	3	–	1.90	2.10**	3.4	6.0	1
Non-modified case	59	34/25	38.8	25	11	–	1.95	1.59**	2.5	4.6	6
Total or mean	80	43/37	42.8	33	14	21	1.94	1.73	2.8	4.9	7

* $p < 0.001$ compared with 3 groups; ** $p < 0.05$ compared with 2 groups.

patients (41.2%) had concurrent ringworm in areas other than the face, and 14 (17.5%) had a hairbrush culture that tested positive for a pathogen. Twenty-one patients (26.3%) had applied topical steroids to treat a rash. The pathogen responsible for tinea faciei was *Trichophyton rubrum* in 35 patients (43.7%), *T. tonsurans* in 19 (23.8%), *T. mentagrophytes* in 3 (3.8%), *T. verrucosum* in 2 (2.5%), *T. violaceum* in 2 (2.5%), *Microsporum canis* in 17 (21.3%), and *M. gypseum* in 2 (2.5%). In all three patients with *T. mentagrophytes*, the teleomorph *Arthroderma vanbreuseghemii* was molecularly identified. Pathogens responsible for tinea faciei vary; the primary pathogens are reported to be *T. tonsurans* in the United States (4), *M. canis* in Italy (5), and *T. verrucosum* in Macedonia (6). The primary pathogen responsible for tinea faciei in Japan is *T. rubrum*, but seven species of pathogens were identified in the current study. Tinea faciei is easily misdiagnosed because of its various clinical symptoms. Tinea must be differentiated from other diseases including discoid lupus erythematosus (DLE), polymorphous light eruption, psoriasis, impetigo, rosacea, and seborrheic dermatitis (1). Thirty-three patients (41.2%) had typical annular lesions, resulting in a score of 2 points for the severity of inflammation, whereas most patients (58.7%) had atypical lesions, resulting in a score of 1 point and 3 points.

Two typical cases will now be presented. The disease in Case 1 was difficult to diagnose since the disease's clinical appearance had been modified by topical steroid use, while the disease in Case 2 should be considered an emerging infectious disease in Japan. Case 1 involved a 64-year-old woman who had applied topical steroids to treat a rash. The pathogen responsible for tinea faciei was *T. rubrum*. The patient had erythematous plaque from her nose to her left cheek (Figure 1). The clinical appearance ruled out DLE. The severity of inflammation was 1 point, and the extent of the lesion was 2 points. Case 2 involved

a 14-year-old judo practitioner who had scaling erythema with infiltration on his left cheek (Figure 2). Incomplete alopecia with several black dots was visible on the occipital scalp. Direct microscopic examination revealed endothrix infection with chains of conidia in and around the hair (Figure 3). A sample, obtained using a circular hairbrush, was cultured and produced brownish-yellow colonies with powdery surface (Figure 4). The results of culturing supported a diagnosis of tinea faciei caused by *T. tonsurans*. The severity of inflammation was 3 points, and the extent of the lesion was 1 point. *T. tonsurans* infection has mainly been reported among judo practitioners since 2001 and has now spread to junior and senior high school judo practitioners in rural areas (7). In the current study, 19 patients with a *T. tonsurans* infection were all teenaged judo practitioners. This Clinic keeps in contact with judo instructors and this Clinic uses a hairbrush culture to periodically examine students for infection. The treatment period for tinea faciei caused by *T. tonsurans* is short because treatment is administered in an early stage.

Table 1 summarizes the clinical features by pathogen. The mean score for the severity of inflammation was 1.94 points and that for extent of lesions was 1.73 points. The corresponding scores were 1.74 and 2.29 points for *T. rubrum*, 1.95 and 1.11 points for *T. tonsurans*, and 2.12 and 1.53 points for *M. canis*, respectively. The mean scores for the severity of inflammation and the extent of lesions were 1.82 and 1.84 points for anthropophilic dermatophytes (*T. rubrum*, *T. tonsurans*, and *T. violaceum*) and 2.14 and 1.50 points for zoophilic dermatophytes (*T. mentagrophytes*, *T. verrucosum*, and *M. canis*), respectively. These findings indicate that anthropophilic fungi resulted in less inflammation and broader lesions, whereas zoophilic fungi resulted in more intense inflammation and smaller lesions. When a small area of erythema (< 3 cm) with intense inflammation was observed on the face, ringworm

caused by zoophilic fungi had to be considered and patients were asked if they had contact with animals. Patients who had applied topical steroids had a mean score for the severity of inflammation of 1.90 points and a mean score of 2.10 points for the extent of lesions. Patients who had not applied topical steroids had a mean score for the severity of inflammation of 1.95 points and a mean score of 1.59 points for the extent of lesions. Mean scores for the severity of inflammation did not differ significantly. However, lesions were significantly larger in patients who had applied topical steroids ($p = 0.026$). Diagnosing tinea faciei based on clinical symptoms is hampered by misuse of topical steroids and the presence of numerous zoophilic fungi causing intense inflammatory symptoms. In addition, the presence of various fungal strains is an important factor to consider. Therefore, scoring the symptoms of tinea faciei is considered to be a useful approach for the clinical diagnosis of tinea faciei.

Acknowledgements

This study was partly supported by Health and Sciences Research Grants for Research on Emerging and Re-emerging Infectious Diseases (H25-shinko-ippan-006) from the Japanese Ministry of Health, Labor, and Welfare.

References

1. Hay RJ. Superficial mycoses. In: Rook's Textbook of Dermatology (Burn T, Breathnach S, Cox N, Griffiths C, eds.). 8th ed., Wiley-Blackwell, Oxford, UK, 2010; pp. 36.29-30.
2. Disease resulting from fungi and yeasts. In: Andrew's Diseases of the Skin: Clinical Dermatology (James WD, Berger T, Elston D, eds.). 11th ed., Saunders Elsevier, Philadelphia, USA, 2011; pp. 291-292.
3. Basnet SB, Basnet NB, Hiruma M, Inaba Y, Makimura K, Kawada A. Mycological examination of the hair samples of 11 school-going Nepalese children suspected of tinea capitis. *Mycoses*. 2000; 43:51-54.
4. Foster KW, Ghannoum MA, Elewski BE. Epidemiologic surveillance of cutaneous fungal infection in the United States from 1999 to 2002. *J Am Acad Dermatol*. 2004; 50:748-752.
5. Nicola A, Laura A, Natalia A, Monica P. A 20-year survey of tinea faciei. *Mycoses*. 2010; 53:504-508.
6. Starova A, Stefanova MB, Skerlev M. Tinea faciei – hypo diagnosed facial dermatoses. *Maced J Med Sci*. 2010; 15:27-31.
7. Shiraki Y, Hiruma M, Hirose N, Sugita T, Ikeda S. A nationwide survey of *Trichophyton tonsurans* infection among combat sport club members in Japan using a questionnaire form and the hairbrush method. *J Am Acad Dermatol*. 2006; 54:622-626.

(Received November 22, 2014; Revised December 11, 2014; Accepted December 21, 2014)

In vitro and *in vivo* anti-MRSA activities of nosokomycins

Ryuji Uchida¹, Hideaki Hanaki², Hidenori Matsui², Hiroshi Hamamoto³, Kazuhisa Sekimizu³, Masato Iwatsuki², Yong-Pil Kim^{2,*}, Hiroshi Tomoda^{1,**}

¹ Graduate School of Pharmaceutical Sciences, Kitasato University, Tokyo, Japan;

² Kitasato Institute for Life Sciences, Kitasato University, Tokyo, Japan;

³ Graduate School of Pharmaceutical Sciences, The University of Tokyo, Tokyo, Japan.

Summary The anti-methicillin-resistant *Staphylococcus aureus* (MRSA) activity of nosokomycins A to D discovered in the silkworm-MRSA infection screening was investigated. The minimum inhibitory concentration (MIC) values of nosokomycins for authentic MRSA and *S. aureus* strains were calculated to be 0.06 to 2.0 µg/mL. They also showed potent inhibitory activity against 54 clinically isolated MRSA strains. Furthermore, nosokomycin A proved effective in the mouse-MRSA infection model.

Keywords: Nosokomycins, silkworm infection assay, anti-MRSA antibiotic, *Streptomyces cyslabdanicus* K04-0144, therapeutic efficacy

1. Introduction

Drug candidates discovered from *in vitro* screening systems sometimes show no therapeutic effects in *in vivo* models using mice, rats, rabbits and so on as a host animal. There are gaps between *in vitro* and *in vivo* assay systems due to the following reasons: membrane permeability of drugs, metabolism of drugs and involvement of host immune systems; therefore, the introduction of *in vivo* assay systems at the early stage of screening programs is effective to fill the gaps, although *in vivo* screening is a time- and cost-consuming method and is therefore unrealistic. On the other hand, there is increased public concern towards eradicating animal experiments from the perspective of animal protection. Furthermore, the implementation of animal experiments is stringently regulated worldwide. Particularly in the European Union, widespread administration of all new drug candidates to healthy animals was forbidden in 1998.

To overcome these problems, researchers

have focused on non-mammalian animals such as Zebrafish (1), *Caenorhabditis elegans* (2), *Drosophila melanogaster* (3), and silkworms (4-8) as alternative hosts for *in vivo* screening systems. On the discovery of antibiotics active against methicillin-resistant *Staphylococcus aureus* (MRSA) from microbial metabolites, we established an *in vivo*-mimic MRSA infection assay using silkworm larvae as a host animal and started to apply this assay to the primary screening for new anti-MRSA antibiotics of microbial origin. In this assay, MRSA-infected silkworm larvae die within 3 day. If drug candidates are effective, silkworm larvae can survive. We predicted that drug candidates discovered by the silkworm infection assay would have higher potential effectiveness in *in vivo* systems than those discovered by *in vitro* assays using paper disks.

During the course of this screening program, nosokomycins A to D (Figure 1) were isolated as potent antibiotics from the culture broth of *Streptomyces cyslabdanicus* K04-0144 (8,9). In this study, *in vitro* and *in vivo* anti-MRSA activities of nosokomycins are described.

2. Materials and Methods

2.1. Materials

Nosokomycins A to D were purified from a culture broth of *Streptomyces cyslabdanicus* K04-0144, as reported (8,9). Vancomycin and linezolid were obtained

*Current address: Faculty of Pharmacy, Iwaki Meisei University, 5-5-1 Chuodai Iino, Iwaki City, Fukushima 970-8551, Japan.

**Address correspondence to:

Dr. Hiroshi Tomoda, Graduate School of Pharmaceutical Sciences, Kitasato University, 5-9-1 Shirokane, Minato-ku, Tokyo 108-8641, Japan.
E-mail: tomudah@pharm.kitasato-u.ac.jp

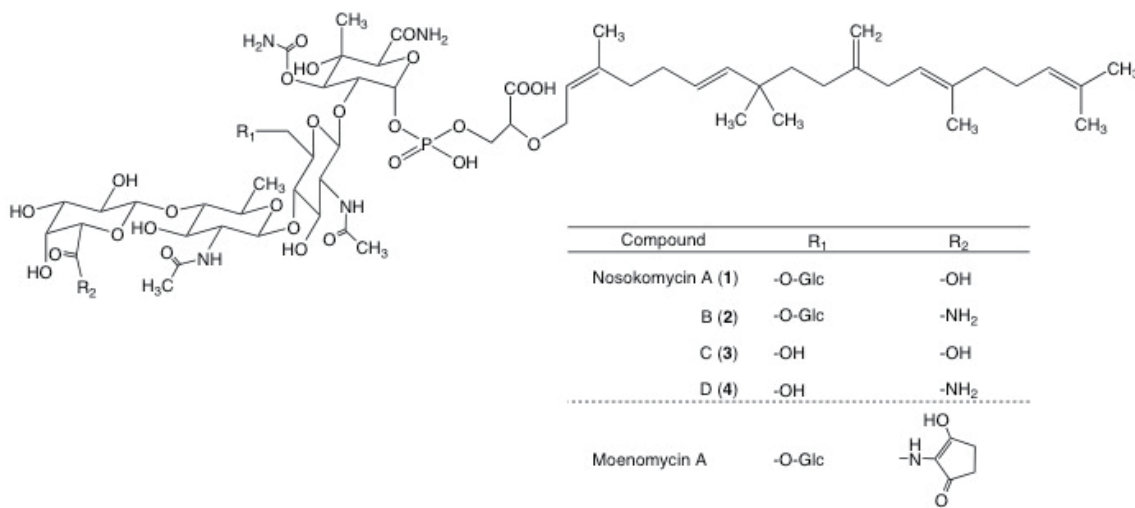


Figure 1. Structures of nosokomycins A to D.

from Wako Pure Chemical Industries (Osaka, Japan). Arbekacin was purchased from Meiji Seika Pharma (Tokyo, Japan). Unless otherwise stated, all other reagents were reagent-grade commercial products.

2.2. Animals

Fertilized silkworm eggs, *Bombyx mori* (Hu•Yo × Tukuba•Ne), were purchased from Ehime Sansyu (Ehime, Japan) and fed artificial food (Silkmate 2S; Nihon Nosan Kogyo; Silkmate; Katakura Industries, Tokyo, Japan) until the fourth-instar larval stage. Female ICR mice (18-20 g, 4 weeks old) were obtained from Charles River (Kanagawa, Japan).

2.3. Microorganisms

Fifty-four MRSA strains, including N315 IR94, N315 IR94 HR-1 and K24, were clinically collected in Japan (10). The origin of other test microorganisms was as follows: *Staphylococcus aureus* FDA209P, *S. aureus* ISP447, *S. aureus* 8325 pEP2104 (partial macrolide and streptogramin B-resistant strain), *S. epidermidis* IFO12648, *Micrococcus luteus* ATCC9341, *Enterococcus faecalis* ATCC21212, *E. faecalis* NTCT12201 (*vanA*-type vancomycin-resistant strain), *Escherichia coli* NIHJ JC-2, *Citrobacter freundii* ATCC8090, *Klebsiella pneumoniae* NCTN9632, *Proteus mirabilis* IFO3849, *P. vulgaris* OX-19, *Morganella morganii* IID Kono, *Serratia marcescens* IFO12648, *Enterobacter cloacae* IFO13535, *E. aerogenes* NCTC10006, *Pseudomonas aeruginosa* 46001, *P. aeruginosa* E-2 (ceftazidime-sensitive strain), and *Acinetobacter calcoaceticus* IFO2552.

2.4. Preparation of microorganism suspension

All microorganisms except *Staphylococcus* sp. were grown overnight at 37°C in Trypticase soy broth (TSB;

BBL Microbiology Systems, Cockeysville, MD, USA). The cultures were diluted with the same broth and adjusted to an optical density at 600 nm of 0.3 (about 10⁸ CFU/mL). *Staphylococcus* sp. was grown overnight at 37°C on Mueller-Hinton agar (MHA; Becton Dickinson, San Jose, CA, USA) containing chocolate horse blood at a final concentration of 10% (v/v), and the colonies were then suspended in a sufficient amount of TSB to make a cell suspension with an optical density at 600 nm of 0.3.

2.5. Determination of minimum inhibitory concentration (MIC) values

MICs of nosokomycins and authentic antibiotics (vancomycin, arbekacin and linezolid) were measured according to the agar dilution method recommended by the National Committee for Clinical Laboratory Standards (NCCLS) (11). For the MIC assay, MHA was used as a medium for test microorganisms except *Staphylococcus* sp., and MHA supplemented with 5% horse blood was used for *Staphylococcus* sp. The bacterial suspensions were then diluted 100-fold with the same fresh broth (about 10⁶ CFU/mL). One loopful (5 μL) of the cell suspension was inoculated onto agar plates containing various concentrations of nosokomycin and authentic antibiotics using an inoculator (Microplanter; Sakuma Seisakusho, Tokyo, Japan). Growth of bacteria was evaluated after 18-h incubation at 37°C. The MIC was defined as the lowest drug concentration that showed 95% growth inhibition of bacteria.

2.6. Population analysis of nosokomycins against clinically isolated MRSA

Resistant subpopulations of 54 clinically isolated MRSA strains (population analysis) were analyzed by the established method (12,13). MRSA culture suspension (50 μL, overnight MRSA culture diluted

to an optical density at 550 nm of 0.3) was spread on MHA plates containing various concentrations of nosokomyins or authentic antibiotics. The plates were incubated at 37°C at 48-h and the number of growth strains was counted.

2.7. *In vivo-mimic MRSA infection assay using silkworm larvae*

An *in vivo-mimic* MRSA infection assay using silkworm larvae was carried out by the established method with some modification (7,8). Hatched silkworm larvae were raised by feeding an artificial diet containing antibiotics (Silk Mate 2S, Nihon Nosan Kogyo, Kanagawa, Japan) in an incubator at 27°C until the fourth molting stage. On the first day of fifth-instar larvae, silkworms were fed an antibiotic-free artificial diet (Silk Mate, Katakura Industries, Saitama, Japan) for 24 h. On the second day, MRSA K-24 (2.5×10^7 CFU in 50 μ L, LB medium containing 10% NaCl) was injected into the hemolymph through the dorsal surface of the silkworms using a disposable 1-mL syringe with a 27G needle (TERUMO, Tokyo, Japan). Immediately (within one hour) after MRSA K-24 injection, a test sample (50 μ L in 10% DMSO) was injected into the hemolymph. When they were maintained in an incubator at 27°C, all the MRSA-infected silkworm larvae without a sample died within 3 days. Under these conditions, when vancomycin (50 μ g per larva) was injected, all silkworms survived, even on day 3.

2.8. *In vivo MRSA infection assay using mice*

The *in vivo* effect of nosokomyin A on systemic MRSA infection was studied using female ICR mice (18-20 g, 4 weeks old) (10). *S. aureus* 92-1191 (highly drug-resistant MRSA; MIC value of methicillin: > 100 μ g/mL) was routinely grown in brain-heart infusion broth (BHI; Becton Dickinson) at 35°C overnight with agitation on a rotary shaker at 45 rpm. Mice were intraperitoneally infected with 1×10^9 CFU of MRSA 92-1191 in 0.1 mL phosphate-buffered saline (pH 7.4) containing 0.01% (w/v) gelatin and 10% (w/v) mucin from swine stomach (Wako Pure Chemical Industries). One hour later, nosokomyin A suspended in saline was subcutaneously injected into the back of mice (*s.c.*) or intravenously administered (*i.v.*) at doses of 3.13, 6.25, 12.5 and 25 mg/kg (five mice per each dose), and the survival rates were recorded for five days. Vancomycin was evaluated under the same conditions.

3. Results

3.1. *Antibacterial activity of nosokomyins A to D against pathogenic microorganisms*

The MIC values of nosokomyins against various pathogenic bacteria including MRSA are shown in Table 1. Under the same conditions, clinically used antibacterial agents, vancomycin, arbekacin and linezolid, were tested (Table 1). Nosokomyins were found to be as active

Table 1. MIC values of nosokomyins against various pathogenic bacteria including MRSA.

Microorganism strain	Nosokomyin				Vancomycin	Arbekacin	Linezolid
	A	B	C	D			
Gram positive bacteria							
<i>S. aureus</i> FDA209P	1.0	≤ 0.25	2.0	1.0	1.0	≤ 0.25	1.0
MRSA N315 IR94	0.06	≤ 0.25	0.125	≤ 0.25	0.50	0.50	1.0
MRSA N315 IR94 HR-1	0.125	≤ 0.25	0.125	≤ 0.25	0.50	1.0	2.0
MRSA K24	0.125	0.125	0.125	0.125	NT	NT	NT
<i>S. aureus</i> ISP447	0.25	≤ 0.25	0.50	≤ 0.25	1.0	≤ 0.25	2.0
<i>S. aureus</i> 8325 (pEP2104)	0.06	≤ 0.25	0.06	0.50	2.0	≤ 0.25	2.0
<i>S. epidermidis</i> IFO12648	4.0	≤ 0.25	8.0	1.0	≤ 0.25	≤ 0.25	2.0
<i>M. luteus</i> ATCC9341	> 16	> 128	> 16	> 128	1.0	≤ 0.25	2.0
<i>E. faecalis</i> ATCC21212	1.0	≤ 0.25	2.0	0.50	4.0	> 32	2.0
<i>E. faecalis</i> NTCT12201 (VanA)	1.0	≤ 0.25	2.0	0.50	> 32	> 32	2.0
Gram negative bacteria							
<i>E. coli</i> NIHJ JC-2	> 16	8.0	> 16	8.0	> 32	> 32	> 32
<i>C. freundii</i> ATCC8090	> 16	64	> 16	64	> 32	0.50	> 32
<i>K. pneumoniae</i> NCTN9632	> 16	8.0	> 16	8.0	> 32	≤ 0.25	> 32
<i>P. mirabilis</i> IFO3849	> 16	8.0	16	8.0	> 32	2.0	> 32
<i>P. vulgaris</i> OX-19	> 16	8.0	4.0	4.0	> 32	2.0	8.0
<i>M. morgani</i> IID Kono	> 16	32	> 16	32	> 32	0.50	> 32
<i>S. marcescens</i> IFO12648	> 16	32	> 16	32	> 32	1.0	> 32
<i>E. cloacae</i> IFO13535	> 16	32	> 16	32	> 32	0.50	> 32
<i>E. aerogenes</i> NCTC10006	> 16	32	> 16	32	> 32	≤ 0.25	> 32
<i>P. aeruginosa</i> 46001	> 16	32	> 16	32	> 32	1.0	> 32
<i>P. aeruginosa</i> E-2	> 16	32	> 16	32	> 32	4.0	> 32
<i>A. calcoaceticus</i> IFO2552	16	8.0	8.0	8.0	> 32	≤ 0.25	> 32

NT; Not tested

as or more active than the three agents against most Gram-positive bacteria. For example, the MIC values of nosokomyocins against multidrug-resistant MRSA N315 IR94 HR-1 (resistant to methicillin, imipenem, ciprofloxacin and tobramycin) were 0.125-0.25 $\mu\text{g}/\text{mL}$, while the three clinically used agents had high MIC values (0.5-2 $\mu\text{g}/\text{mL}$). Among them, nosokomyocins B and D also showed moderate activity against Gram-negative bacteria. Although it is difficult to determine

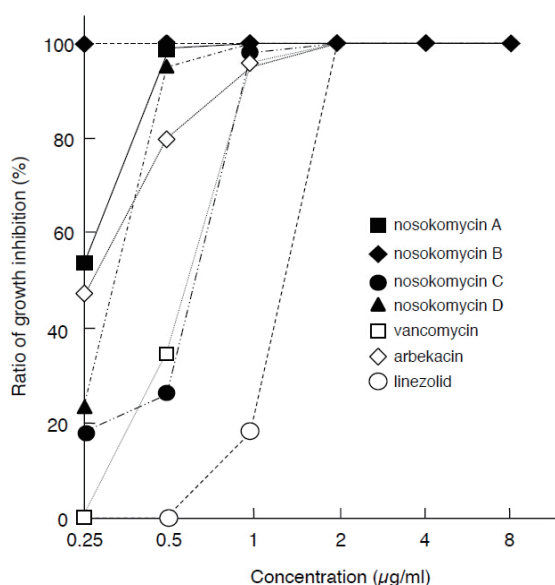


Figure 2. Antibacterial activity of nosokomyocins against 54 clinical isolated MRSA strains.

the potency order of nosokomyocins as antimicrobial agents because of the subtle difference in MIC values, nosokomyocin B appeared to be the most potent.

3.2. Population analysis of nosokomyocins A to D

Since nosokomyocins were found to show potent activity against most Gram-positive bacteria, anti-MRSA activity was investigated in more detail by population analysis using 54 clinically isolated MRSA strains. As shown in Figure 2, the growth of all 54 MRSA strains (100%) was inhibited by 0.25 $\mu\text{g}/\text{mL}$ nosokomyocin B, while the growth of 55%, 22%, and 18% MRSA strains was inhibited by 0.25 $\mu\text{g}/\text{mL}$ nosokomyocins A, D and C, respectively. At 0.5-2 $\mu\text{g}/\text{mL}$, nosokomyocins A, D, and C also showed 100% inhibition of those MRSA strains. From this population analysis, nosokomyocin B showed the most potent anti-MRSA activity, followed by nosokomyocins A, D, and C. Arbekacin was as potent as nosokomyocin D, and vancomycin was as potent as nosokomyocin C. Linezolid was the least among the drugs tested in this analysis.

3.3. Therapeutic efficacy of nosokomyocin A in MRSA-infected silkworm larvae

Nosokomyocins were evaluated in the *in vivo*-mimic MRSA infection assay using silkworm larvae. As shown in Figure 3, when nosokomyocin A (50 μg per larva) was injected into MRSA-infected silkworm larvae,

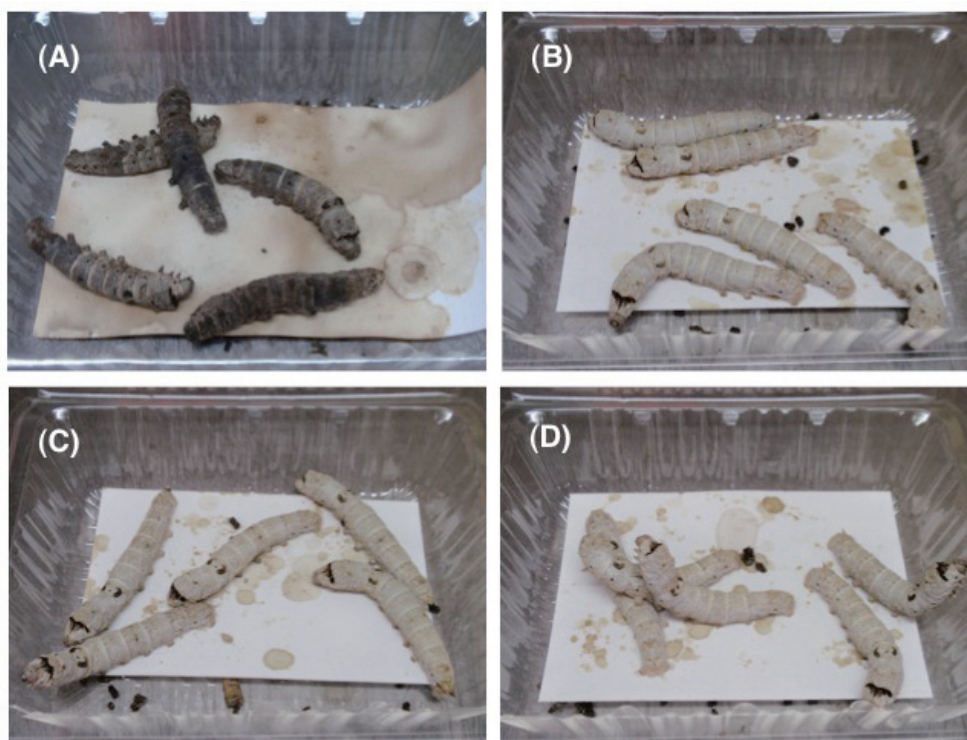


Figure 3. *In vivo* efficacy of nosokomyocin A in silkworm infected with MRSA. (A) MRSA suspension. (B) Nosokomyocin A (25 μg g^{-1} ·larvae). (C) MRSA suspension + nosokomyocin A (25 μg g^{-1} ·larvae). (D) MRSA suspension + vancomycin (25 μg g^{-1} ·larvae).

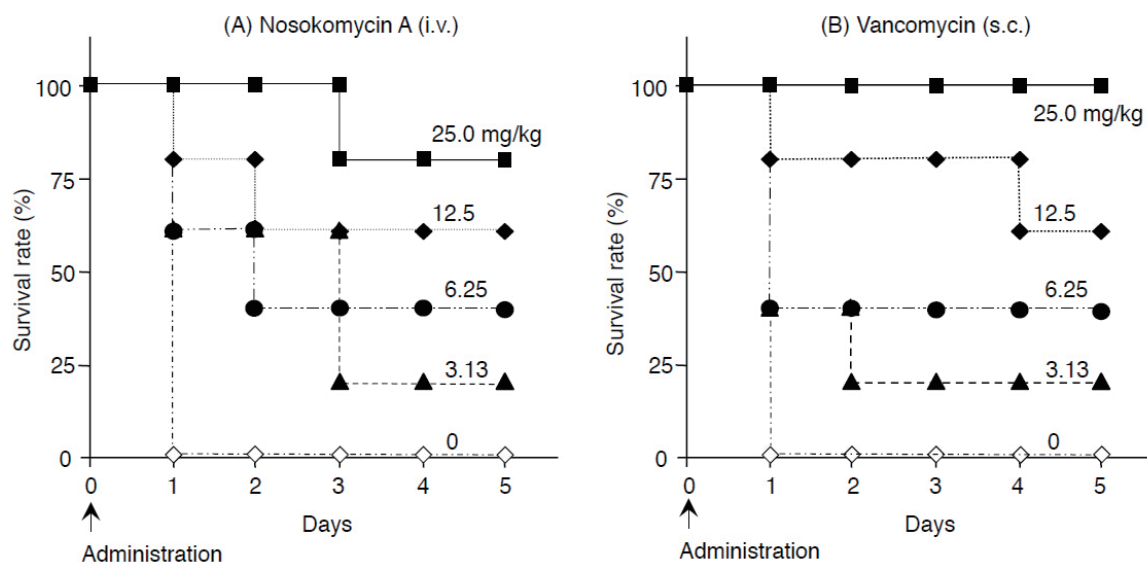


Figure 4. Therapeutic effects of nosokomycin A and vancomycin in mice infected with MRSA. (A) Intravenous administration of nosokomycin A. **(B)** Subcutaneous administration of vancomycin. Drugs were administrated once on day 0.

larvae all survived to at least day 3 (Figure 3C), while untreated larvae became black and died (Figure 3A). Nosokomycin A alone (50 μ g per larva) had no toxic effect on uninfected larvae at least for 3 days (Figure 3B), indicating that the compound showed no toxicity to silkworm larvae. Nosokomycin B (50 μ g per larva) also showed similar therapeutic efficacy for MRSA infected silkworm larvae (data not shown). Under the same conditions, vancomycin (50 μ g per larva) showed the same therapeutic efficacy (Figure 3D).

3.4. Therapeutic efficacy of nosokomycin A in MRSA-infected mice

To confirm its *in vivo* efficacy, nosokomycin A was evaluated in an MRSA-infected mouse assay (7). When MRSA was intraperitoneally infected to mice, all the mice died on day 1 (next day) (Figures 4A and 4B); however, intravenous administration of nosokomycin A (3.12-25 mg/kg, on day 0) to MRSA-infected mice resulted in the dose-dependent survival of mice from MRSA infection (Figure 4A). At 25 mg/kg, 75% mice could survive MRSA infection. Vancomycin also showed *in vivo* efficacy by both subcutaneous (Figure 4B) and intravenous (data not shown) administration to MRSA-infected mice; however, subcutaneous administration of nosokomycin A did not show efficacy even at 25 mg/kg dose (data not shown).

4. Discussion

In this study, *in vitro* and *in vivo* anti-MRSA activities of nosokomycins A to D were investigated. As reported previously, nosokomycins were discovered in the screening using the silkworm-MRSA infection assay (8,9). All nosokomycins showed potent activity against

most Gram-positive pathogenic bacteria with analogous MIC values, and nosokomycins B and D also showed moderate activity against Gram-negative bacteria (Table 1). From MIC data, nosokomycin B appeared to show the most potent anti-microbial activity among the four nosokomycins. From population analysis using 54 clinically isolated MRSA strains (Figure 2), it became clear that nosokomycin B is the most potent, followed by nosokomycins A, D, and C. Thus, it was suggested that the presence of a glucose residue at R1 and an amino residue at R2 in the structure is important for potent anti-MRSA activity. Nosokomycins belong to the phosphoglycolipid moenomycin family. Moenomycin A possesses a glucose residue at R1 and a chromophoric cyclopentenone residue via an amide bond at R2 (Figure 1). To understand, in particular, the importance of the cyclopentenone residue, it will be intriguing to compare anti-MRSA activity between nosokomycin B and moenomycin A, although we could not obtain moenomycin A, because nosokomycin-producing *Streptomyces cylabdanicus* K04-0144 strain did not produce moenomycins. However, it was reported that the anti-*S. aureus* activity of moenomycin A lacking the cyclopentenone moiety decreased tenfold compared with that of moenomycin A (14).

We applied the silkworm-MRSA infection assay to the primary screening method, and discovered nosokomycins from the culture broth of *Streptomyces cylabdanicus* K04-0144 (8,9). This study demonstrated that nosokomycin A proved intravenously active in an *in vivo* MRSA-infected mouse model (Figure 4) (7). Unfortunately, nosokomycin A was inactive by subcutaneous administration in the mouse infection assay, while vancomycin proved active in both administration methods, which might have been due to drug permeability into the bloodstream.

All results showed the usefulness of *in vivo*-mimic MRSA infection assay using silkworm larvae to discover anti-MRSA agents effective in *in vivo* using mammalian animals. We hope this methodology accelerates the discover of anti-infective agents, overcoming many problems such as gaps between *in vitro* and *in vivo* model, animal protection and so on.

Acknowledgements

This work was supported by JSPS KAKENHI Grant Numbers 22590013, 25460130 (to RU) and 21310146 (to HT).

References

- Zon LI, Peterson RT. *In vivo* drug discovery in the zebrafish. *Nat Rev Drug Discov.* 2005; 4:35-44.
- Kwok TCY, Ricker N, Fraser R, Chan AW, Burns A, Stanley EF, McCourt P, Cutler SR, Roy PJ. A small-molecule screen in *C. elegans* yields a new calcium channel antagonist. *Nature.* 2006; 441:91-95.
- Needham AJ, Kibart M, Crossley H, Ingham PW, Foster SJ. *Drosophila melanogaster* as a model host for *Staphylococcus aureus* infection. *Microbiology.* 2004; 150:2347-2355.
- Asami Y, Horie R, Hamamoto H, Sekimizu K. Use of silkworms for identification of drug candidates having appropriate pharmacokinetics from plant sources. *BMC Pharmacol.* 2010; 10:7.
- Kaito C, Akimitsu N, Watanabe H, Sekimizu K. Silkworm larvae as an animal model of bacterial infection pathogenic to humans. *Microb Pathog.* 2002; 32:183-190.
- Hamamoto H, Kurokawa K, Kaito C, Kamura K, Razanajatovo IM, Kusuhara H, Santa T, Sekimizu K. Quantitative evaluation of the therapeutic effects of antibiotics using silkworms infected with human pathogenic microorganisms. *Antimicrob. Agents Chemother.* 2004; 48:774-779.
- Hamamoto H, Urai M, Ishii K, *et al.* Lysocin E is a new antibiotic that targets menaquinone in the bacterial membrane. *Nat Chem Biol.* 2014. doi: 10.1038/nchembio.1710
- Uchida R, Iwatsuki M, Kim YP, Ohte S, Ōmura S, Tomoda H. Nosokomylicins, new antibiotics, discovered in an *in vivo*-mimic infection model using silkworm larvae. I. Fermentation, isolation and biological properties. *J Antibiot.* 2010; 63:151-155.
- Uchida R, Iwatsuki M, Kim YP, Ōmura S, Tomoda H. Nosokomylicins, new antibiotics, discovered in an *in vivo*-mimic infection model using silkworm larvae. II. Structure elucidation. *J Antibiot.* 2010; 63:157-163.
- Hanaki H, Akagi H, Yasui M, Otani T, Hyodo A, Hiramatsu K. TOC-39, a novel parenteral broad-spectrum cephalosporin with excellent activity against methicillin-resistant *Staphylococcus aureus*. *Antimicrob Agents Chemother.* 1995; 39:1120-1126.
- National Committee for Clinical Laboratory Standards. In: Reference method for performance standards for antimicrobial disk susceptibility tests. Approved Standard M2-A8. National Committee for Clinical Laboratory Standards. 8th ed., Wayne, PA, USA, 2003.
- Hiramatsu K, Aritaka N, Hanaki H, Kawasaki S, Hosoda Y, Hori S, Fukuchi Y, Kobayashi I. Dissemination in Japanese hospitals of strains of *Staphylococcus aureus* heterogeneously resistant to vancomycin. *Lancet.* 1997; 350:670-673.
- Takayama Y, Hanaki H, Irinoda I, Kokubun H, Yoshida K, Sunagawa K. Investigation of methicillin-resistant *Staphylococcus aureus* showing diminished susceptibility isolated from a patient with infective endocarditis. *Int J Antimicrob Agents.* 2004; 22:567-573.
- Rühl T, Daghish M, Buchynsky A, Barche K, Volke D, Stempera K, Kempin U, Knoll D, Hennig L, Findeisen M, Oehme R, Giesa S, Ayala J, Welzel P. Studies on the interaction of the antibiotic moenomycin A with the enzyme penicillin-binding protein 1b. *Bioorg Med Chem.* 2003; 11:2965-2981.

(Received December 18, 2014; Revised December 22, 2014; Accepted December 23, 2014)

Human RNA polymerase II-associated protein 2 (RPAP2) interacts directly with the RNA polymerase II subunit Rpb6 and participates in pre-mRNA 3'-end formation

Shotaro Wani, Yutaka Hirose*, Yoshiaki Ohkuma

Laboratory of Gene Regulation, Graduate School of Medicine and Pharmaceutical Sciences, University of Toyama, Toyama, Japan.

Summary

The C-terminal domain (CTD) of the largest subunit of RNA polymerase II (Pol II) is composed of tandem repeats of the heptapeptide Tyr1-Ser2-Pro3-Thr4-Ser5-Pro6-Ser7. The CTD of Pol II undergoes reversible phosphorylation during the transcription cycle, mainly at Ser2, Ser5, and Ser7. Dynamic changes in the phosphorylation patterns of the CTD are responsible for stage-specific recruitment of various factors involved in RNA processing, histone modification, and transcription elongation/termination. Human RNA polymerase II-associated protein 2 (RPAP2) was originally identified as a Pol II-associated protein and was subsequently shown to function as a novel Ser5-specific CTD phosphatase. Although a recent study suggested that RPAP2 is required for the efficient expression of small nuclear RNA genes, the role of RPAP2 in controlling the expression of protein-coding genes is unknown. Here, we demonstrate that the C-terminal region of RPAP2 interacts directly with the Pol II subunit Rpb6. Chromatin immunoprecipitation analyses of the *MYC* and *GAPDH* protein-coding genes revealed that RPAP2 occupied the coding and 3' regions. Notably, siRNA-mediated knockdown of RPAP2 caused defects in 3'-end formation of the *MYC* and *GAPDH* pre-mRNAs. These results suggest that RPAP2 controls Pol II activity through a direct interaction with Rpb6 and participates in pre-mRNA 3'-end formation.

Keywords: RNA polymerase II-associated protein 2, pre-mRNA 3'-end formation, transcription cycle, C-terminal domain phosphatase, gene regulation

1. Introduction

Eukaryotic RNA polymerase II (Pol II) is a multi-subunit enzyme responsible for the transcription of protein-coding mRNAs and a variety of non-coding RNAs. Pol II activity is regulated by phosphorylation of the C-terminal domain (CTD) of its largest subunit (Rpb1), which is composed of multiple repeats of the evolutionarily conserved heptapeptide sequence Tyr1-Ser2-Pro3-Thr4-Ser5-Pro6-Ser7 (1). The repeat number varies between species, ranging from 26 in yeast to 52 in vertebrates (1). The CTD undergoes reversible phosphorylation during the transcription

cycle, predominantly at Ser2, Ser5, and Ser7 of the repeats (2). Multiple kinases and phosphatases act on the CTD in a transcription stage-specific manner, thereby generating different CTD phosphorylation patterns along transcribed genes (2). The dynamically phosphorylated CTD temporally couples transcription with other nuclear processes by serving as a scaffold for the recruitment of various proteins involved in transcription, chromatin modification, and RNA processing (2,3).

Pol II consists of 12 subunits (Rpb1–12); 10 subunits form a catalytic core and the remaining subunits (Rpb4 and Rpb7) form a peripheral subcomplex. Recent proteomics studies identified Pol II assembly intermediates containing subsets of the subunits and suggested that the Pol II complex must be fully assembled in the cytoplasm before entering the nucleus (4). The cytoplasmic assembly and nuclear import of the Pol II complex require a number of novel factors,

*Address correspondence to:

Dr. Yutaka Hirose, Laboratory of Gene Regulation, Graduate School of Medicine and Pharmaceutical Sciences, University of Toyama, 2630 Sugitani, Toyama 930-0194, Japan.
E-mail: yh620@pha.u-toyama.ac.jp

including heat shock protein 90 and its co-chaperone R2TP/Prefoldin-like complex (4), Pol II-associated small GTPase family members (GPN1–3) (5–7), and other Pol II-associated proteins (RNA Pol II-associated protein 1 (RPAP1), RPAP2, and GrinL1A) (7,8).

Human RPAP2 was originally identified as a major Pol II-associated protein by affinity purification and mass spectrometry (8). Forget *et al.* (5) demonstrated that RPAP2 is located mainly in the cytoplasm and shuttles between the cytoplasm and the nucleus, and that RPAP2 binds specifically to the small GTPase GPN1, which functions in Pol II nuclear import. In addition, knockdown of RPAP2 causes the cytoplasmic accumulation of Pol II, suggesting that RPAP2 participates in Pol II nuclear import (5). Human RPAP2 contains zinc finger-like motifs and exhibits a phosphatase activity that is specific for phosphorylated Ser5 (Ser5P) in the Pol II CTD (9,10). A recent study using chromatin immunoprecipitation (ChIP) analyses demonstrated that RPAP2 is recruited to snRNA genes through specific recognition of Ser7P in the Pol II CTD (10). Knockdown of RPAP2 causes defective snRNA expression and a concomitant increase in the level of Ser5-phosphorylated Pol II on the gene encoding U2 snRNA, suggesting that human RPAP2 participates in snRNA gene expression by dephosphorylating Ser5P of Pol II (10). In the ChIP study, exogenously expressed RPAP2 was recruited to the promoter and 5' region of protein-coding genes; however, Ser7 was not required for this recruitment, suggesting the involvement of another molecular interaction between Pol II and RPAP2 (10). Although these findings suggest that RPAP2 participates in snRNA gene expression, the role of RPAP2 in controlling the expression of protein-coding genes is unknown. Furthermore, the distribution of endogenous RPAP2 on human genes has not yet been examined.

Here, biochemical and molecular biological analyses revealed that the C-terminus of human RPAP2 interacted with the Pol II subunit Rpb6 *in vitro*. ChIP analyses showed that endogenous RPAP2 occupied the coding and 3' regions of two Pol II-transcribed genes (*MYC* and *GAPDH*), and knockdown of RPAP2 caused defects in 3'-end formation of these pre-mRNAs. These results suggest that RPAP2 participates both in Pol II assembly (by directly interacting with Rpb6) and in pre-mRNA 3'-end formation.

2. Materials and Methods

2.1. Cell culture and transfection

HEK 293T and HeLa-S3 cells were maintained in Dulbecco's Modified Eagle's Medium (Nissui Pharmaceutical) supplemented with 10% fetal bovine serum (HEK293T) or 5% bovine calf serum (HeLa-S3), 0.7 µg/mL penicillin, 1.5 µg/mL streptomycin, and 2

mM *L*-glutamine. The cells were cultured at 37°C in a humidified incubator containing 5% CO₂. Transfection of siRNAs into HeLa cells was performed as described previously (11).

2.2. Plasmid constructs

The full-length open reading frame (ORF) of human *RPAP2* (NCBI accession no. NM_024813.2) was amplified from HEK293T total RNAs by RT-PCR. The N-terminal (amino acids 1–175) and C-terminal (amino acids 153–612) region of *RPAP2* were amplified by PCR using the full-length cDNA as a template. All of the cDNAs cloned into plasmids were verified by DNA sequencing. To generate the pGEX-RPAP2, pCold II-RPAP2, and pcDNA3-FLAG-RPAP2 expression vectors, the *RPAP2* cDNAs were inserted into the *EcoRI* and *BamHI* sites of the pGEX 6P-1 (GE Healthcare), pCold II (Takara), and pcDNA3-FLAG (Invitrogen) vectors, respectively. The pGEX-2TL(+) vectors containing the human Pol II subunit cDNAs (*RPB3–12*) were a gift from Dr Koji Hisatake (University of Tsukuba). To construct the His (6H)-tagged expression vectors, the *RPB6* and *RPB12* cDNAs were inserted into the *NdeI* and *BamHI* sites of the 6H-pET11d vector. The primers used for cDNA cloning are available upon request.

2.3. Western blotting and antibodies

Preparation of affinity-purified anti-RPAP2 antibodies and western blotting were performed as described previously (11). The following antibodies were used for western blotting: anti-penta His (Qiagen), anti-FLAG (M2; Sigma), anti-Pol II (ARNA-3; Progen), anti-beta-actin (Sigma), and normal rabbit IgG (Millipore). An anti-Pol II antibody (N20; Santa Cruz Biotechnology) was used for ChIP analysis.

2.4. Quantitative RT-PCR (RT-qPCR)

Total RNAs were isolated from siRNA-treated HeLa-S3 cells using Isogen II reagent (Nippon Gene). The first-strand cDNAs were synthesized from total RNA using the PrimeScript™ 1st strand cDNA Synthesis Kit (TaKaRa) and random hexamer primers. The cDNA was quantified using SYBR Premix Ex Taq™ II (TaKaRa) and the Mx3000P real-time PCR system (Stratagene). The primers used for RT-qPCR analyses are available upon request.

2.5. Protein expression and purification

Cold-induced expression of 6H-tagged human RPAP2 in *Escherichia coli* was performed according to the instructions of the manufacturer of the pCold II vector (TaKaRa). Purification of His-tagged recombinant

proteins was performed using Ni-NTA agarose beads (Qiagen), according to the manufacturer's instructions. All GST-fused recombinant proteins were expressed in *E. coli* and purified as described previously (12). Protein concentrations were determined by the Bradford method using bovine serum albumin as a standard.

2.6. GST pull-down assay

GST pull-down assays were performed as described previously (11).

2.7. ChIP assay

ChIP assays were performed as described previously (13). The sequences of the primers used for ChIP assays are available upon request.

3. Results

3.1. Human RPAP2 binds directly to Rpb6 in vitro

Although one group reported that RPAP2 binds directly to Ser7-phosphorylated Pol II (10), another reported that the CTD of Pol II is not essential for the direct interaction between RPAP2 and the purified Pol II complex (5). Hence, it is unclear which subunit of Pol II is the direct binding partner of RPAP2. To address this issue, we performed GST pull-down assays using purified recombinant Pol II subunits (Rpb3-12). The purities of the recombinant proteins used in this study are shown in Supplemental Figures S1 and S2 (<http://www.ddtjournal.com/docindex.php?year=2014&kanno=6>). In the first experiment,

GST-fused Pol II subunits were expressed in bacteria, purified, incubated with 6H-RPAP2, and then pulled down using glutathione-Sepharose. 6H-RPAP2 bound strongly to GST-Rpb6 and GST-Rpb12 (Figure 1A, lanes 6 and 12) and weakly to GST-Rpb5 and GST-Rpb10 (Figure 1A, lanes 5 and 10). Notably, all of these RPAP2-interacting proteins are common subunits of all three classes of RNA polymerases. Next, the 6H and GST tags were exchanged and the GST pull-down assays were repeated. Although 6H-Rpb6 interacted with GST-RPAP2, 6H-Rpb12 scarcely bound to GST-RPAP2 (Figure 1B). It is possible that the N-terminal GST-tag masked or hindered a region of RPAP2 required for its interaction with 6H-Rpb12, but not 6H-Rpb6.

3.2. The C-terminal region of RPAP2 is required for efficient binding to Rpb6

Human RPAP2 comprises 612 amino acids and contains a zinc finger-like motif at its N-terminal region, but does not possess any other specific protein motifs (Figure 1C) (10). To determine which region of RPAP2 is involved in direct binding to Rpb6, we prepared two deletion mutant proteins; the first mutant comprised the N-terminal 175 amino acids (N) and the second comprised the C-terminal 460 amino acids (C) of RPAP2 (Figure 1C). Binding assays using GST-tagged full-length wild type (WT) and mutant RPAP2 proteins demonstrated that both full-length RPAP2 and the C-terminus of the protein bound to GST-Rpb6, whereas the N-terminus did not (Figure 1D). Notably, binding of the C-terminus of RPAP2 to Rpb6 was as efficient as that of the WT protein, suggesting that

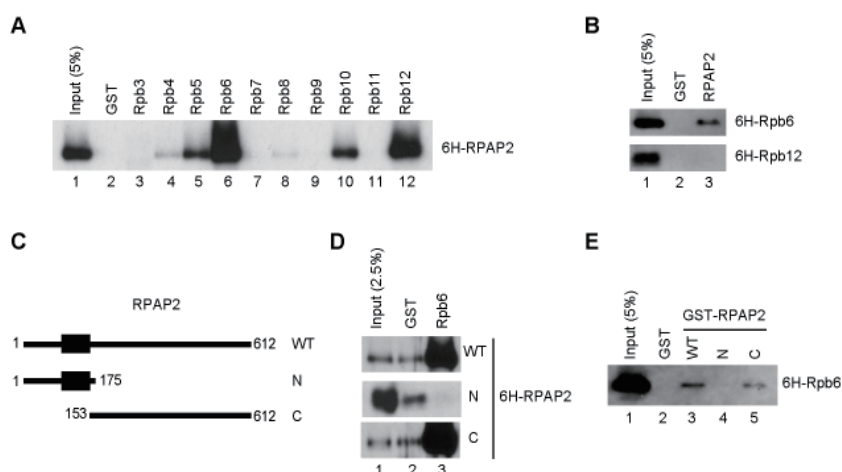


Figure 1. The C-terminus of RPAP2 binds directly to Rpb6. GST pull-down analyses of the interactions between RPAP2 and Pol II subunits (Rpb3–12). **(A)** The indicated GST-tagged Pol II subunits were incubated with 6H-RPAP2 proteins (full-length or deletion mutants) and then pulled down using glutathione-Sepharose beads. Western blotting was performed with an anti-RPAP2 antibody. **(B)** GST-tagged RPAP2 (full-length or deletion mutants) were incubated with 6H-tagged Rpb6 or Rpb12 and then pulled down using glutathione-Sepharose beads. Western blotting was performed with an anti-5His antibody. **(C)** Schematic illustration of the wild type (WT, amino acids 1–612) and deletion mutants (N, amino acids 1–175 amino acids; and C, amino acids 153–612) of RPAP2. **(D)** GST-Rpb6 was incubated with the 6H-RPAP2 proteins shown in **(C)** and then pulled down using glutathione-Sepharose beads. Western blotting was performed with an anti-RPAP2 antibody. **(E)** The GST-RPAP2 proteins shown in **(C)** were incubated with 6H-Rpb6 and then pulled down using glutathione-Sepharose beads. Western blotting was performed with an anti-5His antibody.

the C-terminus is sufficient for the interaction. Next, the 6H and GST tags were exchanged and the GST pull-down assays were repeated. Consistent with the previous result, GST-tagged full-length RPAP2 and the C-terminus mutant bound to 6H-Rpb6, but the N-terminus mutant did not (Figure 1E). However, in the second assay, the binding efficiency of the C-terminus of RPAP2 for 6H-Rpb6 was slightly lower than that of the WT protein. Taken together, these results suggest that the C-terminus of RPAP2 binds directly to the Pol II subunit Rpb6 *in vitro*.

3.3. Characterization of a polyclonal antibody against human RPAP2

Recently, Egloff *et al.* (10) used ChIP assays to analyze

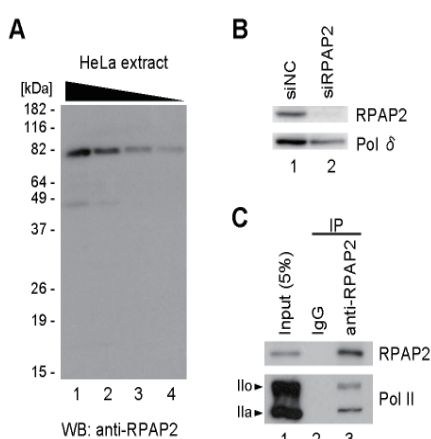


Figure 2. Characterization of a purified polyclonal antibody against human RPAP2. (A) Western blot analysis of HeLa cell total extracts using a purified polyclonal antibody against RPAP2. Lanes 1, 2, 3, and 4 contained 32, 16, 8, and 4 μ g of total protein, respectively. (B) Western blot analyses of lysates from HeLa cells treated with a negative control siRNA (siNC) or a RPAP2-specific siRNA (siRPAP2) for 2.5 days. Western blotting was performed with purified anti-RPAP2 and anti-Pol δ (loading control) antibodies. (C) Immunoprecipitation of endogenous RPAP2 and Pol II using the purified anti-RPAP2 antibody. The antibody was immobilized on protein G beads and incubated with HEK-293T cell extracts. Immunoprecipitated proteins and the input extract (5%) were analyzed by western blotting with the anti-RPAP2 and anti-Pol II (ARNA-3) antibodies. Ilo indicates hyperphosphorylated Rpb1 and Ila indicates hypophosphorylated Rpb1.

the distribution of exogenously expressed RPAP2 on several Pol II-transcribed genes in cultured human cells; however, the distribution of endogenous RPAP2 on these genes remains unclear. To examine its possible roles in controlling gene expression, we analyzed the distribution of endogenous RPAP2 on Pol II-transcribed genes using ChIP assays. A rabbit polyclonal antibody was raised against human RPAP2. Western blot analysis of HeLa whole cell lysates demonstrated that the affinity-purified antibody predominantly recognized a band of approximately 80 kDa, which corresponds to the predicted size of human RPAP2 (Figure 2A). Treatment of HeLa cells with a RPAP2-specific siRNA, but not a non-targeting control siRNA, depleted the 80 kDa antibody-reactive band, confirming that the

purified antibody specifically recognized endogenous RPAP2 (Figure 2B). The affinity-purified antibody also selectively immunoprecipitated endogenous RPAP2 and Pol II (Figure 2C). Taken together, these findings demonstrate that the purified anti-RPAP2 antibody was specific and suitable for ChIP analyses.

3.4. RPAP2 occupies the gene body and 3' region of Pol II-transcribed genes

To examine the distribution of RPAP2 on representative protein-coding genes (*MYC* and *GAPDH*), we performed ChIP assays using the purified anti-RPAP2 antibody and an anti-Pol II (N-20) antibody for comparison. The ChIP signals at several locations within each gene were quantified by real-time PCR (Figures 3A and 3B, upper panels). Consistent with previous reports, Pol II was located predominantly at the regions proximal to the *MYC* and *GAPDH* promoters (Figure 3) (14). On the other hand, RPAP2 was distributed throughout the gene body and 3' region of both genes, without an obvious peak near the promoter (Figure 3). Notably, RPAP2 was also located downstream of the 3'-end processing sites. An intense RPAP2 signal was identified upstream of the *GADPH* transcription start site (position -2056); this signal may have been caused by Pol II-mediated transcription of the 3' region of the *NCAPD2* gene, which is located adjacent to and in the same direction as the *GADPH* gene.

RPAP2 is tightly associated with Pol II; hence, we assumed that the ratio of the RPAP2 ChIP signal to the Pol II ChIP signal represented the ratio of RPAP2-associated Pol II to total Pol II. The RPAP2/Pol II ratio increased towards the center of the gene bodies and peaked at the poly(A) signal sequence of *MYC* (Figure 3A) or an internal region of *GAPDH* (Figure 3B). These results suggest that RPAP2 is increasingly recruited to Pol II towards the 3'-end of at least some protein-coding genes.

3.5. RPAP2 is required for efficient pre-mRNA 3'-end formation

Because the ChIP results showed that RPAP2 occupies the 3' region of protein-coding genes, we hypothesized that it plays a role not only in the early stage of transcription, but also the later stages of this process, including elongation and termination, as well as transcription-associated processes such as 3'-end processing of pre-mRNAs. To address this possibility, we examined the effect of siRNA-mediated knockdown of RPAP2 on pre-mRNA 3'-end formation. Knockdown of RPAP2 by two independent siRNAs was verified by western blotting (Figure 4A) and RT-qPCR (Figure 4B) analyses. To quantitatively evaluate the efficiency of 3'-end formation, the ratio of unprocessed to total (precursor plus mature) *MYC* and *GAPDH*

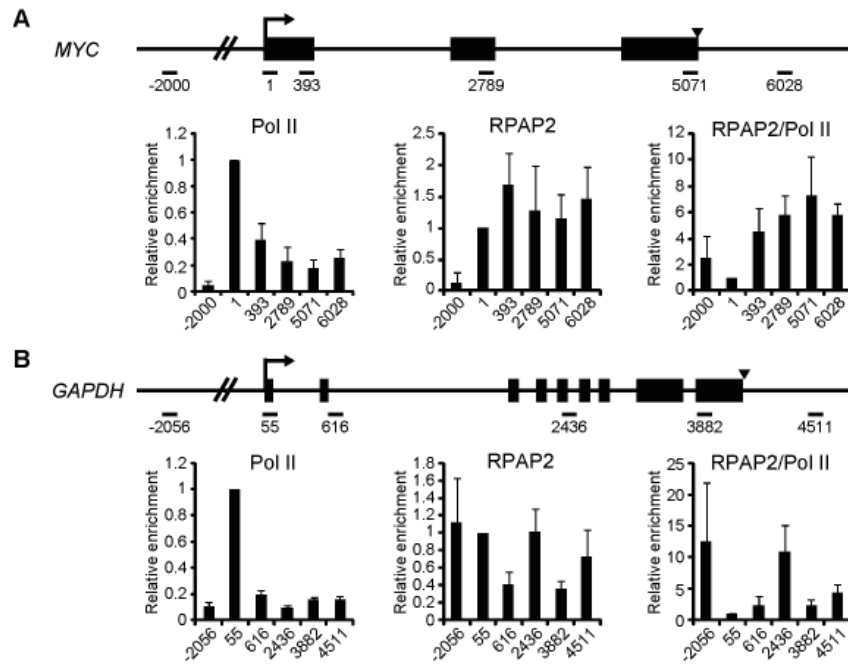


Figure 3. ChIP analyses of the distribution of human RPAP2 on Pol II-transcribed genes. ChIP analyses of the *MYC* (A) and *GAPDH* (B) genes. The upper panels show schematic illustrations of the genes: the transcription start sites are indicated by arrows, the exons are shown as black boxes, and the polyadenylation signals are indicated by arrowheads. The positions of the primer pairs used for RT-qPCR (relative to the transcription start site) are shown below each diagram. The lower panels show the results of ChIP analyses of the indicated regions of the *MYC* and *GAPDH* genes in HEK 293T cells using antibodies against Pol II (N20) or RPAP2. The ratios of the RPAP2 signals to the Pol II signals (RPAP2/Pol II) are also shown. The data were normalized to the region at which the Pol II signal was strongest. Data are expressed as the mean \pm standard deviation of four (*MYC*) or three (*GAPDH*) independent experiments.

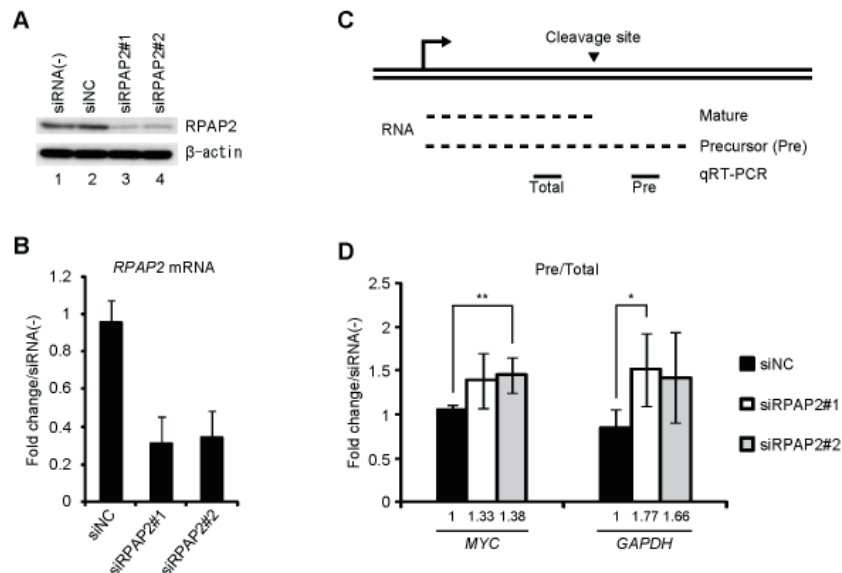


Figure 4. RPAP2 is required for efficient 3'-end formation of the *MYC* and *GAPDH* pre-mRNAs. HeLa cells were transfected with a negative control siRNA (siNC) or with one of two independent RPAP2-specific siRNAs (#1, #2). (A) Western blot analyses of total proteins extracted from the untreated (siRNA(-)) or siRNA-treated cells using antibodies against RPAP2 or β -actin (loading control). (B) RT-qPCR analyses of the efficiency of knockdown of *RPAP2* mRNA by the specific siRNAs. *RPAP2* expression levels were normalized to those of 18S ribosomal RNA. Fold changes were determined relative to the level of RPAP in siRNA(-) cells. Data are expressed as the mean \pm standard deviation of four independent experiments. (C) Schematic illustration of the evaluation of 3'-end formation of pre-mRNAs. DNA is depicted as a double line, the transcription start site is depicted as an arrow, and the cleavage site is denoted by an arrowhead. Transcribed mature and precursor (Pre) RNAs are shown as dashed lines. The short horizontal lines ("Total" and "Pre") indicate the RT-qPCR amplicons used to quantify the total or pre-mRNA transcript. (D) RT-qPCR analyses of the expression levels of total (precursor plus mature) and unprocessed (precursor) *MYC* and *GAPDH* RNAs in siRNA-treated HeLa cells. The ratios of unprocessed to total RNAs (Pre/Total) are shown. Relative expression levels were determined by normalizing the data to the corresponding expression levels in siRNA(-) cells. The numbers below the graphs indicate the -fold increase in the Pre/Total ratio of siRNA-treated cells compared with siNC-treated cells. Data are expressed as the mean \pm standard deviation of four independent experiments. Statistical significance was determined using Student's *t*-test (* $p < 0.05$ and ** $p < 0.01$).

RNAs was determined using RT-qPCR analyses. To detect unprocessed RNAs, first-strand cDNAs were synthesized using random hexamer primers and the cDNAs were amplified by PCR using primer pairs located downstream of the processing sites (Figure 4C). Total RNA levels were detected by amplification of the coding regions. For the *MYC* and *GAPDH* genes, the ratios of unprocessed to total mRNAs in cells treated with the RPAP2-specific siRNAs were approximately 1.3-fold and 1.7-fold higher than those in cells treated with a control siRNA, respectively (Figure 4D). Together with the results of the ChIP analyses, these findings suggest that RPAP2 participates in 3'-end formation of at least some pre-mRNAs.

4. Discussion

This study demonstrates that (i) the C-terminus of human RPAP2 interacts directly with the Pol II subunit Rpb6 *in vitro*, (ii) RPAP2 occupies not only the promoter but also the coding and 3' regions of protein-coding genes, and (iii) knockdown of RPAP2 results in inefficient 3'-end formation of some pre-mRNAs.

The Pol II complex comprises a ten-subunit catalytic core and an Rpb4/Rpb7 subcomplex (15). X-ray analyses of the yeast core Pol II revealed that the two large subunits, Rpb1 and Rpb2, form opposite sides of the active center "cleft" and the Rpb1 side of the cleft forms a mobile "clamp" (16). Rpb6 is positioned at the base of the clamp, close to where the Rpb4/7 subcomplex "stalk" attaches, and where an Rpb1 "linker", which connects to the CTD, emerges from the core surface (15-17). Insertion of the Rpb4/7 stalk into the clamp region affects the clamp movement (15,18). Moreover, newly transcribed RNAs exit the Pol II core *via* the stalk, and the 5' ends of the RNAs contact Rpb7 (19). Therefore, the stalk region of Pol II is thought to function in every stage of the transcription cycle by regulating the clamp motion, as well as in efficient coupling of transcription with RNA processing (19,20). Rpb6 critically contributes to the association of the stalk with the core by interacting directly with Rpb7 (21,22); hence, we speculate that RPAP2 may regulate transcription through a direct interaction with Rpb6.

In contrast to our finding that the C-terminus of human RPAP2 interacts directly with Rpb6, a recent study by Forget *et al.* (5) demonstrated that the N-terminus, but not the C-terminus, of human RPAP2 is required for stable binding to the Pol II complex. Because we did not examine the RPAP2-binding abilities of the two larger subunits of Pol II (Rpb1 or Rpb2), it is possible that the N-terminus of RPAP2 binds stably to the Pol II complex by directly interacting with these subunits. The discrepancy between our results and those of Forget *et al.* might be also explained by other possibilities. For example, the C-terminus of RPAP2 may bind to free Rpb6, but not Rpb6, within the Pol II complex.

Alternatively, the interaction between Rpb6 and the C-terminus of RPAP2 may be transient and may depend on a specific change in the conformation of the Pol II complex. We speculate that a structural change in the Pol II complex may occur at a specific stage of transcription, such as pausing or termination.

At present, the molecular basis of the defective pre-mRNA 3'-end formation caused by knockdown of RPAP2 is unclear. Because there are no reports that RPAP2 interacts directly with 3'-end processing factors, it is possible that RPAP2 indirectly participates in pre-mRNA 3'-end formation. Like its yeast counterpart Rtr1, RPAP2 may function as a phosphatase that is specific for Ser5P in the CTD of Pol II (9,10,23). Recently, our group demonstrated that Ssu72, another Ser5P-specific phosphatase, is required for efficient pre-mRNA 3'-end formation of protein-coding genes in vertebrate cells (13). Based on these observations, we speculate that RPAP2 may regulate pre-mRNA 3'-end formation by controlling the phosphorylation status of the CTD of Pol II because these processes are intimately linked (3). Notably, a recent study demonstrated that Rtr1 also exhibits phosphatase activity that is specific for Tyr1P in the CTD of Pol II (24). Removing the Tyr1P marker from the CTD of Pol II is a prerequisite for the efficient recruitment of 3'-end formation factors to the elongating Pol II complex (25); therefore, RPAP2 may also affect the efficiency of pre-mRNA 3'-end formation by dephosphorylating Tyr1P.

The distributions of RPAP2 on protein-coding genes identified by ChIP analyses (Figure 3) resemble those of Ser2-phosphorylated Pol II (14). A recent study by Ni *et al.* (9) demonstrated that the Pol II-interacting proteins, RPRD1A and RPRD1B/CREPT, both of which contain CTD-interaction domains, interact directly with RPAP2 and serve as scaffolds that coordinate the dephosphorylation of Ser5P. Ni *et al.* (9) also showed that RPRD1A and RPRD1B interact directly with the Ser2P-containing CTD of Pol II and occupy protein-coding genes from the promoter to the 3'-end. Notably, Lu *et al.* (26) demonstrated that RPRD1B/CREPT accelerates tumorigenesis by regulating transcription termination to control the expression of cell-cycle-related genes. Together with the results presented here, these previous findings suggest that RPAP2 participates in transcription elongation and/or termination processes by interacting with Rpb6, or by acting on Ser5P of the CTD of Pol II in collaboration with RPRD1A/B. We are now using ChIP analyses and run-on assays in RPAP2-silenced cells to analyze the Pol II occupancy downstream of the 3'-end processing sites to determine whether RPAP2 participates in transcription termination.

Acknowledgements

We thank Dr. Koji Hisatake (University of Tsukuba) for providing plasmids. We also thank all of our

lab members for helpful discussion. This work was supported by Grants-in-Aid for Scientific Research on Innovative Areas (Y.O.; MEXT KAKENHI grant numbers 24118003 and 25131704) from the Ministry of Education, Science.

References

- Corden JL. Tails of RNA polymerase II. *Trends Biochem Sci.* 1990; 15:383-387.
- Eick D, Geyer M. The RNA polymerase II carboxy-terminal domain (CTD) code. *Chem Rev.* 2013; 113:8456-8490.
- Hsin JP, Manley JL. The RNA polymerase II CTD coordinates transcription and RNA processing. *Genes Dev.* 2012; 26:2119-2137.
- Boulon S, Pradet-Balade B, Verheggen C, Molle D, Boireau S, Georgieva M, Azzag K, Robert MC, Ahmad Y, Neel H, Lamond AI, Bertrand E. HSP90 and its R2TP/Prefoldin-like cochaperone are involved in the cytoplasmic assembly of RNA polymerase II. *Mol Cell* 2010; 399:912-924.
- Forget D, Lacombe AA, Cloutier P, Lavalleye-Adam M, Blanchette M, Coulombe B. Nuclear import of RNA polymerase II is coupled with nucleocytoplasmic shuttling of the RNA polymerase II-associated protein 2. *Nucleic Acids Res.* 2013; 41:6881-6891.
- Carre C, Shiekhattar R. Human GTPases associate with RNA polymerase II to mediate its nuclear import. *Mol Cell Biol.* 2011; 31:3953-3962.
- Forget D, Lacombe AA, Cloutier P, Al-Khoury R, Bouchard A, Lavalleye-Adam M, Faubert D, Jeronimo C, Blanchette M, Coulombe B. The protein interaction network of the human transcription machinery reveals a role for the conserved GTPase RPAP4/GPN1 and microtubule assembly in nuclear import and biogenesis of RNA polymerase II. *Mol Cell Proteomics.* 2010; 9:2827-2839.
- Jeronimo C, Forget D, Bouchard A, Li Q, Chua G, Poitras C, Therien C, Bergeron D, Bourassa S, Greenblatt J, Chabot B, Poirier GG, Hughes TR, Blanchette M, Price DH, Coulombe B. Systematic analysis of the protein interaction network for the human transcription machinery reveals the identity of the 7SK capping enzyme. *Mol Cell.* 2007; 27:262-274.
- Ni Z, Xu C, Guo X, *et al.* RPRD1A and RPRD1B are human RNA polymerase II C-terminal domain scaffolds for Ser5 dephosphorylation. *Nat Struct Mol Biol.* 2014; 21:686-695.
- Egloff S, Zaborowska J, Laitem C, Kiss T, Murphy S. Ser7 phosphorylation of the CTD recruits the RPAP2 Ser5 phosphatase to snRNA genes. *Mol Cell.* 2012; 45:111-122.
- Hirose Y, Iwamoto Y, Sakuraba K, Yunokuchi I, Harada F, Ohkuma Y. Human phosphorylated CTD-interacting protein, PCIF1, negatively modulates gene expression by RNA polymerase II. *Biochem Biophys Res Commun.* 2008; 369:449-455.
- Fan H, Sakuraba K, Komuro A, Kato S, Harada F, Hirose Y. PCIF1, a novel human WW domain-containing protein, interacts with the phosphorylated RNA polymerase II. *Biochem Biophys Res Commun.* 2003; 301:378-385.
- Wani S, Yuda M, Fujiwara Y, Yamamoto M, Harada F, Ohkuma Y, Hirose Y. Vertebrate Ssu72 regulates and coordinates 3'-end formation of RNAs transcribed by RNA polymerase II. *PLoS One* 2014; 9: e106040.
- Glover-Cutter K, Kim S, Espinosa J, Bentley DL. RNA polymerase II pauses and associates with pre-mRNA processing factors at both ends of genes. *Nat Struct Mol Biol.* 2008; 15:71-78.
- Armache KJ, Kettenberger H, Cramer P. Architecture of initiation-competent 12-subunit RNA polymerase II. *Proc Natl Acad Sci U S A.* 2003; 100:6964-6968.
- Cramer P, Bushnell DA, Kornberg RD. Structural basis of transcription: RNA polymerase II at 2.8 angstrom resolution. *Science.* 2001; 292:1863-1876.
- Spahr H, Calero G, Bushnell DA, Kornberg RD. Schizosaccharomyces pombe RNA polymerase II at 3.6-A resolution. *Proc Natl Acad Sci U S A.* 2009; 106:9185-9190.
- Bushnell DA, Kornberg RD. Complete, 12-subunit RNA polymerase II at 4.1-A resolution: implications for the initiation of transcription. *Proc Natl Acad Sci U S A.* 2003; 100:6969-6973.
- Chen CY, Chang CC, Yen CF, Chiu MT, Chang WH. Chang, Mapping RNA exit channel on transcribing RNA polymerase II by FRET analysis. *Proc Natl Acad Sci U S A.* 2009; 106:127-132.
- Werner F, Grohmann D. Evolution of multisubunit RNA polymerases in the three domains of life. *Nat Rev Microbiol.* 2011; 9:85-98.
- Armache KJ, Mitterweger S, Meinhart A, Cramer P. Structures of complete RNA polymerase II and its subcomplex, Rpb4/7. *J Biol Chem.* 2005; 280:7131-7134.
- Tan Q, Prysak MH, Woychik NA. Loss of the Rpb4/Rpb7 subcomplex in a mutant form of the Rpb6 subunit shared by RNA polymerases I, II, and III. *Mol Cell Biol.* 2003; 23:3329-3338.
- Mosley AL, Pattenden SG, Carey M, Venkatesh S, Gilmore JM, Florens L, Workman JL, Washburn MP. Rtr1 is a CTD phosphatase that regulates RNA polymerase II during the transition from serine 5 to serine 2 phosphorylation. *Mol Cell.* 2009; 34:168-178.
- Hsu PL, Yang F, Smith-Kinnaman W, Yang W, Song JE, Mosley AL, Varani G. Rtr1 is a dual specificity phosphatase that dephosphorylates Tyr1 and Ser5 on the RNA polymerase II CTD. *J Mol Biol.* 2014; 426:2970-2981.
- Mayer A, Heidemann M, Lidschreiber M, Schrieck A, Sun M, Hintermair C, Kremmer E, Eick D, Cramer P. CTD tyrosine phosphorylation impairs termination factor recruitment to RNA polymerase II. *Science.* 2012; 336:1723-1725.
- Lu D, Wu Y, Wang Y, Ren F, Wang D, Su F, Zhang Y, Yang X, Jin G, Hao X, He D, Zhai Y, Irwin DM, Hu J, Sung JJ, Yu J, Jia B, Chang Z. CREPT accelerates tumorigenesis by regulating the transcription of cell-cycle-related genes. *Cancer Cell.* 2012; 21:92-104.

(Received November 14, 2014; Accepted November 17, 2014)

Development of mucoadhesive buccal films from rice for pharmaceutical delivery systems

Siriporn Okonogi^{1,*}, Sakornrat Khongkhunthian², Sanchai Jaturasitha³

¹Department of Pharmaceutical Sciences, Faculty of Pharmacy, Chiang Mai University, Chiang Mai, Thailand;

²Department of Restorative Dentistry and Periodontology, Faculty of Dentistry, Chiang Mai University, Chiang Mai, Thailand;

³Department of Animal and Aquatic Science, Faculty of Agriculture, Chiang Mai University, Chiang Mai, Thailand.

Summary

The aim of this work was to investigate the suitable rice varieties for developing pharmaceutical buccal films. Two rice varieties with extreme difference in amylose content were used. Rice powders were chemically modified to yield the carboxymethyl rice prior to film preparation. Scanning electron microscope (SEM) and X-ray diffractometer (XRD) were used to investigate the solid structure of rice powders. The results indicated that amylose content in the rice grains played the effects on the morphology and crystalline structure of the modified rice powders as well as the film properties. The modified rice powders of low amylose content showed halo pattern XRD whereas some crystalline peaks could be observed from the high amylose content modified rice powders. Adding of glycerin caused the films better properties of more transparency and getting rid of air bubbles. High amylose rice films showed more transparency and higher mucoadhesive property and was considered to be suitable for incorporating the drug. Adding of surfactant caused the increase in tensile strength and decrease in elongation of the rice films. The most suitable surfactant for diclofenac buccal rice film is Tween 20. This study demonstrates that rice grains are the promising natural source for pharmaceutical film forming agent. Suitable pharmaceutical buccal films could be developed from the rice with high amylose content.

Keywords: Rice film, mucoadhesive, buccal mucosa, modified starch, carboxymethyl starch

1. Introduction

The systemic delivery of pharmaceutical active ingredients through buccal mucosa is receiving increased attention as for avoiding acid hydrolysis in the gastrointestinal (GI) tract and the hepatic first-pass effect. Buccal films are the most recently developed dosage form for buccal administration. Moreover, buccal mucoadhesive films show several advantages and popular for local therapy (1,2). Films are preferred over adhesive tablets in terms of flexibility and comfort. Films can help protect the wound surface, thus helping to reduce pain and treat the disease more effectively. In addition, they can circumvent

the relatively short residence time of oral gels on the mucosa, which are easily washed away and removed by saliva. Many pharmaceutical buccal delivery bases are made of synthetic polymers, e.g. copolymers of acrylic acid, polyethylene glycol and monomethylether monomethacrylate (3,4), copolymer of polyisobutylene and polyisoprene (5,6), polyvinyl pyrrolidone (7,8), and eudragit (9-11). Blooming use of these polymers has caused serious environmental problems and petroleum as an important resource for originating such polymers is limited. Biodegradable polymers produced from natural raw materials are of great interest nowadays because of environmental benefits and sustainability (12,13). Among these, starch is considered as a promising candidate for developing sustainable materials owing to its complete biodegradability (14), low cost and renewability (15).

Rice (*Oryza sativa* L.) is the most prized cereal crop plant that is cultivated extensively worldwide since it is the principal staple food for half the world's population

*Address correspondence to:

Dr. Siriporn Okonogi, Department of Pharmaceutical Sciences, Faculty of Pharmacy, Chiang Mai University, Chiang Mai, Thailand.
E-mail: okng2000@gmail.com

(16). Rice grain is considered as an important environmentally friendly raw material for starch. Two major components, amylose and amylopectin, are exist in the rice starch (17,18). Many previous studies have demonstrated great variations in the amylose content in rice grains of different varieties, that allow their classification as waxy (1-2% amylose), very low amylose content (2-12%), low amylose content (12-20%), intermediate amylose content (20-25%) and high amylose content (25-33%) (19-21). It was reported that amylose content played an important role on physicochemical properties of the derived rice products (22). Up to date, less of the earlier study reports the effect of rice variety as on the physicochemical property of the rice films in the view point of pharmaceutical delivery system. In the present study, the rice films prepared from two different rice varieties having far different amylose content was firstly compared in order to select the variety for developing the pharmaceutical films.

2. Materials and Methods

2.1. Materials

Milled white rice grains of two different rice varieties from Thailand; a non-glutinous Saohai and a glutinous Niaw Sanpatong harvested in 2013 were used. Monochloroacetic acid and glycerol were purchased from Sigma Chemical Co. (St. Louis, MO). Sodium hydroxide and glacial acetic acid were from RCI Labscan Co., Ltd. (Bangkok, Thailand). All other chemicals and solvents were of AR grade or the highest grade available.

2.2. Preparation of rice powder and analysis of amylose content

Rice powder was prepared by the wet milling method. The rice grains were firstly cleaned and soaked in water at room temperature overnight. The soaked rice was washed twice with deionized water and blended with addition of water in a blender for 10 min. The filtrate passed through the 80-mesh sieve was centrifuged at 15,000 rpm for 15 min. The solid residue was washed with water and filtered through an 80-mesh and received with a 200-mesh screen. The residue collected on the 200-mesh screen was dried at 55°C for 48 h and ground. The ground rice powder after passing through the 80-mesh sieve was kept in a desiccator for further analysis. Amylose content of the rice powders was assayed using the iodine binding method described by Juliano (23).

2.3. Modification of rice

The raw rice powder of each variety was subjected to

chemical modification prior to prepare the films. The reaction was carried out in a 500 mL three necked round-bottom flask, equipped with motor-driven stirrer. An aqueous solution of 50 g sodium hydroxide in 100 mL solution was prepared and firstly mixed with ethanol at a weight ratio of 1:4. The raw rice powder was added and the mixture was stirred. The temperature was raised to 40°C and the mixture was further stirred at 300 rpm for 30 min. Then, monochloroacetic acid was added. The temperature of the mixture was raised to 50°C and further stirred for 3 h. The solid mass was separated and neutralized using glacial acetic acid and washed several times with 85% ethanol until the silver nitrate test for chloride of the filtrate was negative (24). The solid obtained was dried in an oven at 45°C for 48 h, and then pulverized. The white powder of the modified rice after passing the 80-mesh sieve was kept in a desiccator for further experiments.

2.4. Solid structure characterization

The internal solid structure of the rice powders was investigated by X-ray diffractometry (XRD) using a Siemens D-500 X-ray diffractometer with Cu K α radiation at a voltage of 30 kV and 15 mA. The samples were scanned between $2\theta = 5-60^\circ$ with a scanning speed of 5°/min. Prior to testing, the samples were dried and stored in a desiccator.

The external structure of the samples was investigated by SEM using a JEOL JSM-5410LV (Japan) equipped with a large field detector. The acceleration voltage was 10-20 kV under low vacuum mode (0.7-0.8 torr).

2.5. Film preparation

Rice films were prepared from the modified rice powders obtained from each rice variety by casting technique. Exact weight of 5 g of the modified rice powder was dispersed in distilled water. The final volume was adjusted to 100 mL. The dispersions were heated to 90°C in a closed chamber for 2 h and gently stirred in order to obtain clear homogenous liquid gel and avoiding of air bubble formation. In order to study the effects of other additional substances including drugs on the film properties, they were added to this gel before going to further step. Exact portion of the obtained rice gel was poured into a glass petri dish. The gels were spread uniformly over the entire surface and dried at 60°C for 6 days. After drying, cast films were removed. The physical appearance of the films was observed visually.

2.6. Film thickness

Thickness of the films was measured using a precision digital micrometer (Fowler, model FOW52-229-001,

Pennsylvania, USA) with an accuracy of 0.0001 mm. The mean thickness of each film was determined from an average of ten random locations on the film.

2.7. Mechanical properties of the films

The examined mechanical properties of the films included tensile strength and elongation at break were determined using an Instron Universal Testing Machine Model 1000 (H1K-S,UK) with the procedure according to ASTM D 882-80a (25) with the 24 h preconditioning and testing performed at 27 ± 2 °C, $65 \pm 2\%$ RH according to TIS949-2533 (26). The film samples were cut with sharp scissors into 10×70 mm rectangles for each film and used as a test specimen. The initial grip separation and cross-head speed was set at 100 mm and 20 mm/min, respectively. There were ten sample measurements for each kind of rice film.

2.8. Mucoadhesive study of the films

The films were cut into $20 \text{ mm} \times 20 \text{ mm}$ dimensions and subsequently investigated for the mucoadhesive property using a method described by Kundu *et al.* (27) with some modification. After 30 s immersing in water, the wet films were placed on a freshly excised porcine intestinal mucosa, fixed on a glass slide with very thin cellotape so that the exposed mucous membrane was 20×20 mm. Similarly, fresh porcine intestinal mucosa was also fixed on another glass slide, superimposed on the free film surface so that the film laid between the two mucosa bars. The surface area of the film plates and the intestinal mucosa were exactly the same to avoid direct attachment of the mucosa to each other. Finally, the plates were subjected to a little pressure for 2 min. The lower slide was fixed while the other slide was attached to a thread which passed over a system of pulley and was connected to a small plastic container filled with water to confer load. The force of detachment was measured from the load at which detachment of the film from the mucosa occurred.

2.8. Statistic analysis

Descriptive statistics for continuous variables were calculated and reported as a mean±standard deviation. Data were analyzed using a one-way analysis of variance (ANOVA) and Duncan's multiple range test ($p < 0.05$) using Statistica software version 11.

3. Results and discussion

3.1. Solid structure of rice and amylose content

The raw rice flours have similarly outer appearance in comparison with their modified powders when observed visually as seen in Figure 1. The amylose content of the

glutinous NSP was found to be 4% whereas that of the non-glutinous SH was 21%. This extreme difference of amylose content is considered to be due to the variety of the rice. Observation by SEM demonstrates different morphology between NSP and SH varieties as illustrated in Figure 2. Layered organization with some small pieces of supposedly "broken particles" possibly as a result of the preparation process (28) was clearly observed in NSP particles. The chemical method and conditions used in the present study to modify the rice starch to carboxymethyl type caused a significant change to the rice particles and this effect was clearly seen under SEM investigation. The modified SH particles were swollen and the surface edges were obviously unsharpened which some of them were either clustered or merged together. The modified rice particles of NSP displayed more prominent change in shape and surface with extremely higher swelling and merging than SH which some part appeared as complete fusion that the individual particles could not be observed. The surface of the modified NSP also displayed rough and wrinkle. Internal structure investigated by XRD demonstrates some crystalline identical peaks of the raw starch particles indicating that the raw rice powders of both varieties have crystalline structure as seen in Figure 3. After modification, the internal structure of the rice was obviously changed as shown in Figure 4. The XRD



Figure 1. Outer appearance of the rice powders.

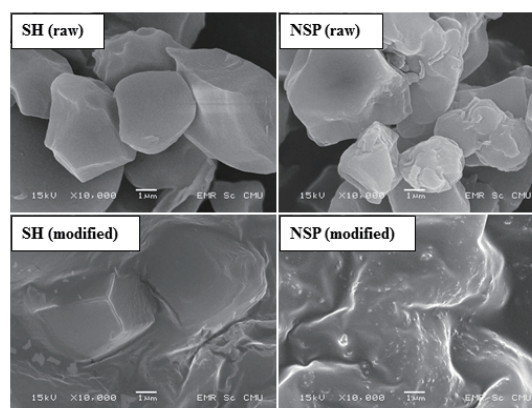


Figure 2. SEM morphology of the rice powders.

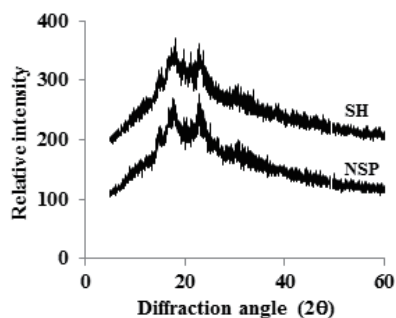


Figure 3. XRD diffractograms of the raw rice powders.

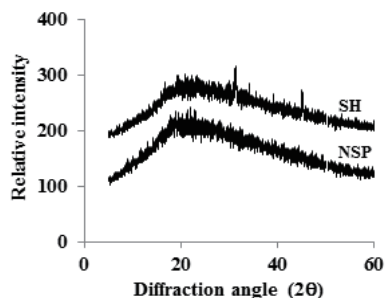


Figure 4. XRD diffractograms of the modified rice powders.

halo patterns were found indicating the destruction of crystalline structure into amorphous form. However, the level of crystalline destruction was different. The internal structure of NSP was completely changed to amorphous structure whereas some crystalline peaks were observed in that of SH. It was concluded that the low amylose content (NSP) rice had higher swelling and obviously higher microstructure change than the high amylose content (SH) variety. Our results indicate the influence of amylose content in the rice starch.

3.2. Effect of additive substance on film appearance and thickness

The film opacity is used to assess the transparency of the films. Preferable pharmaceutical buccal film bases should be transparent, odorless, tasteless, and colorless. The films obtained from 5% modified rice showed slightly white opaque with some small air bubbles and brittle. The received films exhibited rice odor and tasteless. Three common film plasticizers; glycerin, propylene glycol, or polyethylene glycol 400 was used in order to improve film quality. As shown in Figure 5. The plasticizers displayed a role to solve these problems but in different level. No air bubble was seen in the films with all additives but the films added with propylene glycol or polyethylene glycol 400 was still opaque and fragile. NSP films gave similar results but more opaque than those of SH. The best films of both rice varieties were obtained after added with glycerin. Further investigation was done with the effect of glycerin concentration on film thickness. It was found that adding glycerin in the range of 0.75-2.5% caused

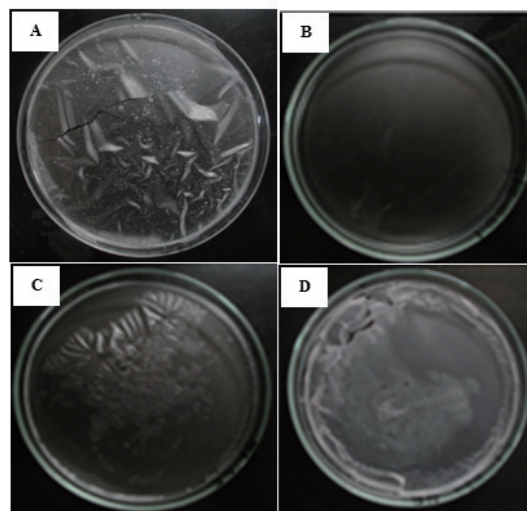


Figure 5. Outer appearance of SH Films without additive substance (A), with 1.5% glycerin (B), 1.5% propylene glycol (C), and 1.5% polyethylene glycol 400 (D).

Table 1. Effect of glycerin on film thickness

Glycerin (%)	Film thickness (mm)	
	SH	NSP
0.00	0.057 ± 0.005	0.058 ± 0.004
0.75	0.054 ± 0.009	0.051 ± 0.016
1.00	0.054 ± 0.008	0.049 ± 0.009
1.25	0.051 ± 0.007	0.047 ± 0.005
1.50	0.051 ± 0.007	0.048 ± 0.009
2.50	0.050 ± 0.004	0.049 ± 0.007

the decrease in film thickness in both rice varieties as seen in Table 1. However, it was observed that the films with more than 1.5% glycerin were slightly liquefied and difficult to get off from the casting mold. Therefore, glycerin 1.5% was selected to add in the film formulation for further study.

3.3. Mucoadhesive property of the films

Mucoadhesive films have been designed to remain in contact with the buccal mucosa for therapeutic purposes for prolonged periods of time. Hence, the measurement of the mucoadhesive strength or time of mucoadhesion is important to respond the desirable property of the buccal films. In these experiments, instead of measuring time of mucoadhesion, the study was focused on determining the mucoadhesive strength or the force of adhesion of the films. The mucoadhesive force of the developed rice films of both rice varieties was found to be obviously different. SH film demonstrated the significantly higher mucoadhesive strength of $191.5 \pm 6.2 \text{ Kg/m}^2$ whereas NSP film exhibited the strength of $137.1 \pm 5.1 \text{ Kg/m}^2$. It was reported that films with high amylose content forms a network of stiff strands and pores present in the network could possibly entrap more water (29). This leads to increase the adhesive bond between the starch polymer in the films and

Table 2. Tensile strength and elongation of the films

Film composition	Tensile strength (kPa)	Elongation (%)
SH 5%, Glycerin 1.5%	0.76 ± 0.12	153 ± 23
SH 5%, Glycerin 1.5%, Drug 0.25%	0.67 ± 0.17	241 ± 21
SH 5%, Glycerin 1.5%, Drug 0.25%, Tween-20 0.1%	2.39 ± 0.19	139 ± 11
SH 5%, Glycerin 1.5%, Drug 0.25%, Tween-80 0.1%	1.23 ± 0.14	101 ± 18
SH 5%, Glycerin 1.5%, Drug 0.25%, Triton-X-100 0.1%	1.63 ± 0.18	132 ± 14

the biological substrates in the mucosa layer such as hydrogen bonds and van der Waals forces (30,31).

3.4. Tensile strength and elongation of the films

A good pharmaceutical buccal film must withstand the normal stress encountered during its application. Tensile strength is the maximum tensile stress sustained by the sample during the tension test. If maximum tensile stress occurs at either the yield point or the breaking point, it is designated tensile strength at yield or at break, respectively (32). In this experiment, the film of SH was selected because of its better properties than that of NSP, such as more transparency and higher mucoadhesive strength. Diclofenac sodium (DS) was used as a model drug because the drug can be used in the buccal cavity for anti-inflammatory and analgesic activity. DS was incorporated into the films formulation to yield the drug percentage of 0.25% in the films. According to enhance the solubility of the drug to be dispersed molecularly and thoroughly the films, three kinds of surfactant; Tween-20, Tween-80, or Triton-X-100 at a concentration of 0.1% was added. The results are shown in Table 2. It was found that the unloaded rice film had high strength with a breaking point at 0.76 ± 0.12 kPa. After drug loading, the tensile strength of the films was slightly decreased with a breaking point at 0.67 ± 0.17 kPa. Interestingly, adding surfactant caused the significant increase in tensile strength of the films. The increasing power was depended on the surfactant type. It was found that among the three surfactants used, Tween-20 showed the highest activity on enhancing of the film strength with a breaking point at 2.39 ± 0.19 kPa. The obvious increasing tensile strength by surfactant was considered to be due to a high formation of intermolecular bonding inside the film. The tensile strength of the films prepared from different type of surfactant was different. This phenomenon indicated the critical type of the surfactant suitable for film-forming components.

Elongation at the break is an indication of the films' flexibility and stretch ability (extensibility), which is determined at the point when the film breaks under tensile testing and is expressed as the percentage of change of the original length of the specimen between

the grips of a film to stretch (extend). It was found that elongation of the films was affected by the incorporated drug and surfactant. The elongation of the drug loading rice film without surfactant was higher than that of the free film. However, adding surfactant caused the decrease of film elongation property. Among three surfactants used, Tween-20 gave the least decrease of elongation.

4. Conclusion

The present study explored the development of pharmaceutical mucoadhesive buccal films using rice as film forming agent. Amylose content in the rice grains showed the effects on the morphology and crystalline structure of the modified rice powders and the film properties. Adding of glycerin caused the films better properties of more transparency and getting rid of air bubbles. High amylose rice films showed more transparency and higher mucoadhesive property and was considered to be suitable for incorporating the drug. Adding of surfactant caused the increase in tensile strength and decrease in elongation of the rice films. The most suitable surfactant of diclofenac buccal rice film is Tween 20.

Acknowledgements

This study work supported by the grants from the National Council Research of Thailand (NRCT), and the Higher Education Research Promotion and National Research University Project of Thailand, Office of the Higher Education Commission.

References

1. Jones DS, Medlicott NJ. Casting solvent controlled release of chlorhexidine from ethylcellulose films prepared by solvent evaporation. *Int J Pharm.* 1995; 114:257-261.
2. Senel S, Ikinici G, Kas S, Yousefi-Rad A, Sargon MF, Hincal AA. Chitosan films and hydrogels of chlorhexidine gluconate for oral mucosal delivery. *Int J Pharm.* 2000; 193:197-203.
3. Shojaei AH, Berner B, Li X. Transbuccal delivery of acyclovir: I. *In vitro* determination of routes of buccal transport. *Pharm Res.* 1998; 15:1182-1188.
4. Shojaei AH, Zhuo SL, Li X. Transbuccal delivery of acyclovir (II): Feasibility, system design, and *in vitro* permeation studies. *J Pharm Pharm Sci.* 1998; 1:66-73.
5. Guo JH. Bioadhesive polymer buccal patches for buprenorphine controlled delivery: Formulation, *in-vitro* adhesion and release properties. *Drug Dev Ind Pharm.* 1994; 20:2809-2821.
6. Guo JH, Cooklock KM. The effects of backing materials and multilayered systems on the characteristics of bioadhesive buccal patches. *J Pharm Pharmacol.* 1996; 48:255-257.
7. Anders R, Merkle HP. Evaluation of laminated mucoadhesive patches for buccal drug delivery. *Int J Pharm.* 1989; 49:231-240.

8. Save T, Shah MU, Ghamande AR, Venkitachalam P. Comparative study of buccoadhesive formulations and sublingual capsules of nifedipine. *J Pharm Pharmacol.* 1994; 46:192-195.
9. Cui Z, Mumper RJ. Buccal transmucosal delivery of calcitonin in rabbits using thin-film composites. *Pharm Res.* 2002; 19:1901-1906.
10. Cui Z, Mumper RJ. Bilayer films for mucosal (genetic) immunization via the buccal route in rabbits *Pharm Res.* 2002; 19:947-953.
11. Jay S, Fountain W, Cui Z, Mumper RJ. Transmucosal delivery of testosterone in rabbits using novel bi-layer mucoadhesive wax-film composite disks. *J Pharm Sci.* 2002; 91:2016-2025.
12. Kinci GI, Senel S, Akincibay H, Kas S, Ercis S, Wilson CG, Hincal AA. Effect of chitosan on a periodontal pathogen *Porphyromonas gingivalis*. *Int J Pharm.* 2002; 235:121-127.
13. Rossi S, Sandri G, Ferrari F, Bonferoni MC, Caramella C. Buccal delivery of acyclovir from films based on chitosan and polyacrylic acid. *Pharm Dev Technol.* 2003; 8:199-208.
14. Araújo MA, Cunha A, Mota M. Enzymatic degradation of starch-based thermoplastic compounds used in prostheses: Identification of the degradation products in solution. *Biomaterials* 2004; 25:2687-2693.
15. Zhang JF, Sun XZ. Mechanical properties of PLA/starch composites compatibilized by maleic anhydride. *Biomacromol.* 2004; 5:1446-1451.
16. Hagenimana A, Ding X, Fang T. Evaluation of rice flour modified by extrusion cooking. *J Cereal Sci.* 2006; 43:38-46.
17. Zhou Z, Robards K, Helliwell S, Blanchard C. Composition and functional properties of rice. *Int J Food Sci Tech.* 2002; 37:849-868.
18. Yu S, Ma Y, Sun DW. Impact of amylose content on starch retrogradation and texture of cooked milled rice during storage. *J Cereal Sci.* 2009; 50:139-144.
19. Coffman WR, Juliano BO. Rice. In: Nutritional quality of cereal grains: Genetic and agronomic improvement (Olson RA, Frey KJ, eds.). Madison, American Society of Agronomy, 1987; pp. 101-131.
20. Ong MH, Blanshard JMV. Texture determinants in cooked, parboiled rice. I: Rice starch amylose and the fine structure of amylopectin. *J Cereal Chem.* 1995; 21:251-260.
21. Frei M, Siddhuraju P, Becker K. Studies on *in vitro* starch digestibility and the glycemic index of six different indigenous rice cultivars from the Philippines. *Food Chem.* 2003; 83:395-402.
22. Lourdin D, Della Valle G, Colonna P. Influence of amylose content on starch films and foams. *Carbohydr Polym.* 1995; 27:261-270.
23. Juliano BO. A simplified assay for milled-rice amylose. *Cereal Sci Today* 1971; 16:334-360.
24. Pfeiffer K, Heinze Th, Lazik W. Starch derivatives of high degree of functionalization. 5. Stepwise carboxymethylation of amylose. *Chem Pap.* 2002; 56:261-266.
25. ASTM, American society of testing and materials. Standard test methods for tensile properties of thin plastic sheeting. D 882 Annual book of ASTM standards, 1995.
26. TIS 949-1990, Thai Industrial standards institute. Standard for oriented polypropylene films, 1990.
27. Kundu J, Patra C, Kundu SC. Design, fabrication and characterization of silk fibroin-HPMC-PEG blended films as vehicle for transmucosal delivery. *Mater Sci Eng C.* 2008; 28:1376-1380.
28. Wang LF, Pan SY, Hu H, Miao WH, Xu XY. Synthesis and properties of carboxymethyl kudzu root starch. *Carbohydr Polym.* 2010; 80:174-179.
29. Muscat, D, Adhikari B, Adhikari R, Chaudhary DS. Comparative study of film forming behaviour of low and high amylose starches using glycerol and xylitol as plasticizers. *J Food Eng.* 2012; 109:189-201.
30. Kinloch AJ. The science of adhesion. Part 1: Surface and interfacial aspects. *J Mater Sci.* 1980; 15:2141-2166.
31. Chickering D, Mathiowitz E. Definitions, mechanisms, and theories of bioadhesion. In: *Bioadhesive Drug Delivery Systems: Fundamentals, Novel Approaches, and Development* (Mathiowitz E, Chickering D, Lehr C, eds.). Marcel Dekker Inc, New York, USA, 1999.
32. ASTM. Standard test method for tensile properties of plastics. D638. In ASTM. Annual book of American standard testing methods (Vol. 15.09, pp. 159e171). Philadelphia, 1991.

(Received October 28, 2014; Accepted December 15, 2014)

Ion-exchange complex of famotidine: sustained release and taste masking approach of stable liquid dosage form

Reham Mokhtar Aman*, Mahasen Mohamed Meshali, Galal Mahmoud Abdelghani

Department of Pharmaceutics, Faculty of Pharmacy, Mansoura University, Mansoura, Egypt.

Summary

A stable controlled release resinate-complex for the highly bitter taste famotidine (FAM) was developed to allow once-daily administration and improve patient compliance especially in pediatric and geriatric medicine. The drug-resinate complexes were prepared in different drug to resin (Amberlite IRP-69) ratios by weight (1:1, 1:2, 1:3, 1:4, 1:5 and 1:6). The optimized drug-resinate complex resulted from 1:6 drug to resin ratio experienced maximum drug loading and sustained release property. Hence, it was subjected to physicochemical characterizations by differential scanning calorimetry (DSC), x-ray diffractometry (XRD), Fourier transform infrared spectroscopy (FTIR) and scanning electron microscope (SEM). The optimized complex was further dispensed in the prepared syrup and the suspension was subjected to accelerated stability study, as mentioned in the International Conference on Harmonization (ICH) guidelines. Furthermore, the gustatory properties of the complex were evaluated on humans. The syrup complied successfully with ICH guidelines and sufficiently alleviated the bitterness of famotidine.

Keywords: Famotidine (FAM), amberlite IRP-69, complexation, physicochemical characterizations, gustatory test

1. Introduction

Famotidine (FAM) is 3-([2-(diaminomethyleneamino)thiazol-4-yl] methylthio)-N'-sulfamoylpropanimidamide (1). It is very slightly soluble in water and in dehydrated alcohol, freely soluble in glacial acetic acid, and highly dissolvable in dilute mineral acids. It has been reported that poor lipophilicity, poor aqueous solubility and susceptibility to gastric degradation may contribute to the low and variable oral bioavailability (2). FAM is classified as a competitive inhibitor of histamine H₂-receptors on the basolateral membrane of parietal cells. It reduces stomach acid production by 90% or more when given in single oral doses of 20 or 40 mg and promotes healing of duodenal ulcers (3). It is useful in treating heartburn, healing ulceration and inflammation of the esophagus resulting from acid (gastroesophageal reflux disease (GERD)). High doses are used for treating conditions characterized by marked increase in acid

secretion such as Zollinger-Ellison syndrome. The current commercially marketable dosage forms for FAM are tablets, capsules and chewable tablets for adults. Additionally, FAM powder for oral suspension was prepared, evaluated and marketed to harmonize pediatric and geriatric patients, but its stability is limited to 30 d after reconstitution (4). FAM has extremely bitter taste which would be highly noticeable when administered as an oral liquid that also suffers from poor stability. Hence, researchers tried several approaches to mask the bitter taste (5).

Ion exchange resins (IER) are cross-linked water insoluble high molecular weight polyelectrolytes that can exchange their mobile ions of equal charge with the surrounding medium reversibly and stoichiometrically (6). Drugs can be loaded onto the resins by an exchanging reaction, and hence, a drug resinate complex is formed.

Amberlite IRP-69 resin is strong cation exchange resin derived from a sulfonated copolymer of styrene and divinylbenzene. It is supplied as sodium salt in the form of dry and fine powder. In addition to taste masking, it is employed as a carrier for cationic drugs and controlled release excipient (7-9).

*Address correspondence to:

Dr. Reham Mokhtar Aman, Department of Pharmaceutics, Faculty of Pharmacy, Mansoura University, Mansoura, Egypt. E-mail: rehamaman@yahoo.com

The present work aims at assessing the possibility of FAM-resinate complex formation with Amberlite IRP-69. The prepared and optimized drug-resinate complex would be subsequently suspended in the prepared syrup. Stability study of this syrup according to International Conference on Harmonization (ICH) guidelines would be of special concern. Previous research by the authors reported an optimized liquid dosage form for an essential drug for pediatric and geriatric medicine (10). The prepared and optimized drug-resinate complex that experienced maximum drug loading would be subjected to physicochemical characterization immediately after preparation by differential scanning calorimetry (DSC), x-ray diffractometry (XRD), Fourier transform infrared spectroscopy (FTIR) and scanning electron microscope (SEM). In addition, accelerated stability study would be performed for the complexes in the dry state and in the prepared syrup.

2. Materials and Methods

2.1. Materials

FAM was kindly supplied by Memphis Chemical Company, Cairo, Egypt. Amberlite IRP-69 and benzalkonium chloride were purchased from Sigma-Aldrich (Saint Louis, MO, USA). Sorbitol and glycerin were obtained from El-Nasr Pharmaceutical Chemical Co., Cairo, Egypt. Sucrose was purchased from United Company for Chemicals, Cairo, Egypt.

2.2. Preparation of drug-resinate complexes

In highly acidic conditions (e.g. 0.1 N HCl, pH 1.2), FAM was demonstrated to be extremely unstable. The degradation process of FAM was reported to be highly dependent on the pH of the solution, although a relatively stable profile for the drug was achieved at pH 4.0 (11).

Drug-resinate complexes were prepared by a single batch process. The time required for constant amount of the drug to react with the resin was taken as the equilibrium time. This was achieved by assaying the supernatant during preparation of the resinate complex. Amberlite resin (50, 100, 150, 200, 250, and 300 mg) was soaked overnight each in a beaker containing 50 mL of HCl (pH 4.0) and stirred with magnetic stirrer (Heidolph, U S A) to facilitate swelling and activation of the resin (12). Fifty mL of FAM solution (1 mg/1mL) in HCl (pH 4.0) was added to each beaker containing the calculated and activated amberlite resin to prepare 1:1, 1:2, 1:3, 1:4, 1:5 and 1:6 drug to resin ratios by weight complexes. The high drug to resin ratio (1:6) was based on its cationic exchange capacity (5 meq/g) (13). The resultant solutions were stirred at room temperature for 24 h.

The FAM-resinate complexes were separated by

decantation, and washed two times with deionized water to remove unassociated drug and other ions. The complexes were then dried in hot air oven (Heraeus GS model B 5042, Germany) for 5 h at 45°C to a constant weight (14) and stored in a tight glass vial.

2.3. Characterization and optimization of the prepared complexes

Complexes of FAM and amberlite were characterized and optimized based on the drug content and *in vitro* drug release using the following methods.

2.3.1. Estimation of FAM content

Samples of the powdered complexes in triplicates were analyzed for FAM's content. Twenty mg samples were weighed and diluted with 10 mL 0.1 N HCl with vigorous shaking followed by sonication in an ultrasonic bath (Sonix USA, SS101H230) for 5 h in order to release and dissolve the drug from complex. The filtered samples were further diluted with 0.1N HCl, and then analyzed for FAM content spectrophotometrically using a UV-Vis double beam scanning spectrophotometer (Labomed, INC, UVD-2950, USA) at 263 nm. The drug-resinate complex with maximum drug content was the optimized one.

2.3.2. *In vitro* drug release studies

The dissolution profiles of untreated pure drug and the drug-resinate complexes were examined using USP type II paddle dissolution apparatus (Six-jars, USP rotating basket, dissolution test apparatus, DA-6D, India) at $37 \pm 0.5^\circ\text{C}$ and 50 rpm. The dissolution medium was 900 mL 0.1 N HCl (pH 1.2). Twenty mg sample of the pure drug or dry complex containing a known amount of FAM equivalent to the pure drug were weighed and each introduced to the dissolution tester cells. At predetermined intervals, 5 mL of the dissolution medium were taken and replaced with an equal volume of fresh dissolution medium in order to maintain the sink condition throughout the experiment. The collected aliquots were filtered and the absorbance of FAM was recorded using a UV-Vis spectrophotometer at 263 nm. Each experiment was done in triplicate and the average percentage released was calculated at each time interval.

2.3.3. Kinetic analysis of the drug release data

To examine the kinetics of drug release, the release data were fitted to models representing zero-order, first-order, Higuchi's square root of time (15) and Korsmeyer-Peppas equation (16). The coefficients of determination (r^2) were determined from regression plots of m vs. t , $\log(m_0 - m)$ vs. t and m vs. $t^{1/2}$, for zero-

order, first-order, and Higuchi's model respectively. In these plots, m represents the cumulative percent of drug released at time t , and $m_0 - m$ is the percentage of the drug remained after time t . For Korsmeyer-Peppas, the equation was:

$$M_t/M_\infty = kt^n \quad (1)$$

Where M_t/M_∞ is the fraction of the drug released after time t and n is a characteristic exponent for the release mechanism. Based on Korsmeyer-Peppas equation, values of the n exponent equal to or less than 0.5 were characteristic of Fickian or quasi-Fickian diffusion, whereas values in the range of 0.5 to 1 were an indication of an anomalous mechanism for drug release (16). On the other hand, a unity value for n would be expected for zero-order release. Models were evaluated using GraphPad Prism 5 software (GraphPad Software Inc., San Diego, CA, version 5.03) computer program.

2.4. Evaluation of the optimized complex

Since complex resulted from 1:6 drug to resin ratio experienced maximum drug loading, the drug-resinate were subjected to physicochemical characterization immediately after preparation by DSC, XRD, FTIR, and SEM. Evaluating molecular properties of drug-resinate complex and comparing them to the drug alone, the resin and their corresponding physical mixture was essential to reveal formation of complex. Furthermore, accelerated stability study was performed for the optimized complex in the dry state and in the prepared syrup for a period of six months. Gustatory test for the fresh suspension of the resinate complex in the prepared syrup was fulfilled.

2.4.1. Differential scanning calorimetry

Differential scanning calorimetry (DSC) was performed for the optimized complex using a Perkin-Elmer Differential Scanning Colorimeter model DSC-4 (New York, USA). It was calibrated with indium (99.99% purity, melting point 156.6°C). Eight mg samples of each of FAM, amberlite IRP-69, physical mixture and dry optimized complex were crimped in standard aluminum pans and heated from 30 to 350°C at a heating rate of 10°C/min under constant purging of dry nitrogen at 30 mL/min. An empty pan, sealed in the same way as the sample, was used as a reference.

2.4.2. X-ray diffractometry

X-ray diffraction patterns (XRD) of FAM, amberlite IRP-69, physical mixture of both and dry optimized complex were obtained using a Diano X-ray diffractometer equipped with Co K α (USA). The tube operated at 45 kv, 9 mA.

2.4.3. Fourier transform infrared spectroscopy

Spectroscopic studies of FAM, amberlite IRP-69, their corresponding physical mixture and dry optimized drug-resinate complex were done by using Mattson 5000 FTIR Spectrophotometer (Madison Instruments, Middleton, Wisconsin, USA). KBr discs were prepared by means of hydrostatic press. The scanning range was 400 to 4,000 cm^{-1} .

2.4.4. Scanning electron microscope

The surface morphology of the samples was examined using scanning electron microscope (SEM) (JSM-6510LV, JEOL, Japan). The powders were fixed on a brass stub using double-sided adhesive tape and then made electrically conductive by coating, in a vacuum, with a thin layer of gold (approximately 150 Å) for 30 s.

2.4.5. Accelerated stability studies of optimized complex

Preparation of syrup The prepared syrup consisted of sucrose 54%, glycerin 5% and sorbitol 4% to retard crystallization of sucrose. The polyols were Generally Recognized as Safe (GRAS) and are listed in the Food and Drug Administration (FDA) (17). Benzalkonium chloride 0.01% was added as a preservative (18). This prepared syrup containing drug-resinate complex has a great advantage of having pH of about 6. At this pH value, the corresponding degradation rate of FAM was reported to be significantly decreased (11).

Accelerated stability study according to the ICH Accelerated stability study as mentioned in ICH guidelines was followed to evaluate physical changes and drug content of the optimized drug-resinate complex on storage (19). The stability study was performed for the complex in the dry state and in the prepared syrup dosage form. Dry resinate complex (137.07 ± 7.23 mg) containing the adult dose (20 mg) was either packed in glass bottles wrapped with aluminum foil, or suspended in 15 mL of the prepared syrup and then placed at ambient conditions ($28 \pm 2^\circ\text{C}/40 \pm 5\%$ RH) for 6 months. Others for accelerated stability study were placed in humidity chamber at ($40 \pm 2^\circ\text{C}/75 \pm 5\%$ RH) for the same period. Relative humidity (RH) was maintained at 75% using saturated solutions of sodium chloride. The RH (75% and 40%) were measured periodically. Drug content of the dry complex as well as the complex suspended in the prepared syrup was analyzed every three-month period as previously described and statistically analyzed.

Special stability experiment was performed monthly for the prepared syrup preparation. Sample of the supernatant was withdrawn, filtered through a Millipore filter (0.45 μm) and analyzed for drug released from the complex, if any. In addition, the pH change of the prepared syrup was monitored at the stipulated

times using digital pH-meter (Beckman Instruments Fullerton, CA 92634, Germany). Re-dispersibility of the prepared syrup preparation was also assessed monthly. The closed glass bottle was inverted through 180° and the number of inversions required for restoration was noted. If uniformity attained in one inversion, then it has 100% re-dispersibility. Every additional inversion decreases the % of ease of re-dispersibility by 5% (20).

2.4.6. Gustatory sensation test

Gustatory test reported by Mady *et al.* (2) for evaluating the taste masking ability of the ternary complexation of FAM was fulfilled for the fresh optimized drug-resinate complex suspension in the prepared syrup with slight modification. Twelve healthy human volunteers, of either sex; in the age group of 23-30 years were selected. The volunteers signed the protocol of the investigation before starting the study. This study was approved by the Scientific Research Ethical Committee at Faculty of Pharmacy, Mansoura University and all the procedures were performed under the terms and conditions of such committee.

Before testing, the volunteers ($n = 12$) were asked to retain the reference solution in their mouths for 10 s, and provide information on its bitterness intensity. Reference solution of the drug suspended in the prepared syrup was used (20 mg pure FAM suspended in 15 mL of the prepared syrup). The determination of the threshold was carried out as follows: immediately after the preparation, each volunteer held about 3 mL of the reference solution in their mouths for 10 s; the volunteers were then requested to recognize this taste and consider it as score 6. After expectoration, the bitterness value was recorded. A numerical scale was used with the following values: 0 = bitterless, 1 = very slightly bitter, 2 = slightly bitter, 3 = moderately bitter, 4 = moderate to strong bitter, 5 = strongly bitter, 6 = very strongly bitter.

Sample consisting of the optimized dry resinate complex (154.3 ± 4.92 mg) containing the adult dose (20 mg) and suspended in 15 mL of the prepared syrup. The volunteers were asked to repeat the same procedure as with the reference solution and to assign a bitterness score for it. The oral cavity was rinsed with distilled water three times to avoid bias. The wash out period between testing different samples was 10 min.

3. Results and Discussion

Taste is considered an important parameter in liquid dosage forms since the taste is perceived in mouth. IER works as a complexing agent and thus eliminates the bitter taste of drugs. For preparation of resinates, batch method was preferred because of its convenience. As the reaction is an equilibrium phenomenon, maximum efficiency in shorter time is best achieved in batch

process. Also, higher swelling efficiency in batch process resulted in more surface area for ion exchange (21). The time to reach equilibrium for drug loading was found to be 24 h. The dissolved drug existed in the protonated ion could displace the hydrogen counterion (H^+) of the sulfonic acid functional group on the ion exchange resin, as depicted in the following equation:



Where Re is an insoluble portion of the resin and FH^+ is FAM ion.

3.1. Characterization and optimization of the prepared complexes

3.1.1. Estimation of FAM content

A linear increase in FAM loading has been recorded with increased resin ratio (Figure 1). The loading of the drug onto the resin was more than (80%) of the drug added for 1:6 drug to resin complex.

3.1.2. *In vitro* drug release studies

Figure 2 illustrates the *in vitro* release characteristics of FAM from different drug-resinate complexes in 0.1 N HCl. For the pure drug, the maximum percentage release reached 100% in 20 min as it is freely soluble in 0.1 N HCl. The existence of hydrogen ions in the dissolution medium (H^+) acted as a cationic counterion and could exchange for the drug in the resinate complex resulting in its liberation. About 60% of the drug was released from the complexes in about one and half h and near total in about 5 h. The sustained release property of strongly cationic exchange resin, with various drugs has been reported by Ngawhirunpat *et al.* (22). This technique may be of value for the

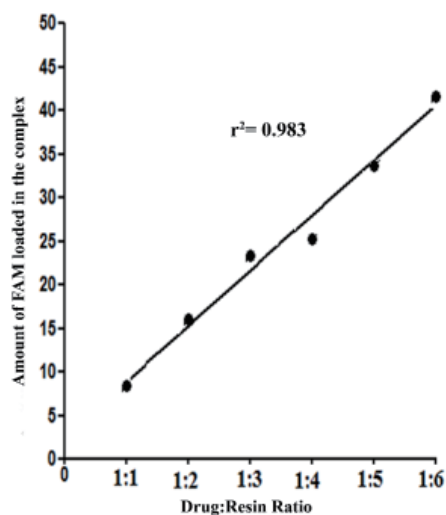


Figure 1. Effect of different drug: resin ratios (1:1 to 1:6) on the amount of FAM loaded in the complex.

pharmaceutical industries, especially in preparing palatable liquid dosage form of FAM with sustained release properties.

3.1.3. Kinetic analysis of the drug release data

The coefficient of determination of the drug release kinetics (r^2) and the exponent "n" for Korsmeyer-Peppas equation were presented in Table 1. The results revealed that there was a linear relationship between the percent drug released from all drug-resinate complexes and the square root of time indicating a typical release pattern according to Higuchi's equation. Mild deviation was noticed with 1:2 drug to resin complex but this will not influence the final conclusion. Since the exponent "n" values were found to be in the range of 0.2107-0.3675 for all the drug-resinate complexes, the result could be described as a quasi-Fickian diffusion mechanism (23). Untreated FAM showed a linear relationship between log percent of drug remaining to be released and time thus following first-order kinetics.

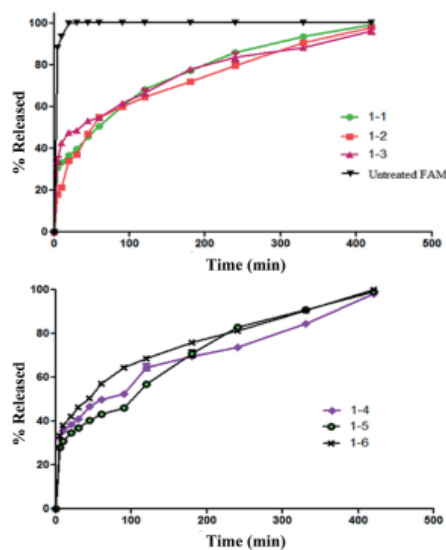


Figure 2. *In vitro* release profiles of untreated FAM and FAM from drug-resinate complexes prepared from different drug: resin ratios (1:1 to 1:6) in 0.1 N HCl. The values were the average of three determinations \pm standard deviation (S.D.).

3.2. Evaluation of the optimized complex

Since complex resulted from 1:6 drug to resin ratio experienced maximum drug loading (Figure 1), the drug-resinate were subjected to physicochemical characterization immediately after preparation by DSC, XRD, FTIR, and SEM. Meanwhile, accelerated stability study was performed for the optimized complex in the dry state and in the prepared syrup. Gustatory test for the fresh suspension of the resinate complex in the prepared syrup was fulfilled.

3.2.1. Differential scanning calorimetry (DSC)

Figure 3 shows the DSC curves of FAM, resin, physical mixture and drug-resinate complex. FAM has an endothermic peak at 166.7°C, indicating the temperature of drug melting, whereas no peak over the range 150-350°C was observed in the DSC curves of the drug-resinate (Figure 3a and d). This indicates that the entrapped drug in the resinate changed from the crystalline to the amorphous state.

The thermal trace shown by the resin was characterized by a broad endothermic peak at 105.5°C as a result of the partial dehydration process of the resin (Figure 3b) (24). The thermogram of the physical mixture of both showed the same peaks of FAM and the resin indicating the absence of complexation among them on physical mixing (Figure 3c).

3.2.2. X-ray diffractometry (XRD)

The XRD patterns of the samples are shown in Figure 4. It appears that the molecular state of FAM is crystalline as it shows several sharp and narrow peaks between 10° and 40° (2 θ) with the maximum peak intensity at 2 θ = 23.973° (d = 3.70898 Å) (Figure 4a). The resin x-ray diffractogram displayed diffused peak due to their amorphous state (Figure 4b) (24).

It was noted that, FAM-resinate physical mixture diffractogram was simply the superimposed spectra of the two components, indicating that no complexation occurred upon physical mixing (Figure 4c). The complete disappearance of crystallinity in case of drug-resinate complex compared to the drug alone or its

Table 1. Kinetic analysis for the percentage drug released from FAM-resinate complexes*

Drug: resin ratio	Coefficient of determination " r^2 "			Korsmeyer-Peppas		Main transport mechanism
	Zero-order	First-order	Higuchi model	r^2	n**	
Untreated FAM	0.9367	0.9595	0.9367	-----	-----	-----
1:1	0.9198	0.9066	0.9895	0.9652	0.2727	Fickian
1:2	0.8662	0.9170	0.9712	0.9818	0.3675	Fickian
1:3	0.9129	0.8961	0.9818	0.9692	0.2107	Fickian
1:4	0.9579	0.8128	0.9860	0.9523	0.2303	Fickian
1:5	0.9662	0.8475	0.9789	0.9265	0.2703	Fickian
1:6	0.9203	0.7170	0.9922	0.9847	0.2393	Fickian

* Analyzed by the regression coefficient method. ** Diffusional exponent indicative of the mechanism of drug release.

physical mixture, confirmed the complex formation between FAM and the resin (Figure 4d).

3.2.3. Fourier transform infrared spectroscopy (FTIR)

The FTIR spectroscopic analysis was performed to augment the results obtained from DSC and XRD (Figure 5). From (Figure 5a), the strong infrared shoulders at $3,505\text{-}3,237\text{ cm}^{-1}$ and $1,640\text{-}1,534\text{ cm}^{-1}$ region are assigned to the stretching and bending vibrations of NH_2 groups in both guanidine and sulfamoyl parts in FAM, respectively (25). The asymmetric and symmetric stretching modes of SO_2 group are generally assigned in $1,325$ and $1,146\text{ cm}^{-1}$, respectively.

The spectra of the physical mixture (Figure 5c) did not show any significant change in the position of the characteristic absorption bands. These spectra appeared

to be consistent with that of FAM and the resin indicating that there was no appreciable interaction between the drug and resin in the physical mixture, which is in accordance with the results from DSC and XRD.

In the FTIR spectra of the resinate complex, however, the absorption bands at $3,505\text{-}3,237\text{ cm}^{-1}$ and $1,640\text{-}1,534\text{ cm}^{-1}$ region disappeared, probably owing to a restriction of the vibration related to complexation process (Figure 5d).

3.2.4. Scanning electron microscope (SEM)

The scanning electron photomicrographs for FAM, the resin, FAM/resin physical mixture and FAM-resinate complex were presented in Figure 6. It appeared that most of the drug crystals are elongated tabular form (Figure 6a), while amberlite resin is irregular in

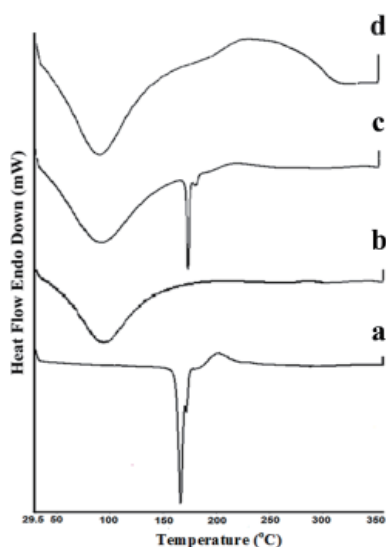


Figure 3. DSC of pure FAM (a), Amberlite IRP-69 resin (b), physical mixture of FAM and the resin (c) and optimized drug-resinate complex (d).

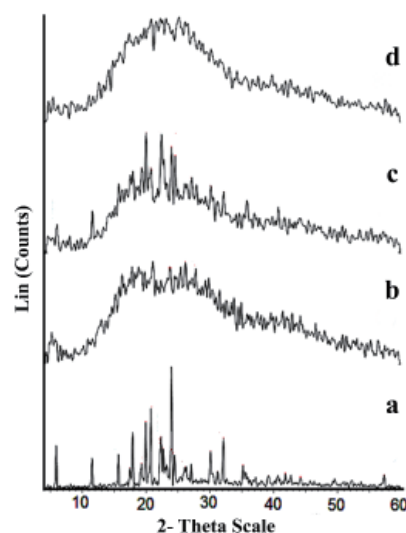


Figure 4. XRD diffractograms of pure FAM (a), Amberlite IRP-69 resin (b), physical mixture of FAM and the resin (c) and optimized drug-resinate complex (d).

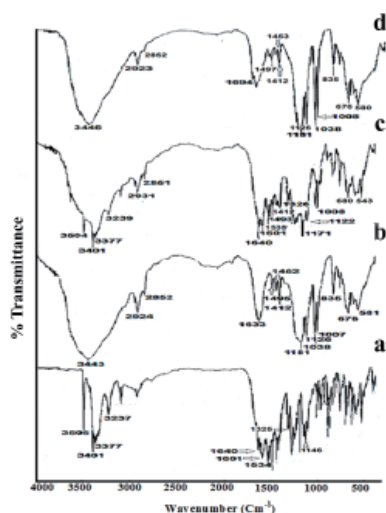


Figure 5. FTIR spectra of pure FAM (a), Amberlite IRP-69 resin (b), physical mixture of FAM and the resin (c) and optimized drug-resinate complex (d).

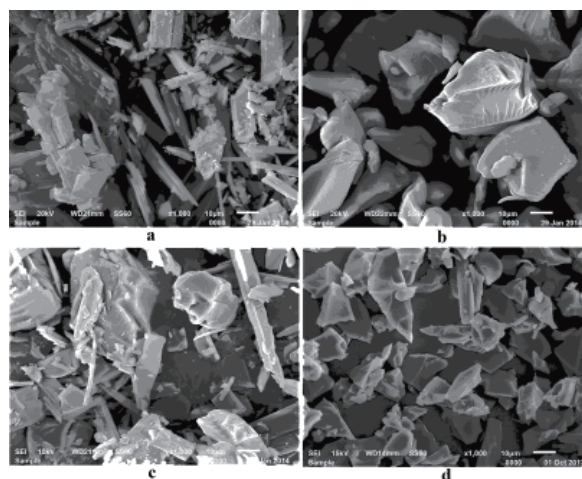


Figure 6. SEM of pure FAM (a), Amberlite IRP-69 resin (b), physical mixture of FAM and the resin (c) and optimized drug-resinate complex (d).

shape and appears as separate pieces (Figure 6b) (24). Physical mixture was observed as a mixture of drug and the resin where it was easy to identify the individual component of FAM and resin (Figure 6c). Meanwhile, FAM-resinate looked different in appearance from the drug, the resin or their physical mixture. The features of drug crystals were not easily detectable indicating formation of a different compound (Figure 6d).

3.2.5. Accelerated stability studies of optimized complex

The stability study was performed for the complex in the dry state and in the prepared syrup dosage form. Both of them did not experience any physical changes at ambient and accelerated stability study conditions for a period of six months. The supernatant of the suspension was nearly free of the drug during the six months period stability study indicating absence of drug leaching into the vehicle after storage. This was assessed by UV scanning of the filtered syrup monthly at 263 nm, using prepared syrup without suspended complex as a blank (Figure 7). From Table 2 it may be concluded that no

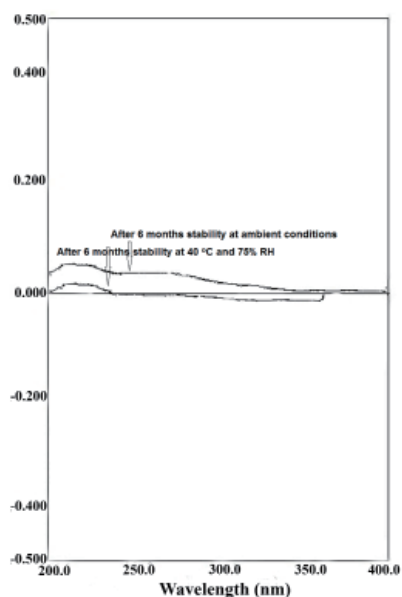


Figure 7. UV scan of the filtered syrup containing the suspended complex after six months of storage at ambient conditions and humidity chamber at ($40 \pm 2^\circ\text{C}/75 \pm 5\%$ RH).

Table 2. Stability studies of dry optimized FAM-resinate complex (1:6 drug to resin ratio) and suspended complex in the prepared syrup

Time	A- Dry complex		B- Suspended complex in prepared syrup	
	Drug content (mg)		Drug content (mg)	
	$40 \pm 2^\circ\text{C}/75 \pm 5\%$ RH	$28 \pm 2^\circ\text{C}/40 \pm 5\%$ RH	$40 \pm 2^\circ\text{C}/75 \pm 5\%$ RH	$28 \pm 2^\circ\text{C}/40 \pm 5\%$ RH
0 Months	20 ± 0.166 mg (100%)	20 ± 0.166 mg (100%)	20 ± 1.694 mg (100%)	20 ± 0.716 mg (100%)
3 Months	19.351 ± 0.251 mg (96.753%)	19.318 ± 0.426 mg (96.658%)	19.442 ± 0.579 mg (97.209%)	19.347 ± 0.532 mg (96.736%)
6 Months	18.989 ± 0.179 (94.947%)	19.070 ± 2.048 (95.342%)	19.298 ± 1.401 (96.488%)	18.898 ± 1.517 (94.493%)
p Value*	0.0013	0.6438	0.7624	0.4507

* Insignificant at $p > 0.001$.

significant difference, ($p > 0.001$) by one-way analysis of variance (ANOVA) (Tukey's test), in drug content was experienced during storage at the two different temperatures.

Furthermore, the pH of the suspension in the prepared syrup originally equal 6 reached values of 5.76 and 4.93 at ambient and accelerated stability conditions, respectively. The number of inversions required to completely re-disperse the suspension ranged from 1-4 times along the stipulated intervals, indicating good re-dispersibility.

The drug-resinate complex prepared to achieve taste masking has the potential to affect the product performance beyond this objective, that is, stability during shelf-life, as well as in the stomach (5).

3.2.6. Gustatory sensation test

The results concerning the bitterness evaluation using consensual volunteers are listed in Table 3. The mean score of 0 for the sample indicated that the optimized complex resulting from 1:6 drug to resin ratio sufficiently alleviated the bitterness of FAM, compared with the reference solution containing the drug alone suspended in the prepared syrup. The complexation with the resin impeded the interaction of FAM with the taste buds. Similar masking effects of the bitter taste of cefetamet pivoxil hydrochloride (an oral third generation cephalosporin antibiotic) using amberlite IRP-69 and amberlite IRP-64 were obtained previously by Sateesha *et al.* (26).

4. Conclusions

Famotidine has an extremely bitter taste and is unstable in acidic medium. A novel controlled release complex with amberlite resin was prepared. The complexation

Table 3. Bitterness score evaluation by a panelist of 12 human volunteers

Formulations	Number of volunteers rating the preparation as						
	0	1	2	3	4	5	6
Reference		7	2	3			
Sample	11	1					

with the resin impeded the interaction of famotidine with the taste buds and sustained its release in the acidic medium. Moreover, complexation was investigated using various physical characterization methods namely differential scanning calorimetry, x-ray diffractometry, Fourier transform infrared spectroscopy and scanning electron microscope. The complex in the dry state and in the prepared syrup dosage form complied with ICH guidelines for stability. Gustatory test on human for drug-resinate complex in the prepared syrup, as well, indicated that the preparation is palatable. Thus, the "patient friendly dosage form" of bitter drug, especially for pediatric, geriatric, bedridden, and non-cooperative patients, was successfully formulated using this technology.

Acknowledgements

The authors wish to thank Memphis Chemical Company, Cairo, Egypt for kindly providing us with famotidine.

References

- Tripathi KD. Essentials of Medical Pharmacology. 5th Ed, New Delhi: Jaypee Brothers Medical Publishers, 2003; p. 588.
- Mady FM, Abou-Taleb AE, Khaled KA, Yamasaki K, Iohara D, Ishiguro T, Hirayama F, Uekama K, Otagiri M. Enhancement of the aqueous solubility and masking the bitter taste of famotidine using drug/SBE-beta-CyD/povidone K30 complexation approach. *J Pharm Sci.* 2010; 99:4285-4294.
- Rang HP, Dale MM, Ritter JM, Flower RJ, Henderson G. Rang and Dale's Pharmacology: The gastrointestinal tract. Elsevier Churchill Livingstone, New York, USA, 2012; pp. 360-371.
- Pepcid AC Advanced Patient Information. <http://www.drugs.com/cons/pepcid-ac.html> (accessed February 08, 2014).
- Mady FM, Abou-Taleb AE, Khaled KA, Yamasaki K, Iohara D, Taguchi K, Anraku M, Hirayama F, Uekama K, Otagiri M. Evaluation of carboxymethyl-beta-cyclodextrin with acid function: improvement of chemical stability, oral bioavailability and bitter taste of famotidine. *Int J Pharm.* 2010; 397:1-8.
- Venkatesh DP, karki R, Goli D, Jha SK. Over view-ion exchange resins in controlled drug delivery system. *WJPPS.* 2013; 2:4764-4777.
- Shamma RN, Basalious EB, Shoukri RA. Development and optimization of a multiple-unit controlled release formulation of a freely water soluble drug for once-daily administration. *Int J Pharm.* 2011; 405:102-112.
- Srikanth MV, Sunil SA, Rao NS, Uhumwangho MU, Ramana Murthy KV. Ion exchange resins as controlled drug delivery carriers. *J Sci Res.* 2010; 2:597-611.
- Abdel-Bary A, Abdel-Monem H, Badawy SS. Microencapsulation of mebeverine hydrochloride resins. *Proceeding of XXI Conf. of Pharm Sci.* February 20, 1989, Cairo, Egypt; pp. 207-225.
- Aman R, Meshali M, Abdelghani G. Optimization and formulation of cinnarizine-loaded chitosan microspheres in liquid dosage form for pediatric therapy. *Drug Deliv Lett.* 2014; 4:128-141.
- Wu Y, Fassihi R. Stability of metronidazole, tetracycline HCl and famotidine alone and in combination. *Int J Pharm.* 2005; 290:1-13.
- Tawakkul MA, Shah RB, Zidan A, Sayeed VA, Khan MA. Complexation of risperidone with a taste-masking resin: novel application of near infra-red and chemical imaging to evaluate complexes. *Pharm Dev Technol.* 2009; 14:409-421.
- Amberlite IRP-69. www.dow.com/amberlite_irp69/html (accessed February 09, 2014).
- Muqtader M, Ali S. Development of famotidine buoyant drug delivery system using natural polymers. *Int J Biopharm.* 2012; 3:17-21.
- Dash S, Murthy PN, Nath L, Chowdhury P. Kinetic modeling on drug release from controlled drug delivery systems. *Acta Pol Pharm.* 2010; 67:217-223.
- Merchant HA, Shoaib HM, Tazeen J, Yousuf RI. Once-daily tablet formulation and *in vitro* release evaluation of cefpodoxime using hydroxypropyl methylcellulose: A technical note. *AAPS PharmSciTech.* 2006; 7:E178-E183.
- Polyols. <http://www.springerreference.com/docs/html/chapterdbid/134984.html> (accessed October 2, 2013).
- Gao R, Shao ZJ, Fan ACL, Witchey-Lakshmanan LC, Stewart DC. Taste masking of oral quinolones liquid preparations using ion exchange resins. U.S. Patent, No. 6,514,492, 2003.
- Sana S, Rajani A, Sumedha N, Mahesh B. Formulation and evaluation of taste masked oral suspension of dextromethorphan hydrobromide. *Int J Drug Dev Res.* 2012; 4:159-172.
- Rani AP, Wessam H. Full Factorial design in formulation of lamotrigine suspension using locust bean gum. *Int J Chem Sci.* 2013; 11:751-760.
- Shende MA, Markandeywar T. Photostability studies and development of fast release nifedipine tablets. *IJPBS.* 2010; 1:1-14.
- Ngawhirunpat T, Goegebakan E, Duangjit S, Akkaramongkolporn P, Kumpugdee-Vollrath M. Controlled release of chlorpheniramine from resins through surface coating with eudragit® RS 100. *Int J Pharm Pharm Sci.* 2010; 2:107-112.
- Beg S, Swain S, Gahoi S, Kohli K. Design, development and evaluation of chronomodulated drug delivery systems of Amoxicillin trihydrate with enhanced antimicrobial activity. *Curr Drug Delivery.* 2013; 10:174-187.
- Fathy M. Interaction of tiramide hydrochloride with amberlite resins: characterization of the interaction and modulation of the release through microencapsulation of the prepared resins. *Bull Pharm Sci. Assiut University.* 2006; 29:111-126.
- Gupta V, Ain S, Babita K, Ain Q, Dahiya J. Solubility enhancement of the poorly water-soluble antiulcer drug famotidine by inclusion complexation. *IJPSN.* 2013; 6:1983-1989.
- Sateesha SB, Rajamma AJ, Shekar HS, Divakar G. Formulation development and rheological studies of palatable cefetamet pivoxil hydrochloride dry powder suspension. *Daru.* 2011; 19:118-125.

(Received November 13, 2014; Revised December 4, 2014; Accepted December 21, 2014)

Central nervous system infection with non-tuberculous mycobacteria: A report of that infection in two patients with AIDS

Rentian Cai¹, Tangkai Qi¹, Hongzhou Lu^{1,2,3,*}

¹Department of Infectious Disease, Shanghai Public Health Clinical Center, Fudan University, Shanghai, China;

²Huashan Hospital affiliated to Fudan University, Shanghai, China;

³Medical College of Fudan University, Shanghai, China.

Summary Meningitis caused by non-tuberculous mycobacteria (NTM) has a low incidence and is a rare form of NTM infection. In an increasing number of cases, however, disseminated mycobacterial infection is noted in acquired immune deficiency syndrome (AIDS). Described here are two patients with AIDS who were infected with NTM. Both patients eventually died, but one did receive anti-NTM treatment. Non-tuberculous mycobacterial meningitis must be suspected in patients with AIDS who present with prolonged fever and brain symptoms, and anti-NTM drugs should be promptly administered if necessary.

Keywords: Non-tuberculous mycobacteria, meningitis, AIDS

1. Introduction

Non-tuberculous mycobacteria (NTM) are organisms that typically live free in the environment in soil, water, milk, food, aerosols, and wild and domestic animals. NTM are *Mycobacterium* species but do not include the *M. tuberculosis* complex (*M. tuberculosis*, *M. africanum*, *M. bovis*, *M. microti*, *M. canetti*, and *M. leprae*). However, NTM include *Mycobacterium avium* complex (MAC), *M. kansasii*, rapidly growing mycobacteria (RGM), *M. flavescens*, *M. scrofulaceum*, *M. szulgai*, and *M. goodnae*. NTM can cause a wide variety of infections, including pulmonary, lymphatic, skin, soft tissue, skeletal, and catheter-related infections (1).

NTM infections are relatively common in patients with acquired immune deficiency syndrome (AIDS) and especially is those with a CD4 T lymphocyte cell count < 50 cells/ μ L. Although NTM can cause serious pulmonary and disseminated infection in some patients (2), central nervous system (CNS) infections with brain lesions are rare. Moreover, there are no reports in China of patients infected with HIV who have developed meningitis due to NTM.

Reported here are two patients with AIDS who were subsequently infected with NTM. The process of diagnosis and treatment of these two patients may provide a useful reference for treatment of NTM meningitis.

2. Case report

2.1. Case 1

A 48-year-old man who was infected with HIV had a fever for 3 months and weakness in both lower limbs for 1 week that went without treatment.

On admission, the patient had white patches in his mouth and grade 4 muscle strength in his lower limbs. However, he had normal muscle tone. The presumptive diagnoses were: 1. AIDS; 2. a fungal infection of the oral cavity; and 3. a CNS infection.

Two days after admission, a chest CT scan revealed multiple opacities in both lungs and enlarged lymph nodes in the mediastinum. Brain MRI images are shown in Figure 1A. The patient's CD4 T and CD8 T cell counts are shown in Table 1. A lumbar puncture was performed and the results of cerebrospinal fluid (CSF) analysis are shown in Table 1. Based on this information, tubercular meningitis was considered and isoniazid, rifampicin, ethambutol, and pyrazinamide were given as anti-tuberculosis therapy. However, the muscle strength in both lower limbs gradually decreased,

*Address correspondence to:

Dr. Hongzhou Lu, Department of infectious diseases, Shanghai Public Health Clinical Center, 2901Caolang Road, Jinshan District, Shanghai 201508, China.
E-mail: luhongzhou@fudan.edu.cn

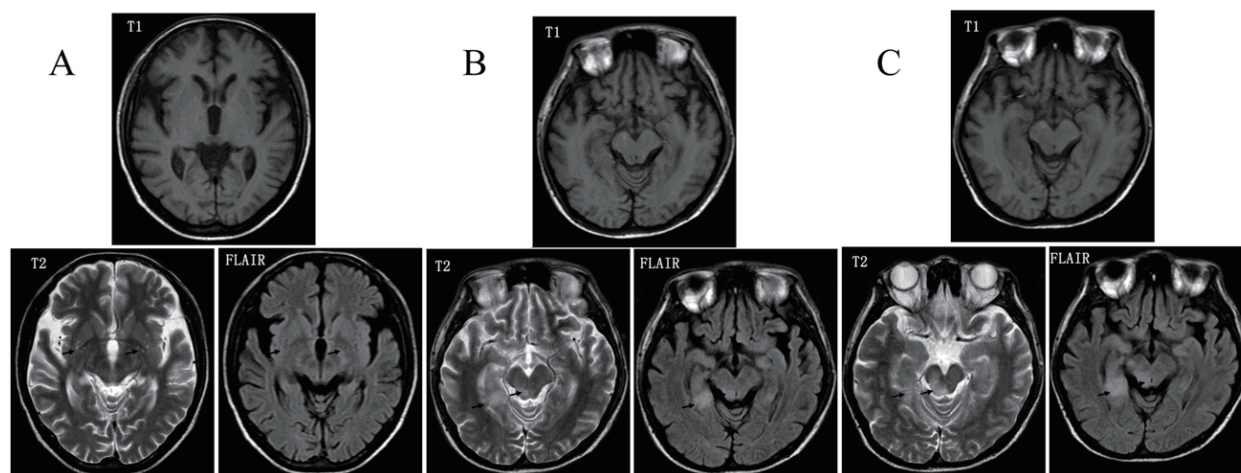


Figure 1. Brain MRI images of two patients. (A) Brain MR imaging revealed both basal ganglia had areas of abnormal signal intensity including hypointensity on T1WI and FLAIR images and hyperintensity on T2WI. Cerebral ventricle dilation and encephalatrophy were also evident. (B) Brain MRI imaging revealed multiple lesions in the cerebrum, cerebellum, and brainstem. Imaging revealed hypointensity in T1WI and hyperintensity in T2WI and FLAIR images. (C) Brain MR imaging revealed multiple lesions in the cerebrum, cerebellum, and brainstem. Imaging revealed hypointensity in T1WI and hyperintensity in T2WI and FLAIR images. There were no significant changes in comparison to image findings in B.

Table 1. Results of laboratory tests of blood and CSF from two patients

Sample	Test	Case 1	Case 2
Blood	Glucose (mmol/L) (the same time as the 1st lumbar puncture)	8.36	4.9
	CD4 count (/ μ L)	2	4
	CD8 count (/ μ L)	75	122
	T-SPOT.TB	N	NA
CSF	Pressure (mmH ₂ O)	150	160
The 1st lumbar puncture	Total leukocyte count (/ μ L)	124	2
	Multinucleated cells (%)	90	NA
	Lymphocytes (%)	10	NA
	Pandy test	WP	N
	Chloride (mmol/L)	113	116
	Glucose (mmol/L)	2.15	2.02
	Protein (mg/L)	428	314
Blood	Glucose (mmol/L) (the same time as the 2nd lumbar puncture)	6.67	5.54
CSF	Pressure (mmH ₂ O)	55	120
The 2nd lumbar puncture	Total leukocyte count (/ μ L)	300	24
	Multinucleated cells (%)	90	NA
	Lymphocytes (%)	10	NA
	Pandy test	P	WP
	Chlorine (mmol/L)	110	118
	Glucose (mmol/L)	1.99	2.54
	Protein (mg/L)	2314	514

NA, not available; N, negative; P, positive; WP, weakly positive.

and urinary retention occurred. Consequently, a lumbar puncture was performed again on the 6th day after admission. The results of CSF analysis are shown in Table 1. Based on the results of CSF analysis, tubercular meningitis was diagnosed again: low glucose levels, low chlorine levels, and smears positive for acid-fast bacilli. However, T-SPOT.TB test results were negative, suggesting the infection was not tuberculosis. The same anti-tuberculosis regimen was maintained. On the 14th

day after admission, muscle strength in the patient's lower limbs was grade 0. The patient lost confidence in the treatment and voluntarily discharged himself from the hospital.

Nine days after discharge, the first CSF culture revealed NTM. The patient's family was informed of the results so that the patient could receive anti-NTM treatment rather than anti-tuberculosis treatment. Unfortunately, the patient had died 7 days after discharge.

2.2. Case 2

A 27-year-old man had symptoms of a dry cough and fever for 6 months and progressive dyspnea for 10 days that went without treatment prior to admission. The man was in a coma for 4 days and he was taken to another hospital. Chest CT scans revealed extensive interstitial hyperplasia, fibrosis, and exudate in both lungs. There were nodular shadows from the posterior segment in the upper lobe of the right lung and as well as pleural thickening. Brain CT scans revealed atrophied frontal and temporal lobes. The preliminary diagnosis was a lung infection. The therapeutic regimen included tracheal intubation with a ventilator, imipenem and cilastatin sodium, norvancomycin, azithromycin, sulfamethoxazole (SMZ), caspofungin, and nutritional support.

The man was admitted to this Hospital because he tested positive for HIV. The preliminary diagnoses were AIDS, a lung infection, and type 1 respiratory failure.

Because the pathogenic microorganism had not been identified, medications included SMZ and caspofungin for *Pneumocystis carinii*, the anti-viral oseltamivir, norvancomycin for Gram-positive bacteria, imipenem and cilastatin sodium for Gram-negative bacteria, azithromycin for mycoplasma, and gamma globulin to improve immunity.

In the first 2 days after admission, CD4 T and CD8 T cell counts were determined (Table 1). On the 3rd day after admission, the patient recovered consciousness. An acid-fast bacilli sputum smear was positive, so tuberculosis infection was considered. Isoniazid, rifampicin, ethambutol, and pyrazinamide were administered as anti-tuberculosis therapy. On the 8th day after admission, anti-retroviral treatment (ART) was begun with tenofovir, lamivudine, and efavirenz. A bedside chest radiograph revealed diffuse inflammation in the lungs with no significant changes. Therefore, tigecycline and amikacin were substituted for norvancomycin. A tracheotomy was performed and the patient was placed on a ventilator. On the 10th day after admission, results of a sputum culture revealed *Acinetobacter baumannii* that was highly drug-resistant. On the 12th day after admission, HIV RNA was 102,000.00 copies/mL. However, caspofungin treatment was sufficient and thus stopped. Fluconazole was used as an anti-fungal agent. Seventeen days after admission, the lung lesions improved and the patient was able to breathe on his own, so mechanical ventilation was stopped. Results of a blood culture revealed mycobacteria and suggested a disseminated mycobacterial disease. Moxifloxacin was added to enhance the anti-tuberculosis regimen.

On the 21st day after admission, the mycobacterium was identified as NTM. Consequently, rifampin, ethambutol, amikacin, azithromycin, and moxifloxacin were used for anti-NTM therapy, and isoniazid and

pyrazinamide were discontinued. Twenty-nine days after admission, the patient's condition improved. Antibiotic therapy was de-escalated, with minocycline substituted for tigecycline and cefoperazone-sulbactam substituted for imipenem and cilastatin sodium. On the 38th day after admission, voriconazole was prescribed as an anti-fungal agent because there was no further improvement of lung lesions. Raltegravir was used as the ART regimen rather than efavirenz because of potential interaction between efavirenz and voriconazole. Fifty days after admission, the lung lesions improved and voriconazole was stopped. On day 51, however, the patient was lethargic and he was unable to speak or even signal his desire to defecate or urinate. Brain MRI images are shown in Figure 1B. A lumbar puncture was performed and the results of CSF analysis are shown in Table 1. A diagnosis of NTM meningitis was considered most likely. Therefore, anti-NTM therapy was continued. On the 57th day after admission, the patient developed dysphagia, which may have been due to encephalopathy associated with HIV infection. Lopinavir and ritonavir tablets, which readily penetrated into the central nervous system, were substituted for efavirenz. Rifabutin was also used instead of rifampin. A lumbar puncture was performed again (Table 1). A subsequent brain MRI is shown in Figure 1C. A chest CT scan revealed that the pulmonary lesions had improved slightly. Sixty-eight days after admission, the first CSF culture revealed NTM. The diagnosis of NTM meningitis was clear and anti-NTM therapy was continued. On day 74, convulsions manifested and the patient lost consciousness. Sodium valproate and carbamazepine were used to control the convulsions. The patient's parents refused use of a ventilator, and 76 days after admission the patient died.

3. Discussion

Saritsiri *et al.* studied 71 patients infected with HIV who were subsequently infected with NTM (3). They noted MAC in 62% of those patients, *M. kansasii* in 15.5%, and RGM in 8.4%. None of the HIV-infected patients they studied had meningitis due to NTM. This finding suggests that MAC infection may constitute the primary form of NTM infection. Medication given to the two patients described here followed the treatment for MAC because there are no guidelines for treatment of meningitis due to NTM. Meningitis due to NTM is rare but often fatal (4).

The two patients reported here presented with weight loss, a chronic cough, a prolonged fever, and nervous system disorders. Biochemical analysis of CSF revealed normal CSF pressure, low levels of chlorine and glucose, and high levels of protein. The patient in Case 1 had muscle strength in his lower limbs and he was diagnosed with tubercular meningitis. Anti-tuberculosis treatment was administered until hospital

discharge although the results of the T-SPOT.TB test, a moderately specific and sensitive test for the diagnosis of tuberculosis (5,6), were negative. The patient in Case 2 presented with a severe pulmonary infection including bacteria, fungi, and NTM. Anti-NTM treatment was started before the emergence of new nervous system symptoms and before the definitive diagnosis of NTM meningitis. However, the patient died after 55 days of anti-NTM treatment. The species of NTM was not identified further. The therapeutic regimen was based on treatment of MAC, the most common species of NTM (7). Drug options for treating disseminated MAC disease include clarithromycin or azithromycin, rifabutin, ethambutol, amikacin or streptomycin, and levofloxacin or moxifloxacin (2). Azithromycin, ethambutol, amikacin, and moxifloxacin were selected and rifampicin was used initially but was switched to rifabutin. Rifampicin, rifabutin, and moxifloxacin are readily able to permeate the blood-brain barrier. Ethambutol has moderate ability to permeate the blood-brain barrier in patients with meningitis. Azithromycin and amikacin have limited ability to permeate the blood-brain barrier. Limited drug selection and time-consuming procedures to diagnose NTM meningitis might be factors for the high mortality rate of NTM meningitis. In a study of 15 patients with MAC meningitis and AIDS, Jacob *et al.* found that the in-hospital mortality rate was 67% (8). However, some of those patients were lost to follow-up.

Recent studies (since 2000) regarding NTM meningitis are predominantly case reports. Dickerman *et al.* reported isolated intracranial MAC infection in a patient (9). The patient was initially treated with a cocktail of anti-MAC medications, including clarithromycin, ethambutol, and rifampin, for 4 months. However, the CNS lesions in the right aspect of the cerebellum continued to grow. Surgery to clear the lesion was successful and the patient remained free of recurrent disease for longer than 2 years. The authors recommended a conventional systemic antibiotic regimen as the first-line treatment for intracranial infections and suggested neurosurgical intervention in cases of medically refractory intracranial infections. However, the patient in that report did not have AIDS. Sharma *et al.* reported that PCR was able to detect co-infection of TB and MAC in CSF from two AIDS patients with meningitis (10). However, neither of the patients received prompt anti-NTM treatment and both died. These previous studies indicate that MAC meningitis is a terminal event in the clinical evolution of AIDS.

Based on previous reports and the two patients reported here, treatment of NTM meningitis requires a

rapid and accurate method of its diagnosis (*e.g.* PCR) and various methods of treatment (*e.g.* neurosurgery). If a patient tests positive for acid-fast bacilli but the T-SPOT.TB test is negative, NTM infection should be suspected.

Acknowledgements

This work was supported by a grant from The 12th Five-Year Major New Drug Discovery Science and Technology (2012ZX09303013). The authors also wish to thank both patients with HIV infection for their cooperation with the report.

References

1. Wagner D, Young LS. Nontuberculous mycobacterial infections: A clinical review. *Infection*. 2004; 32:257-270.
2. Centers for Disease Control and Prevention, National Institutes of Health, HIV Medical Association of the Infectious Diseases Society of America. Guidelines for the Prevention and Treatment of Opportunistic Infections in HIV-Infected Adults and Adolescents. 2013. Q1-Q10.
3. Saritsiri S, Udomsantisook N, Suankratay C. Nontuberculous mycobacterial infections in King Chulalongkorn Memorial Hospital. *J Med Assoc Thai*. 2006; 89:2035-2046.
4. Flor A, Capdevila JA, Martin N, Gavalda J, Pahissa A. Nontuberculous mycobacterial meningitis: Report of two cases and review. *Clin Infect Dis*. 1996; 23:1266-1273.
5. Chen J, Zhang R, Wang J, Liu L, Zheng Y, Shen Y, Qi T, Lu H. Interferon-gamma release assays for the diagnosis of active tuberculosis in HIV-infected patients: A systematic review and meta-analysis. *PLoS One*. 2011; 6:e26827.
6. Cai R, Chen J, Guan L, Sun M, Sun Y, Shen Y, Zhang R, Liu L, Lu H. Relationship between T-SPOT.TB responses and numbers of circulating CD4+ T-cells in HIV infected patients with active tuberculosis. *Biosci Trends*. 2014; 8:163-168.
7. Johnson MM, Odell JA. Nontuberculous mycobacterial pulmonary infections. *J Thorac Dis*. 2014; 6:210-220.
8. Jacob CN, Henein SS, Heurich AE, Kamholz S. Nontuberculous mycobacterial infection of the central nervous system in patients with AIDS. *South Med J*. 1993; 86:638-640.
9. Dickerman RD, Stevens QE, Rak R, Dorman SE, Holland SM, Nguyen TT. Isolated intracranial infection with *Mycobacterium avium* complex. *J Neurosurg Sci*. 2003; 47:101-105; discussion 105.
10. Sharma K, Sharma A, Modi M, Singh G, Kaur H, Varma S, Sharma M. PCR detection of co-infection with *Mycobacterium tuberculosis* and *Mycobacterium avium* in AIDS patients with meningitis. *J Med Microbiol*. 2012; 61:1789-1791.

(Received September 22, 2014; Revised December 11, 2014; Accepted December 21, 2014)

Subject Index (2014)

Policy Forum

Systematic evidence-based clinical practice guidelines are ushering in a new stage of standardized management of hepatocellular carcinoma in Japan.

Song PP, Tang W, Hasegawa K, Kokudo N
2014; 8(2):64-70. (DOI: 10.5582/ddt.8.64)

Reviews

Pharmacological effects and clinical applications of ultra low molecular weight heparins.

Liu Z, Ji SL, Sheng JZ, Wang FS
2014; 8(1):1-10. (DOI: 10.5582/ddt.8.1)

Daily hydroxyl radical scavenging capacity of mammals.

Ienaga K, Park CH, Yokozawa T
2014; 8(2):71-75. (DOI: 10.5582/ddt.8.71)

Perspectives on a combined test of multi serum biomarkers in China: Towards screening for and diagnosing hepatocellular carcinoma at an earlier stage.

Zhang KM, Song PP, Gao JJ, Li GH, Zhao X, Zhang SG
2014; 8(3):102-109. (DOI: 10.5582/ddt.2014.01026)

A map describing the association between effective components of traditional Chinese medicine and signaling pathways in cancer cells *in vitro* and *in vivo*.

Xia JF, Chen JL, Zhang ZM, Song PP, Tang W, Kokudo N
2014; 8(4):139-153. (DOI: 10.5582/ddt.2014.01032)

Advances in the study of molecularly targeted agents to treat hepatocellular carcinoma.

Chen JL, Gao JJ
2014; 8(4):154-164. (DOI: 10.5582/ddt.2014.01031)

The progress in adjuvant therapy after curative resection of liver metastasis from colorectal cancer.

Zhang W, Song TQ
2014; 8(5):194-200. (DOI: 10.5582/ddt.2014.01037)

Chemical constituents and bioactivities of *Colla corii asini*.

Wang DL, Ru WW, Xu YP, Zhang JL, He XX, Fan GH, Mao BB, Zhou XS, Qin YF
2014; 8(5):201-207. (DOI: 10.5582/ddt.2014.01038)

Drug induced pulmonary parenchymal disease.

Prasad R, Gupta P, Singh A, Goel N
2014; 8(6):232-237. (DOI: 10.5582/ddt.2014.01046)

Brief Reports

Design, synthesis and biological evaluation of naphthalimide-based fluorescent probes for α 1-adrenergic receptors.

Zhang W, Chen LZ, Ma Z, Du LP, Li MY
2014; 8(1):11-17. (DOI: 10.5582/ddt.8.11)

Design, synthesis and biological evaluation of 4-chromanone derivatives as I_{Kr} inhibitors.

Wang R, Liu ZZ, Du LP, Li MY
2014; 8(2):76-83. (DOI: 10.5582/ddt.8.76)

Synthesis and biological evaluation of novel indoline-2,3-dione derivatives as antitumor agents.

Li PZ, Tan YM, Liu GY, Liu Y, Liu JZ, Yin YZ, Zhao GS
2014; 8(3):110-116. (DOI: 10.5582/ddt.2014.01012)

Isotryptoquivaline F, a new quinazolinone derivative with anti-TNF- α activity from *Aspergillus* sp. CM9a.

Xue H, Xu QY, Lu CH, Shen YM
2014; 8(5):208-211. (DOI: 10.5582/ddt.2014.01039)

Human mediator subunit MED15 promotes transcriptional activation.

Nakatsubo T, Nishitani S, Kikuchi Y, Iida S, Yamada K, Tanaka A, Ohkuma Y
2014; 8(5):212-217. (DOI: 10.5582/ddt.2014.01036)

Several herbal compounds in Okinawa plants directly inhibit the oncogenic/aging kinase PAK1.

Nguyen BCQ, Taira N, Tawata S
2014; 8(6):238-244. (DOI: 10.5582/ddt.2014.01045)

Clinical features of 80 cases of tinea faciei treated at a rural clinic in Japan.

Noguchi H, Jinnin M, Miyata K, Hiruma M, Ihn H
2014; 8(6):245-248. (DOI: 10.5582/ddt.2014.01049)

Original Articles

Antioxidant activity of *Rafflesia kerrii* flower extract.

Puttipan R, Okonogi S
2014; 8(1):18-24. (DOI: 10.5582/ddt.8.18)

The comparative study of acetyl-11-keto-beta-boswellic acid (AKBA) and aspirin in the prevention of intestinal adenomatous polyposis in *APC^{Min/+}* mice.

Wang RQ, Wang Y, Gao ZH, Qu XJ
2014; 8(1):25-32. (DOI: 10.5582/ddt.8.25)

Combination treatment of ligustrazine piperazine derivate DLJ14 and adriamycin inhibits progression of resistant breast cancer through inhibition of the EGFR/PI3K/Akt survival pathway and induction of apoptosis.

Chen JH, Wang WF, Wang HY, Liu XY, Guo XL
2014; 8(1):33-41. (DOI: 10.5582/ddt.8.33)

Fibroblast growth factor-2 inhibits mineralization of osteoblast-like Saos-2 cells by inhibiting the functioning of matrix vesicles.

Liu C, Cui YZ, Luan J, Zhou XY, Liu ZX, Han JX
2014; 8(1):42-47. (DOI: 10.5582/ddt.8.42)

A combination of oral uracil-tegafur plus leucovorin (UFT + LV) is a safe regimen for adjuvant chemotherapy after hepatectomy in patients with colorectal cancer: Safety report of the UFT/LV study.

Saiura A, Yamamoto J, Hasegawa K, Oba M, Takayama T, Miyagawa S, Ijichi M, Teruya M, Yoshimi F, Kawasaki S, Koyama H, Makuuchi M, Kokudo N
2014; 8(1):48-56. (DOI: 10.5582/ddt.8.48)

A lesson from Japan: Research and development efficiency is a key element of pharmaceutical industry consolidation process.

Shimura H, Masuda S, Kimura H
2014; 8(1):57-63. (DOI: 10.5582/ddt.8.57)

Metabolites from *Aspergillus versicolor*, an endolichenic fungus from the lichen *Lobaria retigera*.

Dou YL, Wang XL, Jiang DF, Wang HY, Jiao Y, Lou HX, Wang XN
2014; 8(2):84-88. (DOI: 10.5582/ddt.8.84)

Exploring the influence of renal dysfunction on the pharmacokinetics of ribavirin after oral and intravenous dosing.

Gupta SK, Kantesaria B, Glue P
2014; 8(2):89-95. (DOI: 10.5582/ddt.8.89)

Synthesis and crystal structure of 6-fluoro-3-hydroxypyrazine-2-carboxamide.

Shi FY, Li ZT, Kong LJ, Xie YC, Zhang T, Xu WF
2014; 8(3):117-120. (DOI: 10.5582/ddt.2014.01028)

Effectiveness of Chinese prescription Kangen-karyu for dyslipidemia, using 3T3-L1 adipocytes and type 2 diabetic mice.

Park CH, Rhyu DY, Noh JS, Park CM, Yokozawa T
2014; 8(3):121-131. (DOI: 10.5582/ddt.2014.01024)

Design of amphiphilic oligopeptides as models for fine tuning peptide assembly with plasmid DNA.

Goparaju GN, Gupta PK
2014; 8(4):165-172. (DOI: 10.5582/ddt.2014.01029)

Subcellular localization of KL-6 mucin in intraductal papillary mucinous neoplasm of the pancreas.

Inagaki Y, Seyama Y, Hasegawa K, Tang W, Kokudo N
2014; 8(4):173-177. (DOI: 10.5582/ddt.2014.01027)

Enhancement of solubility of dexibuprofen applying mixed hydrotropic solubilization technique.

El-Houssieny BM, El-Dein EZ, El-Messiry HM
2014; 8(4):178-184. (DOI: 10.5582/ddt.2014.01019)

Formulation, optimization, and evaluation of a transdermal patch of heparin sodium.

Patel RP, Gaiakwad DR, Patel NA
2014; 8(4):185-193. (DOI: 10.5582/ddt.2014.01030)

R-eriodictyol and S-eriodictyol exhibited comparable effect against H₂O₂-induced oxidative stress in EA.hy926 cells.

Li HZ, Li C, Shen T, Zhao LJ, Ren DM
2014; 8(5):218-224. (DOI: 10.5582/ddt.2014.01033)

***In vitro* and *in vivo* anti-MRSA activities of nosokomycins.**

Uchida R, Hanaki H, Matsui H, Hamamoto H, Sekimizu K, Iwatsuki M, Kim YP, Tomoda H
2014; 8(6):249-254. (DOI: 10.5582/ddt.2014.01050)

Human RNA polymerase II-associated protein 2 (RPAP2) interacts directly with the RNA polymerase II subunit Rpb6 and participates in pre-mRNA 3'-end formation

Wani S, Hirose Y, Ohkuma Y
2014; 8(6):255-261. (DOI: 10.5582/ddt.2014.01044)

Development of mucoadhesive buccal films from rice for pharmaceutical delivery systems.

Okonogi S, Khongkhunthian S, Jaturasitha S

2014; 8(6):262-267. (DOI: 10.5582/ddt.2014.01041)

Ion-exchange complex of famotidine: sustained release and taste masking approach of stable liquid dosage form.

Aman RM, Meshali MM, Abdelghani GM

2014; 8(6):268-275. (DOI: 10.5582/ddt.2014.01043)

Case Reports

Management of inappropriate sinus tachycardia with ivabradine in a renal transplant recipient.

Goyal VK, Godara S, Sadasukhi TC, Gupta HL

2014; 8(3):132-133. (DOI: 10.5582/ddt.2014.01023)

Central nervous system infection with non-tuberculous mycobacteria: A report of that infection in two patients with AIDS.

Cai R, Qi T, Lu HZ

2014; 8(6):276-279. (DOI: 10.5582/ddt.2014.01047)

Commentaries

Three-dimensional imaging technology offers promise in medicine.

Karako K, Wu Q, Gao JJ

2014; 8(2):96-97. (DOI: 10.5582/ddt.8.96)

Current clinical uses of the biomarkers for hepatocellular carcinoma.

Huang JW, Zeng Y

2014; 8(2):98-99. (DOI: 10.5582/ddt.8.98)

Can gamma-glutamyl transferase levels contribute to a better prognosis for patients with hepatocellular carcinoma?

Wang ZG, Song PP, Xia JF, Inagaki Y, Tang W, Kokudo N

2014; 8(3):134-138. (DOI: 10.5582/ddt.2014.01025)

HDAC1/3 dual selective inhibitors - New therapeutic agents for the potential treatment of cancer.

Li XY, Xu WF

2014; 8(5):225-228. (DOI: 10.5582/ddt.2014.01034)

Drug development for controlling Ebola epidemic – A race against time.

Gao JJ, Yin L

2014; 8(5):229-231. (DOI: 10.5582/ddt.2014.01040)

Letter

Suggestions to the media to help us cope with the A/H7N9 crisis in China.

Sun Y, Lu HZ

2014; 8(2):100-101. (DOI: 10.5582/ddt.8.100)

Guide for Authors

1. Scope of Articles

Drug Discoveries & Therapeutics welcomes contributions in all fields of pharmaceutical and therapeutic research such as medicinal chemistry, pharmacology, pharmaceutical analysis, pharmaceuticals, pharmaceutical administration, and experimental and clinical studies of effects, mechanisms, or uses of various treatments. Studies in drug-related fields such as biology, biochemistry, physiology, microbiology, and immunology are also within the scope of this journal.

2. Submission Types

Original Articles should be well-documented, novel, and significant to the field as a whole. An Original Article should be arranged into the following sections: Title page, Abstract, Introduction, Materials and Methods, Results, Discussion, Acknowledgments, and References. Original articles should not exceed 5,000 words in length (excluding references) and should be limited to a maximum of 50 references. Articles may contain a maximum of 10 figures and/or tables.

Brief Reports definitively documenting either experimental results or informative clinical observations will be considered for publication in this category. Brief Reports are not intended for publication of incomplete or preliminary findings. Brief Reports should not exceed 3,000 words in length (excluding references) and should be limited to a maximum of 4 figures and/or tables and 30 references. A Brief Report contains the same sections as an Original Article, but the Results and Discussion sections should be combined.

Reviews should present a full and up-to-date account of recent developments within an area of research. Normally, reviews should not exceed 8,000 words in length (excluding references) and should be limited to a maximum of 100 references. Mini reviews are also accepted.

Policy Forum articles discuss research and policy issues in areas related to life science such as public health, the medical care system, and social science and may address governmental issues at district, national, and international levels of discourse. Policy Forum articles should not exceed 2,000 words in length (excluding references).

Case Reports should be detailed reports of the symptoms, signs, diagnosis, treatment, and follow-up of an individual patient. Case reports may contain a demographic profile of the patient but usually describe an unusual or novel occurrence. Unreported or unusual side effects or adverse interactions involving medications will also be considered. Case

Reports should not exceed 3,000 words in length (excluding references).

News articles should report the latest events in health sciences and medical research from around the world. News should not exceed 500 words in length.

Letters should present considered opinions in response to articles published in Drug Discoveries & Therapeutics in the last 6 months or issues of general interest. Letters should not exceed 800 words in length and may contain a maximum of 10 references.

3. Editorial Policies

Ethics: Drug Discoveries & Therapeutics requires that authors of reports of investigations in humans or animals indicate that those studies were formally approved by a relevant ethics committee or review board.

Conflict of Interest: All authors are required to disclose any actual or potential conflict of interest including financial interests or relationships with other people or organizations that might raise questions of bias in the work reported. If no conflict of interest exists for each author, please state "There is no conflict of interest to disclose".

Submission Declaration: When a manuscript is considered for submission to Drug Discoveries & Therapeutics, the authors should confirm that 1) no part of this manuscript is currently under consideration for publication elsewhere; 2) this manuscript does not contain the same information in whole or in part as manuscripts that have been published, accepted, or are under review elsewhere, except in the form of an abstract, a letter to the editor, or part of a published lecture or academic thesis; 3) authorization for publication has been obtained from the authors' employer or institution; and 4) all contributing authors have agreed to submit this manuscript.

Cover Letter: The manuscript must be accompanied by a cover letter signed by the corresponding author on behalf of all authors. The letter should indicate the basic findings of the work and their significance. The letter should also include a statement affirming that all authors concur with the submission and that the material submitted for publication has not been published previously or is not under consideration for publication elsewhere. The cover letter should be submitted in PDF format. For example of Cover Letter, please visit <http://www.ddtjournal.com/downloadcentre.php> (Download Centre).

Copyright: A signed JOURNAL PUBLISHING AGREEMENT (JPA) must be provided by post, fax, or as a scanned file before acceptance of the article. Only forms with a hand-written signature are accepted. This copyright will ensure the widest possible dissemination of information. A form facilitating transfer of copyright can be downloaded by clicking the appropriate link and can be returned to the e-mail address or fax number noted on the form (Please visit

Download Centre). Please note that your manuscript will not proceed to the next step in publication until the JPA form is received. In addition, if excerpts from other copyrighted works are included, the author(s) must obtain written permission from the copyright owners and credit the source(s) in the article.

Suggested Reviewers: A list of up to 3 reviewers who are qualified to assess the scientific merit of the study is welcomed. Reviewer information including names, affiliations, addresses, and e-mail should be provided at the same time the manuscript is submitted online. Please do not suggest reviewers with known conflicts of interest, including participants or anyone with a stake in the proposed research; anyone from the same institution; former students, advisors, or research collaborators (within the last three years); or close personal contacts. Please note that the Editor-in-Chief may accept one or more of the proposed reviewers or may request a review by other qualified persons.

Language Editing: Manuscripts prepared by authors whose native language is not English should have their work proofread by a native English speaker before submission. If not, this might delay the publication of your manuscript in Drug Discoveries & Therapeutics.

The Editing Support Organization can provide English proofreading, Japanese-English translation, and Chinese-English translation services to authors who want to publish in Drug Discoveries & Therapeutics and need assistance before submitting a manuscript. Authors can visit this organization directly at <http://www.iacmhr.com/iac-eso/support.php?lang=en>. IAC-ESO was established to facilitate manuscript preparation by researchers whose native language is not English and to help edit works intended for international academic journals.

4. Manuscript Preparation

Manuscripts should be written in clear, grammatically correct English and submitted as a Microsoft Word file in a single-column format. Manuscripts must be paginated and typed in 12-point Times New Roman font with 24-point line spacing. Please do not embed figures in the text. Abbreviations should be used as little as possible and should be explained at first mention unless the term is a well-known abbreviation (e.g. DNA). Single words should not be abbreviated.

Title page: The title page must include 1) the title of the paper (Please note the title should be short, informative, and contain the major key words); 2) full name(s) and affiliation(s) of the author(s); 3) abbreviated names of the author(s); 4) full name, mailing address, telephone/fax numbers, and e-mail address of the corresponding author; and 5) conflicts of interest (if you have an actual or potential conflict of interest to disclose, it must be included as a footnote on the title page of the manuscript; if no conflict of interest exists for each author, please state "There is no conflict of interest to disclose"). Please visit [Download Centre](#) and refer to the title page of the manuscript sample.

Abstract: The abstract should briefly state the purpose of the study, methods, main findings, and conclusions. For article types including Original Article, Brief Report, Review, Policy Forum, and Case Report, a one-paragraph abstract consisting of no more than 250 words must be included in the manuscript. For News and Letters, a brief summary of main content in 150 words or fewer should be included in the manuscript. Abbreviations must be kept to a minimum and non-standard abbreviations explained in brackets at first mention. References should be avoided in the abstract. Key words or phrases that do not occur in the title should be included in the Abstract page.

Introduction: The introduction should be a concise statement of the basis for the study and its scientific context.

Materials and Methods: The description should be brief but with sufficient detail to enable others to reproduce the experiments. Procedures that have been published previously should not be described in detail but appropriate references should simply be cited. Only new and significant modifications of previously published procedures require complete description. Names of products and manufacturers with their locations (city and state/country) should be given and sources of animals and cell lines should always be indicated. All clinical investigations must have been conducted in accordance with Declaration of Helsinki principles. All human and animal studies must have been approved by the appropriate institutional review board(s) and a specific declaration of approval must be made within this section.

Results: The description of the experimental results should be succinct but in sufficient detail to allow the experiments to be analyzed and interpreted by an independent reader. If necessary, subheadings may be used for an orderly presentation. All figures and tables must be referred to in the text.

Discussion: The data should be interpreted concisely without repeating material already presented in the Results section. Speculation is permissible, but it must be well-founded, and discussion of the wider implications of the findings is encouraged. Conclusions derived from the study should be included in this section.

Acknowledgments: All funding sources should be credited in the Acknowledgments section. In addition, people who contributed to the work but who do not meet the criteria for authors should be listed along with their contributions.

References: References should be numbered in the order in which they appear in the text. Citing of unpublished results, personal communications, conference abstracts, and theses in the reference list is not recommended but these sources may be mentioned in the text. In the reference list, cite the names of all authors when there are fifteen or fewer authors; if there are sixteen or more authors, list the first three followed by *et al.* Names of journals should

be abbreviated in the style used in PubMed. Authors are responsible for the accuracy of the references. Examples are given below:

Example 1 (Sample journal reference):
Nakata M, Tang W. Japan-China Joint Medical Workshop on Drug Discoveries and Therapeutics 2008: The need of Asian pharmaceutical researchers' cooperation. *Drug Discov Ther.* 2008; 2:262-263.

Example 2 (Sample journal reference with more than 15 authors):
Darby S, Hill D, Auvinen A, *et al.* Radon in homes and risk of lung cancer: Collaborative analysis of individual data from 13 European case-control studies. *BMJ.* 2005; 330:223.

Example 3 (Sample book reference):
Shalev AY. Post-traumatic stress disorder: Diagnosis, history and life course. In: *Post-traumatic Stress Disorder, Diagnosis, Management and Treatment* (Nutt DJ, Davidson JR, Zohar J, eds.). Martin Dunitz, London, UK, 2000; pp. 1-15.

Example 4 (Sample web page reference):
World Health Organization. The World Health Report 2008 – primary health care: Now more than ever. http://www.who.int/whr/2008/whr08_en.pdf (accessed September 23, 2010).

Tables: All tables should be prepared in Microsoft Word or Excel and should be arranged at the end of the manuscript after the References section. Please note that tables should not in image format. All tables should have a concise title and should be numbered consecutively with Arabic numerals. If necessary, additional information should be given below the table.

Figure Legend: The figure legend should be typed on a separate page of the main manuscript and should include a short title and explanation. The legend should be concise but comprehensive and should be understood without referring to the text. Symbols used in figures must be explained.

Figure Preparation: All figures should be clear and cited in numerical order in the text. Figures must fit a one- or two-column format on the journal page: 8.3 cm (3.3 in.) wide for a single column, 17.3 cm (6.8 in.) wide for a double column; maximum height: 24.0 cm (9.5 in.). Please make sure that artwork files are in an acceptable format (TIFF or JPEG) at minimum resolution (600 dpi for illustrations, graphs, and annotated artwork, and 300 dpi for micrographs and photographs). Please provide all figures as separate files. Please note that low-resolution images are one of the leading causes of article resubmission and schedule delays. All color figures will be reproduced in full color in the online edition of the journal at no cost to authors.

Units and Symbols: Units and symbols conforming to the International System of Units (SI) should be used for physicochemical quantities. Solidus notation (*e.g.* mg/kg, mg/mL, mol/mm²/min) should be used. Please refer to the SI Guide www.bipm.org/en/si/ for standard units.

Supplemental data: Supplemental data might be useful for supporting and enhancing your scientific research and Drug Discoveries & Therapeutics accepts the submission of these materials which will be only published online alongside the electronic version of your article. Supplemental files (figures, tables, and other text materials) should be prepared according to the above guidelines, numbered in Arabic numerals (*e.g.*, Figure S1, Figure S2, and Table S1, Table S2) and referred to in the text. All figures and tables should have titles and legends. All figure legends, tables and supplemental text materials should be placed at the end of the paper. Please note all of these supplemental data should be provided at the time of initial submission and note that the editors reserve the right to limit the size and length of Supplemental Data.

5. Submission Checklist

The Submission Checklist will be useful during the final checking of a manuscript prior to sending it to Drug Discoveries & Therapeutics for review. Please visit [Download Centre](#) and download the Submission Checklist file.

6. Online submission

Manuscripts should be submitted to Drug Discoveries & Therapeutics online at <http://www.ddtjournal.com>. The manuscript file should be smaller than 5 MB in size. If for any reason you are unable to submit a file online, please contact the Editorial Office by e-mail at office@ddtjournal.com

7. Accepted manuscripts

Proofs: Galley proofs in PDF format will be sent to the corresponding author *via* e-mail. Corrections must be returned to the editor (proof-editing@ddtjournal.com) within 3 working days.

Offprints: Authors will be provided with electronic offprints of their article. Paper offprints can be ordered at prices quoted on the order form that accompanies the proofs.

Page Charge: A page charge of \$140 will be assessed for each printed page of an accepted manuscript. The charge for printing color figures is \$340 for each page. Under exceptional circumstances, the author(s) may apply to the editorial office for a waiver of the publication charges at the time of submission.

(Revised February 2013)

Editorial and Head Office:

Pearl City Koishikawa 603
2-4-5 Kasuga, Bunkyo-ku
Tokyo 112-0003
Japan
Tel: +81-3-5840-9697
Fax: +81-3-5840-9698
E-mail: office@ddtjournal.com

JOURNAL PUBLISHING AGREEMENT (JPA)

Manuscript No.:

Title:

Corresponding author:

The International Advancement Center for Medicine & Health Research Co., Ltd. (IACMHR Co., Ltd.) is pleased to accept the above article for publication in Drug Discoveries & Therapeutics. The International Research and Cooperation Association for Bio & Socio-Sciences Advancement (IRCA-BSSA) reserves all rights to the published article. Your written acceptance of this JOURNAL PUBLISHING AGREEMENT is required before the article can be published. Please read this form carefully and sign it if you agree to its terms. The signed JOURNAL PUBLISHING AGREEMENT should be sent to the Drug Discoveries & Therapeutics office (Pearl City Koishikawa 603, 2-4-5 Kasuga, Bunkyo-ku, Tokyo 112-0003, Japan; E-mail: office@ddtjournal.com; Tel: +81-3-5840-9697; Fax: +81-3-5840-9698).

1. Authorship Criteria

As the corresponding author, I certify on behalf of all of the authors that:

- 1) The article is an original work and does not involve fraud, fabrication, or plagiarism.
- 2) The article has not been published previously and is not currently under consideration for publication elsewhere. If accepted by Drug Discoveries & Therapeutics, the article will not be submitted for publication to any other journal.
- 3) The article contains no libelous or other unlawful statements and does not contain any materials that infringes upon individual privacy or proprietary rights or any statutory copyright.
- 4) I have obtained written permission from copyright owners for any excerpts from copyrighted works that are included and have credited the sources in my article.
- 5) All authors have made significant contributions to the study including the conception and design of this work, the analysis of the data, and the writing of the manuscript.
- 6) All authors have reviewed this manuscript and take responsibility for its content and approve its publication.
- 7) I have informed all of the authors of the terms of this publishing agreement and I am signing on their behalf as their agent.

2. Copyright Transfer Agreement

I hereby assign and transfer to IACMHR Co., Ltd. all exclusive rights of copyright ownership to the above work in the journal Drug Discoveries & Therapeutics, including but not limited to the right 1) to publish, republish, derivate, distribute, transmit, sell, and otherwise use the work and other related material worldwide, in whole or in part, in all languages, in electronic, printed, or any other forms of media now known or hereafter developed and the right 2) to authorize or license third parties to do any of the above.

I understand that these exclusive rights will become the property of IACMHR Co., Ltd., from the date the article is accepted for publication in the journal Drug Discoveries & Therapeutics. I also understand that IACMHR Co., Ltd. as a copyright owner has sole authority to license and permit reproductions of the article.

I understand that except for copyright, other proprietary rights related to the Work (e.g. patent or other rights to any process or procedure) shall be retained by the authors. To reproduce any text, figures, tables, or illustrations from this Work in future works of their own, the authors must obtain written permission from IACMHR Co., Ltd.; such permission cannot be unreasonably withheld by IACMHR Co., Ltd.

3. Conflict of Interest Disclosure

I confirm that all funding sources supporting the work and all institutions or people who contributed to the work but who do not meet the criteria for authors are acknowledged. I also confirm that all commercial affiliations, stock ownership, equity interests, or patent-licensing arrangements that could be considered to pose a financial conflict of interest in connection with the article have been disclosed.

Corresponding Author's Name (Signature):

Date:

